



Comparison between simulated and observed LHC beam backgrounds in the ATLAS experiment at $E_{\text{beam}} = 4 \text{ TeV}$

The ATLAS Collaboration

Results of dedicated Monte Carlo simulations of beam-induced background (BIB) in the ATLAS experiment at the Large Hadron Collider (LHC) are presented and compared with data recorded in 2012. During normal physics operation this background arises mainly from scattering of the 4 TeV protons on residual gas in the beam pipe. Methods of reconstructing the BIB signals in the ATLAS detector, developed and implemented in the simulation chain based on the FLUKA Monte Carlo simulation package, are described. The interaction rates are determined from the residual gas pressure distribution in the LHC ring in order to set an absolute scale on the predicted rates of BIB so that they can be compared quantitatively with data. Through these comparisons the origins of the BIB leading to different observables in the ATLAS detectors are analysed. The level of agreement between simulation results and BIB measurements by ATLAS in 2012 demonstrates that a good understanding of the origin of BIB has been reached.

1 Introduction

Proton losses in the Large Hadron Collider (LHC) ring upstream¹ of the ATLAS experiment [1], due to interactions with either residual gas in the beam pipe (beam–gas scattering) or with machine elements such as collimators, result in beam-induced background (BIB). Although the rates are negligible compared to particle debris from almost 10^9 proton–proton (pp) collisions per second, BIB has particular features that render it potentially problematic: it is characterised by particles almost parallel to the beam line, which can produce elongated clusters with large energy deposition in the innermost tracking detectors based on silicon pixel technology. At high rates, these abnormally large clusters can affect data-taking efficiency [2]. Furthermore, a potential background for physics analyses arises from high-energy muons, originating mostly from pion and kaon decay in the hadronic showers induced by beam losses. These muons can deposit large amounts of energy in calorimeters through radiative processes. Such energy depositions, which are not associated with a hard scattering at the interaction point (IP), can be reconstructed as *fake jets* leading to missing transverse momentum if overlaid with a collision event. Especially in searches for some exotic physics processes [3–6], fake jets represent a non-negligible background that must be well controlled and subtracted.

Although BIB has had no detrimental effects on ATLAS operation so far, the continuous striving for better LHC luminosity performance might change this situation in the future. A thorough understanding of the sources and nature of BIB, which is crucial when planning upgrades to the LHC, can only be achieved by a combination of measurements and simulations. A validation of the latter is the main purpose of this work.

A lot of experience with BIB was gained at the Tevatron and HERA colliders [7–9]. The first simulation predictions for BIB at the LHC were presented more than 20 years ago [10] and have been refined several times thereafter [11–14]. Throughout the LHC operation, BIB is routinely monitored and analysed by ATLAS [15, 16]. In this paper, comparisons between detailed simulations using the FLUKA Monte Carlo (MC) simulation package [17, 18] and measurements [16] of BIB during the 2012 LHC run, with a proton beam energy of 4 TeV, are presented.

2 The LHC accelerator and the ATLAS experiment

The LHC accelerator and the ATLAS experiment are described in detail in Refs. [19] and [1] respectively. Only a summary, focused on aspects relevant to the studies and simulations of BIB, is given here.

2.1 The LHC

The LHC, shown schematically in Figure 1, consists of eight arcs that are joined by long straight sections (LSSs) of ~ 500 m length. In the middle of each LSS there is an interaction region (IR); the ATLAS experiment is situated in IR1. The LHC beam-cleaning equipment is located in IR3 and IR7, for momentum and betatron cleaning respectively. The principal performance parameters of LHC operation in 2012 are listed in Table 1.

¹ Upstream and downstream are defined relative to the beam direction.

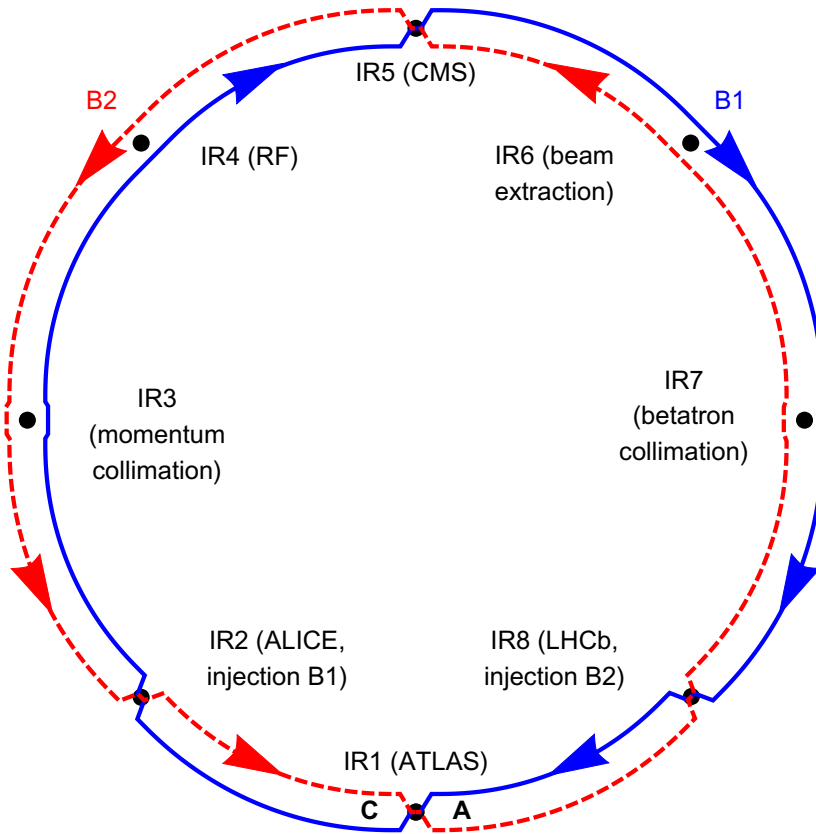


Figure 1: The general layout of the LHC [19], showing the eight interaction regions. The counter-circulating beams are shown schematically, i.e. their separation is not to scale. The ATLAS convention of labelling sides by ‘A’ and ‘C’ is indicated. The figure is adapted from Ref. [20].

Table 1: LHC parameters during operation as a pp collider in the second half of 2012. The parameter β^* refers to the value of the optical β -function at the collision point.

Parameter	Value
Beam energy [TeV]	4.0
Protons per bunch [10^{11}]	~ 1.5
Number of bunches per beam	1374
Bunch spacing [ns]	50
Vertical crossing angle in IR1 [μrad]	145.0
β^* in IR1 [m]	0.6

A schematic layout of IR1, up to 165 m from the interaction point (IP, at $z = 0$), is shown in Figure 2, where the separation of the two counter-rotating beams is illustrated. Copper absorbers (TAS), which protect the superconducting inner triplets from collision debris, are located between $|z| = 19$ m and $|z| = 20.8$ m and have an aperture of $r = 17$ mm. The final focus is provided by the quadrupoles of the inner triplets on each side of the IP, between $|z| = 23$ m and $|z| = 54$ m. The beam trajectories are separated at $|z| \approx 70$ m inside

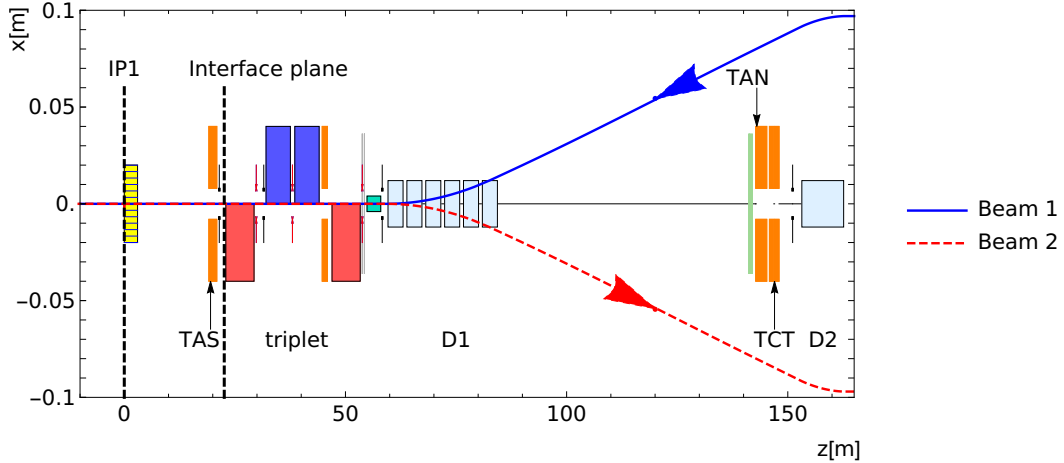


Figure 2: Layout of the IR1 region showing the z -location of LHC beam-line elements and schematic beam trajectories. The x -coordinates refer only to the positions of the beams, not to the beam-line elements. The beams are separated by the D1 magnet and recombined into parallel trajectories by the D2 magnet. The tertiary collimator (TCT) is only on the incoming beam, just before the neutral particle absorber (TAN). The sense of focusing of the four triplet elements is indicated by the colour of the boxes (red = vertical, blue = horizontal) for the incoming beam. The interface plane is explained in Section 5.

the separation dipoles D1 and recombined in dipoles D2 at $|z| \approx 160$ m, which bring the two beams into parallel trajectories at a distance of 194 mm from each other. The dipole D2 is superconducting and is protected by the neutral particle absorber (TAN), which intercepts energetic neutrons and photons emitted from the IP at very small angles.

The 400.79 MHz frequency of the LHC radio-frequency (RF) system and the revolution time of 88.9244 μ s form 35640 buckets that can be filled with particles. In the 2012 LHC run, every 20th bucket was filled giving a bunch spacing of 50 ns. In order to facilitate monitoring of BIB, a few (typically six per beam in 2012) unpaired bunches are included in each LHC bunch pattern. Having no counterpart in the other beam to collide with, these bunches provide the LHC experiments with a rather clean measurement of BIB.

2.2 The ATLAS experiment

The ATLAS experiment is one of the two general-purpose detectors at the LHC. With a length of 46 m and a diameter of 25 m, it is optimised to study proton–proton collisions at the highest available energies and luminosities.

In this study, the right-handed ATLAS coordinate system is used. The origin is at the nominal IP and the azimuthal angle ϕ is measured relative to the x -axis, which points towards the centre of the LHC ring. Side A of ATLAS is defined as the side of the incoming, clockwise, LHC beam-1 while the side of the incoming beam-2 is labelled C, as illustrated in Figure 1. The z -axis points from C to A, i.e. along the beam-2 direction. The pseudorapidity is given by $\eta = -\ln \tan(\theta/2)$, where θ is the polar angle relative to the z -axis. The transverse momentum is defined as $p_T = p \sin \theta$, where p is obtained from the energy deposits in the calorimeters, assuming them to be massless.

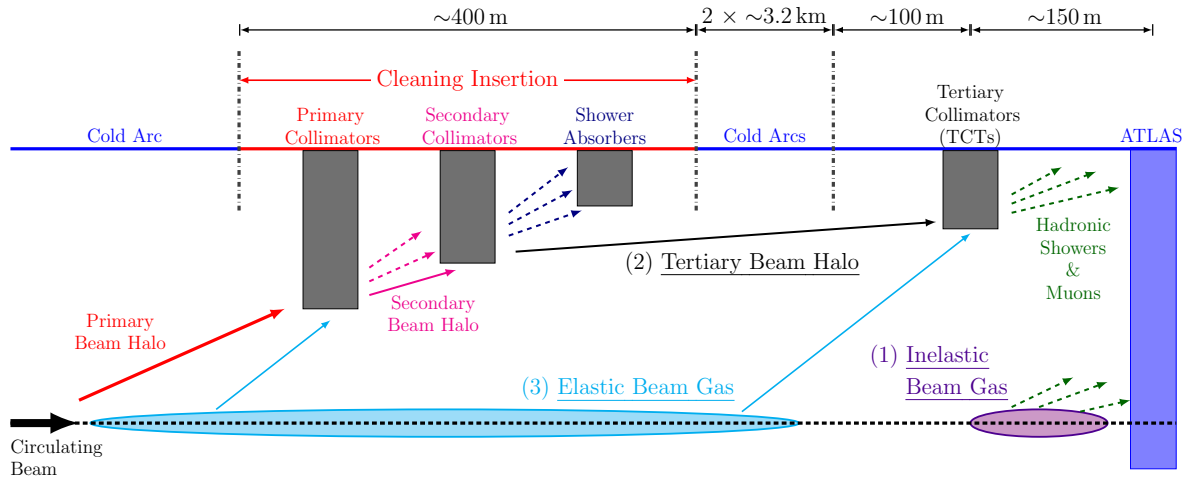


Figure 3: Schematic illustration of the three sources of BIB reaching ATLAS: (1) nearby inelastic beam–gas collisions, (2) tertiary beam halo losses on the TCT and (3) protons deflected by elastic beam–gas collisions and hitting the TCT. The cleaning insertions are 6.7 km away from ATLAS and the elastic beam–gas events are distributed around the entire accelerator ring. The distance from the beam to the collimators is a few millimetres.

ATLAS includes a dedicated beam conditions monitor (BCM) [21] for beam background measurements. The BCM consists of four small diamond modules on each side of the IP, at $z = \pm 1.84$ m, at a mean radial distance of $r = 55$ mm ($|\eta| \approx 4.2$) from the beam line. The modules are arranged in a cross: two in the horizontal and two in the vertical plane. Each module has two back-to-back sensors with an active area of 8×8 mm² and a total thickness of 1 mm.

The inner detector [22] is subdivided into a pixel detector immediately outside the beam pipe, a silicon-strip tracker and an outer transition-radiation tracker. These are inside a solenoid, which produces a 2 T magnetic field along the z -axis. The inner detector is used to determine the momentum of charged particles in the pseudorapidity range $|\eta| < 2.5$.

The calorimeter system, which measures the energy of the particles, includes a high-granularity liquid-argon (LAr) electromagnetic barrel calorimeter with lead as absorber; it has a half-length of ~ 3 m and extends radially from $r = 1.5$ m to 2.0 m, thus covering pseudorapidities up to $|\eta| = 1.5$. Between $r = 2.3$ m and 4.3 m a scintillator-tile hadronic barrel calorimeter (Tile) with steel as absorber and ~ 6 m half-length covers pseudorapidities up to $|\eta| = 1.7$. The calorimeter system is extended, up to $|\eta| = 3.2$, by electromagnetic and hadronic endcaps based on LAr technology. These have lengths, along z , of 0.6 m and 1.8 m respectively.

The calorimeters are surrounded by a muon spectrometer based on three large air-core superconducting toroidal magnets with eight coils each: one barrel toroid and two endcap toroids positioned inside the barrel at the ends of the central solenoid.

3 Beam-induced background

Beam induced background originates from three different beam-loss processes, which are illustrated in Figure 3 and detailed below.

Inelastic proton interactions with residual gas inside the beam pipe (labelled 1 in Figure 3), in the vicinity of the IP, constitute the dominant source of BIB in ATLAS. Hadronic and electromagnetic showers, but in particular high-energy muons produced by these interactions, can enter ATLAS and be detected by the BIB monitoring system. It was shown in previous studies [10] that inelastic beam–gas collisions up to distances of ~ 500 m from the IP contribute to the background.

A small fraction of BIB arises from beam halo, which is continuously repopulated by scattering of particles from the beam due to various processes such as elastic collisions at the experiments and with residual gas, noise on the RF system and feedback, intrabeam scattering, resonances and instabilities. The superconducting magnets of the LHC require very efficient halo-cleaning, which is realised by a multi-step cleaning system [23]. The primary and secondary collimators of the cleaning insertions in IR3 and IR7 intercept most of the off-momentum and betatron halo. A small fraction of the protons escape these insertions and constitute the tertiary halo (labelled 2 in Figure 3) which is intercepted by the tertiary collimators (TCTs), located at distances of $z \approx 150$ m from each experimental IP. Protons impinging on the TCTs can also originate from elastic beam–gas interactions (labelled 3 in Figure 3), which deflect protons out of the beam, around the whole accelerator ring. The losses on the TCTs create showers, which can propagate all the way to the IP. Dedicated tests [24] during 2015 and 2016 showed that, in normal physics conditions, total losses on the TCTs contribute of the order of only 1% to the total BIB seen in ATLAS. Thus they are not considered in this paper.

The rate of beam–gas interactions is proportional to the residual gas pressure and the beam intensity. The latter is a property of the beams and is measured by the LHC with percent-level accuracy, but the pressure and molecular composition of the residual gas varies as a function of position around the accelerator. After pumping down of the LHC beam vacuum, a small amount of gas remains stuck on the beam-pipe surface. These gas molecules can be desorbed by synchrotron radiation or charged particles hitting the beam-pipe walls. The rate of outgassing depends on the intensity of the radiation and therefore the dynamical pressure depends on beam intensity and energy. In addition, the surface characteristics and temperature have a large influence on the residual pressure. The residual gas consists of H_2 , CH_4 , CO_2 and CO . Their relative fractions depend on local temperature, radiation load and surface characteristics of the beam pipe. In cryogenic sectors the gas condenses on the cold walls, but is relatively easily released by irradiation. Almost all room-temperature sectors of the LHC beam pipe are coated with a non-evaporable getter material [25], which provides distributed pumping along the beam line for all common gases except CH_4 . Therefore, methane is the dominant gas species in room-temperature sections, including the D1 dipole. Inside cryogenic magnets where the cold bore is at 1.9 K, notably those of the inner triplet and the LHC arc, all gases except hydrogen stick relatively firmly on the surface, so the dominant gas is H_2 . The magnets in the LSS, from D2 to the arc, are operated at 4.5 K. At this temperature all gases are more easily desorbed and here CO_2 is the most abundant gas species. Vacuum pumps produce local minima in the pressure and corresponding gradients which result in gas diffusion from sections with higher pressure towards the pumps.

The room-temperature sections of the LHC are equipped with vacuum gauges, but between these measurement points the pressure has to be obtained from simulations. The simulation models are based on theory and laboratory measurements of desorption rates and gas composition [26]. The amount of gas on the surfaces depends on the beam-conditioning history: when gas is desorbed and pumped out during beam operation the rate of outgassing slowly goes down. The state of surface conditioning, at any given time, has to be empirically estimated based on prior experience. Thus, the simulations depend on the local characteristics and temperature of the beam pipe, local pumping speeds, beam intensity and the estimated effects of the beam-conditioning history. The overall uncertainty in the local pressure due to knowledge

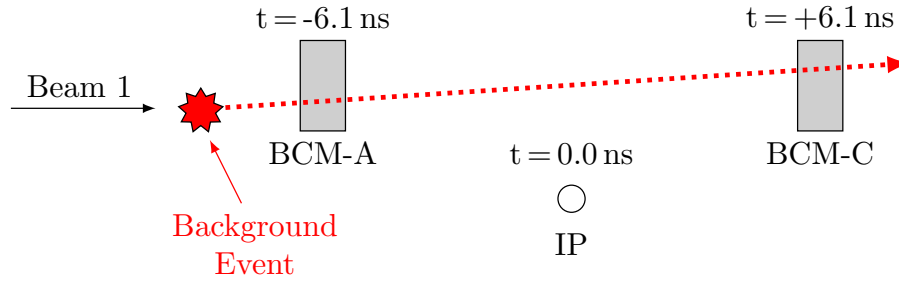


Figure 4: Illustration of the BCM background trigger signature for beam-1. The dotted line represents the trajectory of one particle hitting the upstream and downstream BCM modules. For beam-1 the early hit is on side A and the in-time hit on side C. For beam-2 the direction is reversed. The trigger can also be fired by two different particles, the only requirement being that any of the four modules on one side of the IP has an early hit and any of those on the opposite side has an in-time hit.

of these parameters, especially of the state of surface conditioning, is estimated to be a factor of ~ 3 . Since both the surface characteristics and the intensity of radiation vary as a function of position, this uncertainty is not a global scale factor of the entire pressure distribution; it is possible that the pressure is underestimated in some regions and overestimated in others.

4 Background monitoring methods

The rates of BIB are measured by the BCM and the calorimeters, which are described in Section 2.2. They both provide low-level trigger signals which can be used for real-time background monitoring, and also record the data for detailed offline analysis. Only the unpaired bunches are used for monitoring and analysis of BIB. For inelastic beam–gas background these can be assumed to be perfectly representative of colliding bunches.

4.1 BCM background rates

Hits in the BCM modules are counted above a threshold of 250 keV, which corresponds to roughly 40% of the energy deposition of a minimum-ionising particle in 1 mm of diamond. Particles from beam losses reach upstream BCM detectors 6.1 ns before the nominal collision time, i.e. the passage of the bunch at the IP at $t = 0$, and produce *early* hits. Both the BIB and collision products from the IP produce *in-time* hits in the downstream detectors at $t = +6.1$ ns.

A BCM background trigger signature, illustrated in Figure 4, consists of an early hit in any module on the upstream side and an in-time hit in any module on the downstream side. The time windows of the background trigger are 5.46 ns wide and nominally centred at $t = \pm 6.25$ ns. The BCM has sub-nanosecond time resolution and the nominal centre of the trigger window is aligned with the LHC collision time to an accuracy better than 2 ns.

Due to the built-in direction requirement, the BCM background trigger is able to distinguish which beam the background originates from. In 2012 a single BCM background trigger, which fired on events in either direction, was used to collect events for the offline analysis.

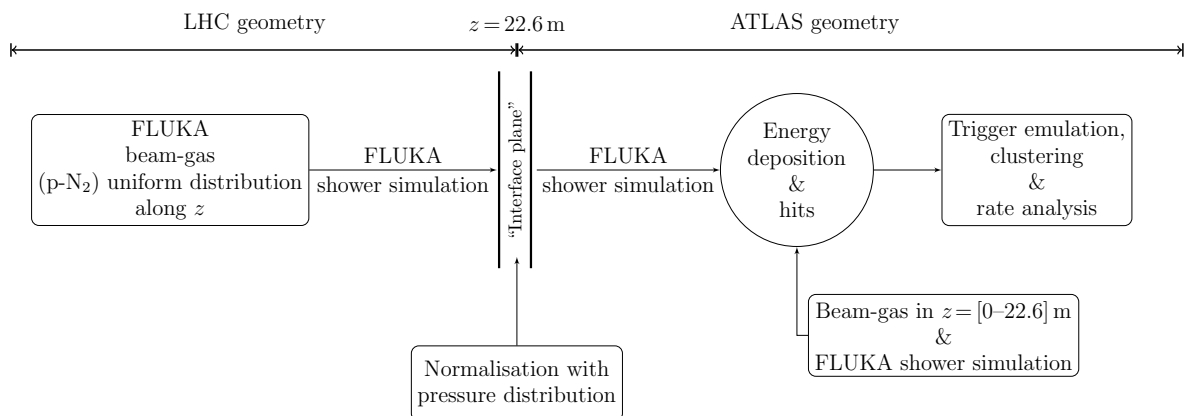


Figure 5: Flowchart of the two-step process for simulation of beam–gas events. Particles crossing the interface plane are stored in a file, and normalised using the appropriate pressure distribution before being injected into the ATLAS simulation. The trigger emulation, clustering and rate analysis are performed on the custom FLUKA output.

4.2 Fake jets in calorimeters

The barrel and endcap calorimeters have nanosecond time resolution and contribute to a jet trigger with a p_T threshold of 10 GeV at the electromagnetic scale, which is used to select fake-jet candidates induced by BIB in unpaired bunches. The jets are reconstructed with the anti- k_t jet algorithm [27] with radius parameter $R = 0.4$ using the FastJet software package [28]. The inputs to this algorithm are topologically connected clusters of calorimeter cells [29], seeded by cells with an energy at least four standard deviations above the measured noise. These topological clusters are calibrated at the electromagnetic scale. The reconstructed jets are corrected for contributions from additional pp interactions in the same and neighbouring bunch crossings as described in Ref. [29]. In order to suppress instrumental backgrounds, standard data-quality requirements are imposed [30]. Data from periods affected by calorimeter noise bursts are excluded from the analysis.

5 Simulation framework

The simulation of the inelastic beam–gas events was performed with FLUKA using a two-step approach – a method first introduced in Ref. [10] and illustrated in Figure 5. The advantage of dividing the simulation into accelerator- and detector-specific parts is that it leaves more flexibility in the choice of simulation tools. This approach also saves computational resources since the results of the first step, simulation of particle transport and showering in the accelerator structures, can be used for several studies of the impact on the ATLAS detector.

The first step is discussed in detail in Ref. [31]: beam–gas events with a uniform distribution in a z -range from 22.6 m to 546.6 m were generated with FLUKA as inelastic p – N_2 interactions. Although the residual gas composition varies along the ring and H_2 is most abundant in 1.9 K sections, the much larger interaction cross-sections of the other gas species causes them to dominate the interaction rate, especially in the LSS. Nitrogen is therefore considered to represent a good average of the atomic composition of the residual gas [14]. Using a generic gas species and a uniform distribution of events has the advantage that the same simulation results can be used with different pressure distributions. Unlike most previous studies [10–13],

all simulations in this work were performed without any Monte Carlo variance reduction techniques,² in order to preserve correlations within individual events. This is a prerequisite for reconstructing the trigger signatures. In the first simulation step, the secondaries produced in the beam–gas interactions are transported to a virtual *interface plane* at $z = 22.6$ m upstream of the IP. The choice of this z -location is motivated by the fact that it is on the IP-side of the closest inner-triplet magnet. Thus it naturally separates the experimental area, where a detailed FLUKA geometry of the ATLAS detector is available, from the LHC accelerator with its own geometry and magnetic field modelling. For all particles reaching this plane the positions, four-momenta and times of flight are recorded and serve as input to subsequent detector simulations. For a complete description of the background, especially in the BCM with its low hit threshold, particles have to be transported down to low energies to ensure that all potential hits are simulated. Since this is very CPU-intensive, only six million inelastic events were simulated, transporting particles down to a kinetic energy of 20 MeV. This value of 20 MeV is chosen in order to stay above low-energy nuclear reactions which are the source of a large number of low-energy particles. Such particles are absorbed locally but, due to their abundance, their simulation is costly in terms of CPU time. Six million events are not enough for the fake-jet studies, so a second sample of 300 million p -N₂ interactions was generated with a threshold of 20 GeV.³ This 20 GeV threshold corresponds to the minimum energy of the muon needed to create a fake jet with sufficient transverse momentum to fire the jet trigger used in this study.

The rate of p -N₂ interactions as a function of z , shown by the solid histogram in Figure 6, is obtained from an equivalent N₂ density distribution of the residual gas, $\rho_{\text{N}_2}(z)$. The partial densities (ρ_i) of all residual gas species at the location z are taken from the simulated pressure distribution and weighted by the ratio of inelastic proton–molecule (σ_i) to p -N₂ (σ_{N_2}) cross-sections:

$$\rho_{\text{N}_2}(z) = \sum_i \frac{\rho_i(z) \cdot \sigma_i}{\sigma_{\text{N}_2}}, \quad (1)$$

where i runs over H₂, CH₄, CO and CO₂. The absolute normalisation of all simulated rates in this paper is fixed by the interaction rates shown in Figure 6. Since these are derived from the pressure distribution, they are subjected to the uncertainty in the pressure simulations, discussed in Section 3.

The events used as input to the ATLAS simulations are sampled according to their z -coordinate, using the rate distribution of inelastic interactions, shown in Figure 6. The dotted histogram in Figure 6 shows, as a function of z , the rate of those events for which at least one particle has reached the interface plane. A comparison of the two histograms in Figure 6 reveals that practically all events produced at $z \lesssim 150$ m give contributions, while only $\sim 1\%$ of events with $z > 300$ m result in particles at the interface plane.

In order to account for beam–gas events between the IP and the interface plane, p -N₂ events were generated separately for $z < 22.6$ m with a z -distribution sampled directly from the inelastic interaction probability in that region, i.e. left of the dashed vertical line in Figure 6.

The particles at the interface plane, as well as those generated at $z < 22.6$ m, were transported through the ATLAS experimental area and detector using a dedicated FLUKA geometry model [32]. The magnetic

² Variance reduction refers to favouring some regions of phase space at the cost of others in order to achieve faster convergence of the estimates in the favoured regions. While significantly reducing the computational effort, the disadvantage of these methods is that they do not preserve correlations within events.

³ In order to further increase the number of fake jets, all events were used twice. Since the probability for a muon to experience a large radiative energy loss is very low, only 5% of the events gave a fake jet on both trials. Even in these cases the jet p_T was different, i.e. only the azimuthal angle was strongly correlated.

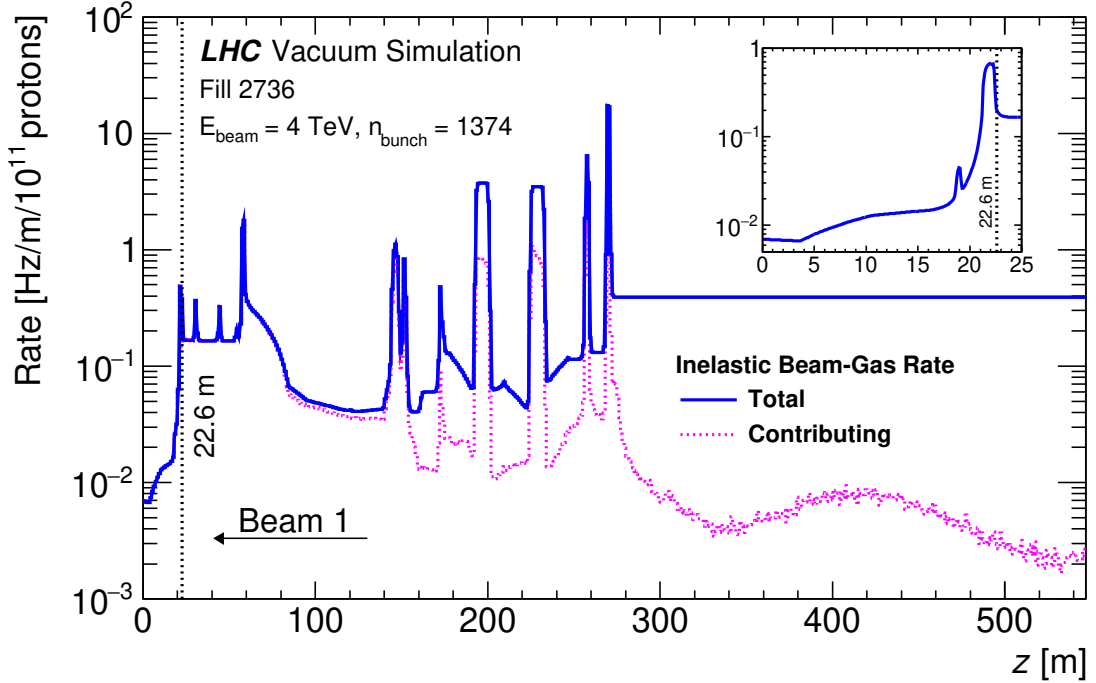


Figure 6: Inelastic beam–gas interaction rate of beam-1 in IR1 as a function of distance from the IP at the start of data-taking in LHC fill 2736. The beam moves towards negative z , i.e. from right to left in the figure. The total rate (solid blue histogram) reflects the residual gas pressure. The dotted histogram shows the rate of interactions which contribute at least one particle with kinetic energy $E > 20$ MeV at the interface plane at $z = 22.6$ m. The prominent peaks between $z \approx 150$ m and $z \approx 270$ m correspond to the positions of the TCT, the D2 dipole ($T = 4.5$ K), Q4–Q6 quadrupoles ($T = 4.5$ K) and cold-warm transitions at the exit of the arc. The pressure in the LHC cold arc ($T = 1.9$ K), starting at ~ 270 m, is assumed constant. The small inset shows the interaction rate on the IP side of the interface plane in more detail.

fields produced by the ATLAS magnets were implemented as two-dimensional maps covering the entire detector radius and extending in z up to the interface plane. The propagation and showering of the particles through ATLAS was simulated with FLUKA, which provides accurate simulation of all relevant physics processes. Besides full simulation of hadronic and electromagnetic showers, FLUKA provides detailed transport of muons through matter with complete modelling of all energy loss processes and explicit production of secondary particles in radiative events. Compared to the full ATLAS simulation [33] based on GEANT 4 [34], the disadvantage of choosing FLUKA is that an exact modelling of the detector response is not available. In particular, digitisation and reconstruction of e.g. tracks and jets cannot be performed in FLUKA simulations with a level of detail comparable to real data. Dedicated algorithms were incorporated in the FLUKA simulation in order to record quantities of interest, namely energy depositions and detector hits, on an event basis. The rates of fake jets and events with the BCM background trigger signature were estimated using custom reconstruction algorithms during the post-processing of the simulation output.

The geometry of the BCM detector was modelled, including both the sensitive detector and the services. The transport threshold in the ATLAS simulations was set to 100 keV, so that all particles able to generate hits in the BCM detector were included in the simulations. Neutrons were always transported to thermal energies and their capture by nuclei, with associated photon emission, was simulated.

Table 2: Radial and longitudinal extent of the ATLAS calorimeter regions and bin sizes (δr , δz) as implemented in the FLUKA geometry. An azimuthal binning of 36 bins of 10 degrees each is used in all calorimeter regions. The endcaps at the negative (‘-’) side of ATLAS are mirror images of the positive (‘+’) ones.

Calorimeter	r_{\min} [mm]	r_{\max} [mm]	z_{\min} [mm]	z_{\max} [mm]	δr [mm]	δz [mm]
Barrel LAr	1471	2009	-3172	3172	107.6	396.5
Barrel Tile	2285	3885	-6000	6000	160.0	400.0
Endcap1 (+)	475	2075	3670	6120	160.0	408.3
Endcap2 (+)	300	475	3670	4650	87.5	490.0

Due to the 20 MeV transport threshold the LHC simulations do not include particles down to 100 keV. This has no significant influence on the results, since particles starting from the interface plane will not reach the BCM directly: most of them are intercepted by the TAS. Those which pass through its small central aperture have to traverse the beam-pipe wall at a very shallow angle, which implies a high probability for an inelastic interaction. This was verified by checking that the BCM trigger rates as a function of the z -coordinate of the origin of the event, as obtained from the “fully 100 keV” simulation of events on the IP side of the interface plane, join smoothly with the rates from the “mixed 20 MeV & 100 keV” simulation of events beyond $z = 22.6$ m. In the simulations the threshold of a BCM module is accounted for by considering as a hit each charged particle with a kinetic energy above 250 keV, entering the sensitive area of a BCM module. This simplification is motivated by the fact that a particle deposits in the module at least the minimum-ionising equivalent or its total kinetic energy, whichever is smaller. The sensitivity of the results to the choice of threshold was evaluated by varying it between 100 keV and 1 MeV. The simulated BCM trigger rate was affected by only a few percent. The arrival time and the identifier of the module entered are used to reconstruct the BCM background triggers from the recorded data and simulation output. Each hit results in a dead time of the affected BCM module, the duration of which depends on the energy but is typically 10–20 ns. For simplicity only the first hit in each BCM module, in a ± 12.5 ns window around $t = 0$, is considered, both in the simulations and the data.

Since fake jets are mainly produced by radiative energy losses of high-energy muons, the computational effort was significantly reduced by selecting only muons from the sample with a 20 GeV threshold. The propagation and showering in ATLAS was simulated with a 100 keV transport threshold. The fake-jet rates are estimated by recording, event by event, the local energy depositions in the different calorimeter regions which are described in Table 2. After the simulation of each event, the energy depositions are analysed.

Since FLUKA is not part of the standard ATLAS simulation software, it does not benefit from the sophisticated ATLAS jet-reconstruction tools. Instead, a much simplified algorithm is used to assess the fake-jet rate in the simulations. A cluster is formed by summing the energy depositions in $3 \times 3 \times 3 = 27$ (r , ϕ , z)-bins, centred around the maximum deposition. In the barrel calorimeters this clustering produces jets with angular dimensions comparable to those of the ATLAS jet-reconstruction algorithm. Each deposition is used only once, starting with the highest in any bin. If the cluster energy is large enough to exceed the 10 GeV transverse-energy threshold, the cluster is counted as a fake jet. The position of the fake jet is determined from the energy-weighted average of the bins considered. Likewise the jet time is determined from the energy-weighted time of the individual depositions. Depositions at times larger than 50 ns are excluded in order to prevent small depositions with very large delay, e.g. from thermal neutron capture,

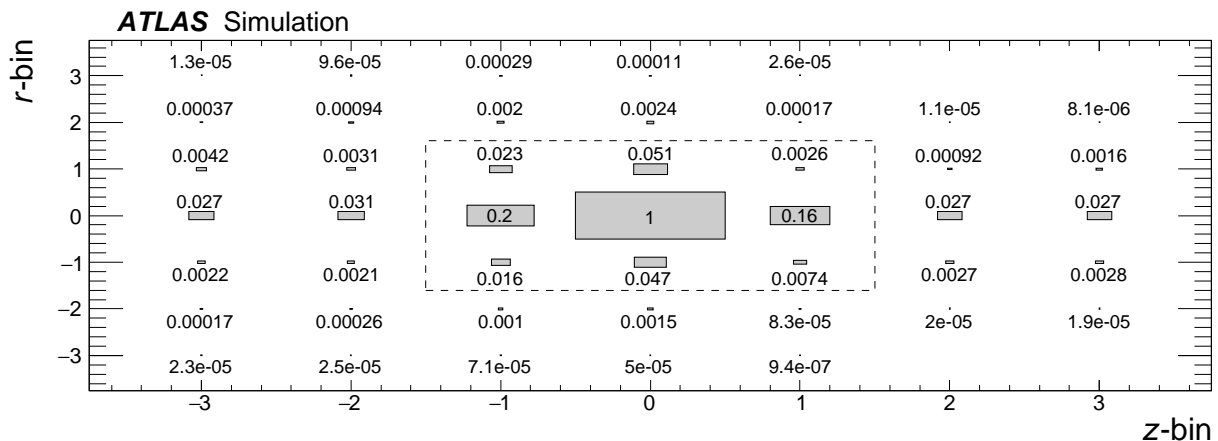


Figure 7: The r - z projection of the average fractional energy distribution, found in the FLUKA simulations for jets with $p_T > 16$ GeV in the barrel LAr calorimeter. The beam direction is from right to left in the plot. The values are summed over seven bins in azimuth, centred at the maximum, and normalised such that for each event the maximum bin is 1.0. Before averaging over all events, they are aligned such that the largest deposition is at the centre of the plot. The r and z bin numbers shown in the plot are relative to the centre. The dashed box indicates the 3×3 r - z bins used for determining the jet energy (summed over azimuthal bins).

to influence the average time. This procedure is fully consistent with the reconstruction of jet time in ATLAS data, which also takes into account only depositions in a narrow time window.

In order to assess the systematic uncertainty due to the energy spread, sums over more bins were explored and it was found that an extension of the sum in r and ϕ adds almost no energy to the cluster. In z , however, taking the sum over more bins results in a larger cluster energy. Figure 7 shows the r - z projection of the average energy fraction in the different bins around the maximum. The energy is well contained in the central 3×3 bins. The continuous energy loss of the passing muon, about 1 GeV per metre in the calorimeters, is reflected as a row of almost constant values for r -bin = 0 and $|z$ -bin > 1 in Figure 7. A wider summing range in z mostly adds this ionisation energy loss of the muon, which would be a non-negligible contribution to the lowest jet energies considered in this study. The average energy lost by the muon, however, is below the threshold of the ATLAS jet reconstruction, so in data only upward fluctuations of the muon energy loss are likely to be combined into the jet, if they happen close enough to the large radiative loss. Therefore an energy sum over $3 \times 3 \times 3$ bins is considered a good approximation to the reconstruction algorithm applied to the data.

6 Comparison with data

The principal objective of this work is to validate, through comparisons with data, the simulation methods described in Section 5. For this purpose, events collected with the BCM background and low- p_T jet triggers during 2012 are analysed. The vacuum simulations assume the beam conditions at the start of LHC fill 2736, which correspond to the parameters listed in Table 1 and are typical of the operation in the second half of 2012. Only fills with the same bunch pattern as in fill 2736 are considered in the analysis. Data affected by more than 20% trigger dead time are rejected and a dead-time correction is applied to the remaining data. In order to remove the effect of the beam intensity, which decreases in the course of a fill,

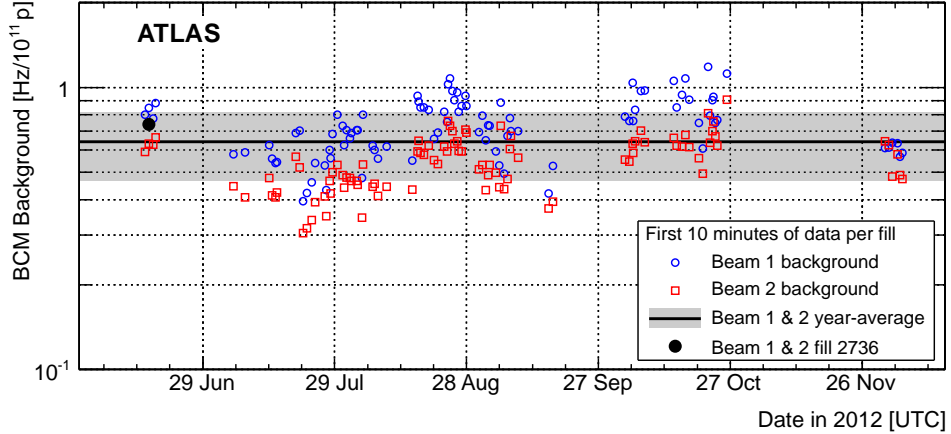


Figure 8: BCM background rate during the first ten minutes of data-taking in each fill with 1374 bunches. The average and standard deviation, resulting from the combined effect of fill-to-fill variation and difference between the beams, are shown by the black line and shaded area respectively. Data taken during a period with instrumental noise in the BCM, lasting through most of November, are excluded [16]. Only fills where data-taking started promptly after beams were brought into collision and which provided at least ten minutes of data are included. The solid black circle in mid June shows the average of beam-1 and beam-2 backgrounds in fill 2736, for which the pressure distribution has been simulated.

all results are normalised to 10^{11} protons. However, since the residual gas pressure follows the decrease of beam intensity over a LHC fill, fill-averaged beam–gas rates are lower than those at the start of a fill.

6.1 BCM background

In Figure 8 the BCM background rates during the first ten minutes of data-taking are shown for all LHC fills included in the analysis. The direction information provided by the BCM is used to reject events in the direction opposite to the unpaired bunches, which are used for the background measurement. Such wrong-direction signals can arise either from *ghost charge*⁴ in the opposite beam or from accidental background signatures involving hits from *afterglow* [16]. Although the data are selected such that they should correspond to the same beam conditions, a significant fill-to-fill variation and slightly increasing trend over the year can be seen. The BCM background from beam-1 is found to be systematically higher than from beam-2. The relative difference, averaged over all the data in Figure 8, is 28%. Since the simulations make no distinction between the two beams, they are compared with the average. Although, at $\pm 14\%$, the difference between the beams is small compared to the fill-to-fill variation, it is included in the variation in the data quoted in Table 3.

Table 3 compares the simulated BCM beam background rates with the start-of-fill and the fill-averaged data taken in 2012. The simulated rate of $1.2 \text{ Hz}/10^{11}$ protons is almost twice the measured start-of-fill value. Figure 8 shows separately the observed BCM background rate in fill 2736, for which the pressure simulations are performed. With a rate of $0.72 \text{ Hz}/10^{11}$ protons it falls close to the upper edge of the fill-to-fill variation and thus closer to the simulated value than the 2012 average shown in Table 3.

⁴ Ghost charge is formed by beam protons that have escaped their initial RF-bucket and been recaptured in nominally empty buckets.

Table 3: Simulated BCM background rates compared with ATLAS data. The rates correspond to events giving, in the BCM, a background signature that is consistent with the direction of the unpaired bunch. The simulations correspond to the start of data-taking, while the last two columns illustrate the difference in background between averaging over the first ten minutes of data-taking in each fill and averaging over entire fills. For the data, the uncertainty in the average corresponds to one standard deviation of the mean of all fills. For the simulations it indicates the statistical uncertainty. The fill-to-fill variation includes the difference between beam-1 and beam-2. The last row indicates the possible range of the simulated rate, due to the estimated uncertainty of the pressure simulation, discussed in Section 3.

	MC simulation [0–546.6] m	Data Fill Start	Data All Fill
Average rate [Hz/10 ¹¹ protons]	1.2	0.642	0.463
Uncertainty in average rate	0.4%	2.0%	2.3%
Fill-to-fill rate variation	—	27%	34%
Pressure uncertainty [Hz/10 ¹¹ protons]	0.4–3.6	—	—

In the inner triplet, p -H₂ scattering contributes about 90% of the beam–gas interactions, while the simulations are based on p -N₂ events. Equation (1) ensures that the correct number of beam–gas collisions is generated in the simulations, but it does not account for differences in the collision dynamics, especially the multiplicity of produced secondaries. In order to estimate the possible dependence of the background rate on the target nuclide, the less CPU-intensive simulations at $z < 22.6$ m were repeated with p -H₂ events. The rate was found to decrease by about 15%. Assuming a similar reduction for the inner-triplet region, where most of the BCM background originates from (see Section 7), the use of proton–N₂ events overestimates the BCM trigger rate by up to 15%.

Even after accounting for this correction, the observed difference between simulation and data is larger than the fill-to-fill variation, but remains well within the estimated uncertainty range of the simulation, which is dominated by knowledge of the pressure distribution.

In Figure 9 the distribution of particle arrival times at the BCM modules in the simulation is compared with data. The histograms represent the time distribution of hits in upstream BCM modules for events which give the BCM background signature in beam-1 unpaired bunches. The plain FLUKA simulations yield a very narrow time distribution with a vertical rising edge. In the analysis, this is smeared by the 0.25 ns time fluctuation due to the LHC bunch length of 75 mm.⁵ A larger broadening effect comes from the instrumental resolution and time alignment of the BCM. In order to account for these, the rising edge of the simulated time distribution is fitted to that in data with the time alignment and time resolution as free parameters. Values of -1.0 ns and 0.55 ns are found for these parameters respectively. The fit yields an uncertainty of about 10% in both parameters. The observed time shift is well within the 2 ns alignment tolerance specified for the BCM. The fitted time resolution is about 30% better than that found in test-beams [21]. However, it agrees, within its 10% uncertainty, with the resolution derived from in-situ monitoring of the time difference between hits in upstream and downstream modules in collision events recorded by the BCM detector.

The data shown in Figure 9 are extracted from the events recorded during the first ten minutes of each LHC fill. A determination of the fill-to-fill variation for each bin is not feasible since, especially in the tail

⁵ The centre of the bunch passes the IP at $t = 0$, but the background event can originate from any proton within the bunch.

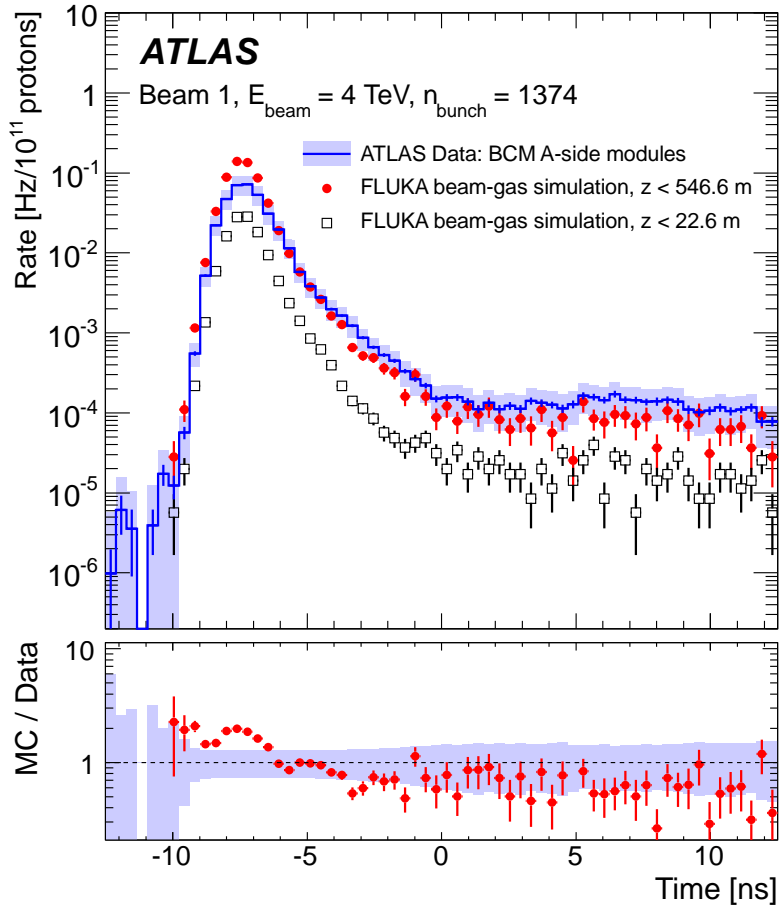


Figure 9: Comparison of the time distribution of BCM hits in ATLAS unpaired-bunch data (blue histogram) with FLUKA simulation (red circles). The bunch passes the IP at $t = 0$ ns. The histograms show the early hits per upstream BCM module for events which have fired the BCM beam-background trigger in the beam-1 direction. The black open squares show the contribution from beam-gas events within the ATLAS experimental area $z < 22.6$ m, while the red solid circles show the total, i.e. $z < 546.6$ m. The errors shown on the simulation are statistical only. The blue band indicates the fill-to-fill and module-to-module variation of the data and the error bars show the uncertainty in the mean value. The lower panel shows the ratio of simulation to data, taken between the red circles and the blue histogram. Only data from the first ten minutes of ATLAS data-taking in each LHC fill are considered.

region, the very low counting rate causes many bins to have zero counts for a single fill. If, however, the shape of the distribution is assumed to be invariant between fills, the fill-to-fill variation of each bin can be taken as 27%, which is the value given in Table 3 for the total rate. The blue band shown around the data in Figure 9 illustrates this fill-to-fill variation, but takes also into account the total counting statistics in each bin. The uncertainty in the mean value in each bin is determined from the data in all fills and shown by the smaller error bars on the data. For the simulations, only the statistical uncertainties are shown. The error bars on the ratio of simulation to data are based on the statistical uncertainties only. If the shape of the distribution is correctly reproduced by the simulation, the ratio should be a constant. However, since the simulations correspond to a particular fill, this constant can deviate from unity by the amount of the fill-to-fill variation. The allowed range (1σ), ignoring the uncertainty arising from the pressure distribution, is indicated by the blue band.

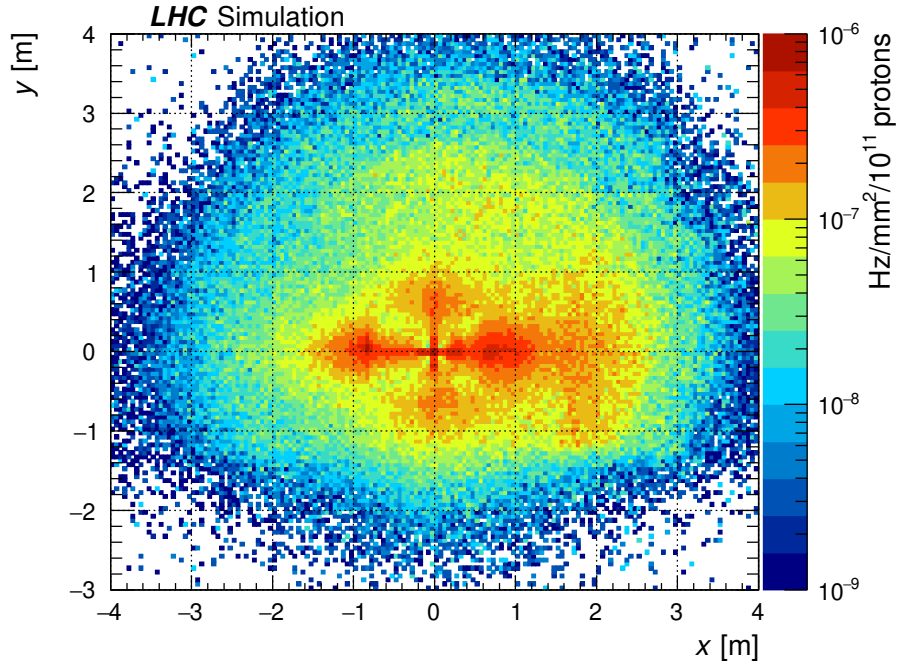


Figure 10: Simulated x - y distribution of muons with energy $E > 20$ GeV entering the ATLAS experimental area at $z = 22.6$ m. The beam passes at $(x, y) = (0, 0)$. The plot is based on Ref. [31] and constitutes the input to the study described in this paper. The rate corresponds to the pressure conditions at the start of fill 2736.

The ratio shown in Figure 9 indicates that the peak is overestimated by the simulations, while the tail at positive times is underestimated, i.e. the peak-to-tail ratio is larger in the simulations than in data and, consequently, the falling slope is slightly steeper. The open squares in Figure 9 show that the events within the ATLAS experimental area contribute only 20% to the total hit rate but the shape, especially the peak-to-tail ratio, is similar to that of the total rate. If the tail were due to delayed arrival of some particles from distant events, i.e. due to a dependence between time spread and distance to the event, then it should not appear for the beam-gas events at $z < 22.6$ m. The fact that a tail of similar height, relative to the peak, is seen in both distributions indicates that the delayed particles are due to a local effect. The simulated hits in the tail are found to be caused by particles with a kinetic energy below ~ 10 MeV and if the solenoidal field is turned off in the simulations, the tail is suppressed. These findings indicate that the tail is due to low-energy particles looping in the magnetic field and accumulating a delay due to the longer path along the helix. Since such low-energy particles have a short range in matter already a slightly too large amount of material in the simulation geometry, with respect to reality, is sufficient to explain the observed underestimation.

6.2 Fake-jet background

Most of the fake jets are produced by radiative energy losses of high-energy muons in the calorimeters. Such fake jets have a very different topology from collision jets: they do not point to the IP and are almost entirely of electromagnetic nature with very little hadronic activity. Therefore the simulation results are compared with jet data calibrated to the electromagnetic energy scale rather than with fully calibrated

Table 4: Simulated fake-jet rates compared with ATLAS data. Only jets with $p_T > 16 \text{ GeV}$ and $|\eta| < 1.5$ are considered. The simulations correspond to the start of data-taking, while the last two columns illustrate the difference in background between averaging over the first ten minutes of data-taking in each fill and averaging over entire fills. For the data, the uncertainty in the average corresponds to one standard deviation of the mean of all fills. For the simulations it indicates the statistical uncertainty. The fill-to-fill variation includes the difference between beam-1 and beam-2. The last row indicates the possible range of the simulated rate, due to the estimated uncertainty of the pressure simulation, discussed in Section 3.

	MC simulation [0–546.6] m	Data Fill Start	Data All Fill
Average rate [Hz/10 ¹¹ protons]	0.0053	0.0046	0.0037
Uncertainty in average rate	1.0%	3.4%	2.2%
Fill-to-fill rate variation	—	56%	39%
Pressure uncertainty [Hz/10 ¹¹ protons]	0.002–0.015	—	—

jets, which are corrected for the non-compensating response of the calorimeter to hadrons. Possible jets from collisions of the protons in the unpaired bunch with ghost charge in the other beam are removed by rejecting events for which a primary vertex has been reconstructed from the tracks measured by the inner detector. Only the highest- p_T jet in each event is included in the analysis. In the endcap calorimeters, hadronic showers can contribute to the fake jets. Since only muons are considered in the simulations, the analysis is restricted to $|\eta| < 1.5$, i.e. the barrel calorimeters. These are at large radii and shadowed by other detector elements so hadronic showers from the beam line cannot reach them.

Figure 10 shows the x - y distribution of muons with energy $E > 20 \text{ GeV}$ reaching the interface plane. This distribution reflects the geometry of the LHC tunnel, and also the effect of some beam-line magnets. The tunnel’s radius of 2.2 m and the floor at $y = -1.1 \text{ m}$ produce a relatively sharp edge in the muon flux. The higher rate seen on the inside of the ring at $y \approx \pm 1 \text{ m}$, between $x \approx 1.5 \text{ m}$ and $x \approx 2.5 \text{ m}$, is due to the offset of the beam line relative to the centre of the tunnel, leaving more free space for pions and kaons to decay into muons on the inside of the ring. The “hot spots” seen around $x \approx \pm 0.8 \text{ m}$ are mainly due to bending of the off-momentum muons by the D1 and D2 dipoles of the LSS. The vertical spread at $x = 0$ is probably due to bending in the quadrupoles of the inner triplet, although the crossing angle might also have some influence on this.

In Table 4 the rates of simulated fake jets, created by the muons shown in Figure 10, are compared with the data from all relevant fills in 2012. Systematic uncertainties may arise from the jet reconstruction used in the simulations. The studies described in Section 5 show that increasing the extent over which the jet energy is integrated in the simulations from $3 \times 3 \times 3$ bins to a very wide $7 \times 7 \times 7$ bins increases the jet rate by 20%. However, since this increase is due to including the ionisation energy loss of the passing muon, it does not seem justified to consider it as a systematic uncertainty, but rather an upper limit thereof. Thus the uncertainty from the jet reconstruction algorithm is considered negligible compared with the uncertainty from the pressure distribution. The latter is estimated to be a factor of three, which means that the high level of agreement between simulations and data, seen in Table 4, must be largely fortuitous.

The offset in arrival time, at given z , between the proton bunch and a beam background muon originating from that bunch, is negligible. Therefore, when the beam background muon reaches an upstream point $P(r, z)$ in the calorimeter, the proton bunch still has to cover a distance $|z|$ to reach the IP and then the produced secondary particles have to travel a distance $s = \sqrt{r^2 + z^2}$ to reach P , as illustrated in Figure 11.

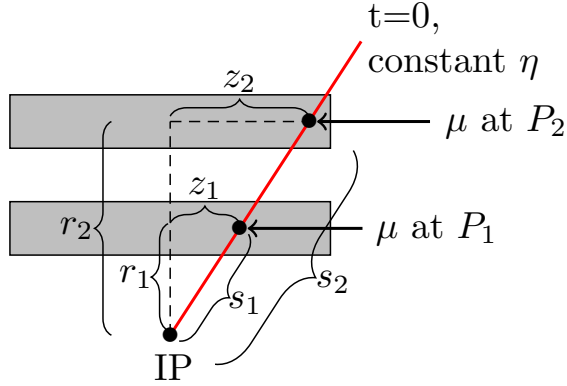


Figure 11: Schematic illustration of reconstructed arrival time of beam background muons compared with collision jets in the calorimeter regions. The two grey boxes represent two different calorimeters and the red solid line represents $t = 0$, corrected for the time of flight of particles coming from the IP.

For a downstream P the expression for s is the same, but in this case the muon has to cover the additional distance $|z|$. The calorimeter timing is such that for each point P the arrival time of a secondary particle produced in collisions at the IP is 0. Thus the relative time Δt of a beam background muon at P is given by

$$\Delta t = -\left(\sqrt{r^2 + z^2} \pm |z|\right)/c \quad (2)$$

where c is the speed of light and $+|z|$ and $-|z|$ correspond to the upstream and downstream sides respectively. Equation (2) shows that fake jets due to BIB always arrive early, i.e. have $\Delta t < 0$. A characteristic *banana* shape is seen in the η - Δt plane, shown in Figure 12; this arises from the definition of η and the dependence of jet time on z and r .

The number of fake-jet counts in the data is low. To maximise the amount of data when studying distributions of fake jets, in the following plots data from entire fills are used while the simulations correspond to the higher rate at the start of a fill. In order to compensate for this, the MC results have been scaled by the ratio of "All Fill" to "Fill Start" values given in Table 4.

Figure 12 compares the distribution in the η - Δt plane of fake jets seen in ATLAS data with the simulated rate of energy deposition clusters having $p_T > 16$ GeV. The pedestal, i.e. entries outside the banana area, seen in Figure 12(a) is mostly due to beam-gas and off-momentum halo background from ghost charge [16], a contribution that is not included in the simulations.⁶ A time-smearing due to the LHC bunch length has been applied to the simulated jet times. The instrumental time resolution of the calorimeters depends on η and the calorimeter cell energy. For Figure 12(b) the instrumental resolution was determined by fitting the width of the downstream tail of the banana shape in simulation, between $\eta = -3$ and $\eta = -2$, to the data. The fitted value of 0.5 ns is consistent with the range of resolutions measured for the ATLAS calorimeters. The dashed horizontal lines indicate the jet-trigger time window of ± 12.5 ns. Entries falling outside these lines are not seen in data, unless the event was selected by another trigger or has a sufficiently energetic subleading jet within the trigger window. The position and curvature of the banana pattern within the trigger window is well reproduced by the simulations, which indicates that the jet times are correctly simulated.

⁶ The data in the η - Δt plot are restricted to LHC fills prior to 3rd August when the LHC made chromaticity changes which caused a significant increase of ghost charge [16].

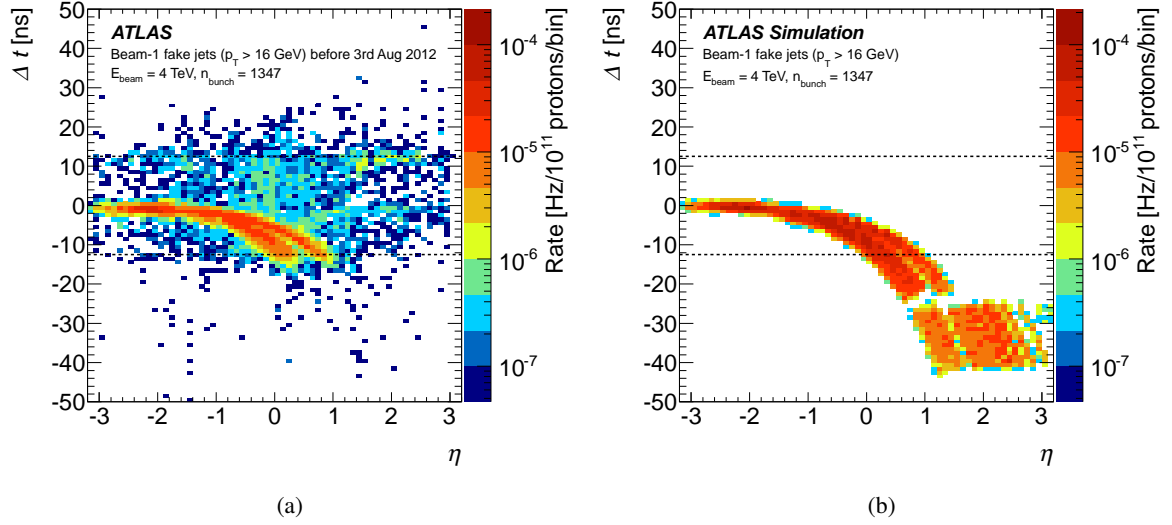


Figure 12: (a) Fake-jet counts in unpaired bunches in the pseudorapidity–time (η – Δt) plane for beam-1 in ATLAS data and (b) the simulated rate of energy deposition clusters with $p_T > 16$ GeV in the η – Δt plane. The width of the bins is 1 ns in time and 0.1 units in η . The FLUKA simulations, which correspond to the start-of-fill conditions, have been scaled by the ratio of the total "All Fill" to "Fill Start" rates, shown in Table 3.

The curvature of the banana shape depends on the radial position in the calorimeter: as indicated by Eq. (2) and Figure 11, fake jets at P_2 will have a larger time advance than those at P_1 due to the difference in radial position. In Figure 12, two banana shapes with slightly different curvature can be distinguished. The upper and lower tails correspond to fake jets in the LAr and Tile calorimeters respectively. At higher $|\eta|$ on the downstream side the bananas merge and the fake-jet times approach $\Delta t = 0$, although a small negative offset remains due to the dependence on r in Eq. (2). Very early fake jets, with $\Delta t < -20$ ns, are seen in the simulations. These are all in the upstream part of the barrel Tile calorimeter or the upstream endcaps. Falling outside the trigger window, they are not seen in the data. However, a minor concentration of jets at $\eta \approx 2$ and $\Delta t \approx 10$ ns can be distinguished in Figure 12(a). It is caused by upstream fake jets associated with the following bunch, which arrives 50 ns later. These jets are reproduced by the simulations and are seen at the same η but at $\Delta t \approx -40$ ns in Figure 12(b).

Figure 13 compares transverse-momentum and azimuthal-angle distributions of the simulated fake jets with data. For these comparisons, jets within the banana area are extracted from data in order to minimise the contribution from the pedestal. As in the case of Figure 9, the low count rates prevent an estimation of the fill-to-fill variation in individual bins. The same approach as described for Figure 9 is adopted, i.e. the blue band shows the fill-to-fill variation determined from the total rates and the small error bars show the uncertainty in the mean value in each bin.

The transverse-momentum distribution of the simulated fake jets, shown in Figure 13(a), continues on a rising slope below ~ 15 GeV, while the data dip down. This is due to the jet trigger, used to select the data, which reaches full efficiency only above ~ 15 GeV. When full trigger efficiency is reached, the simulations agree well with the data up to $p_T \approx 50$ GeV, but towards higher transverse momenta the simulation tends to overestimate the data.

In Figure 13(b) an additional requirement of $p_T > 16$ GeV is applied in order to select events above the trigger efficiency turn-on. The azimuthal distribution of fake jets from BIB is well reproduced at a

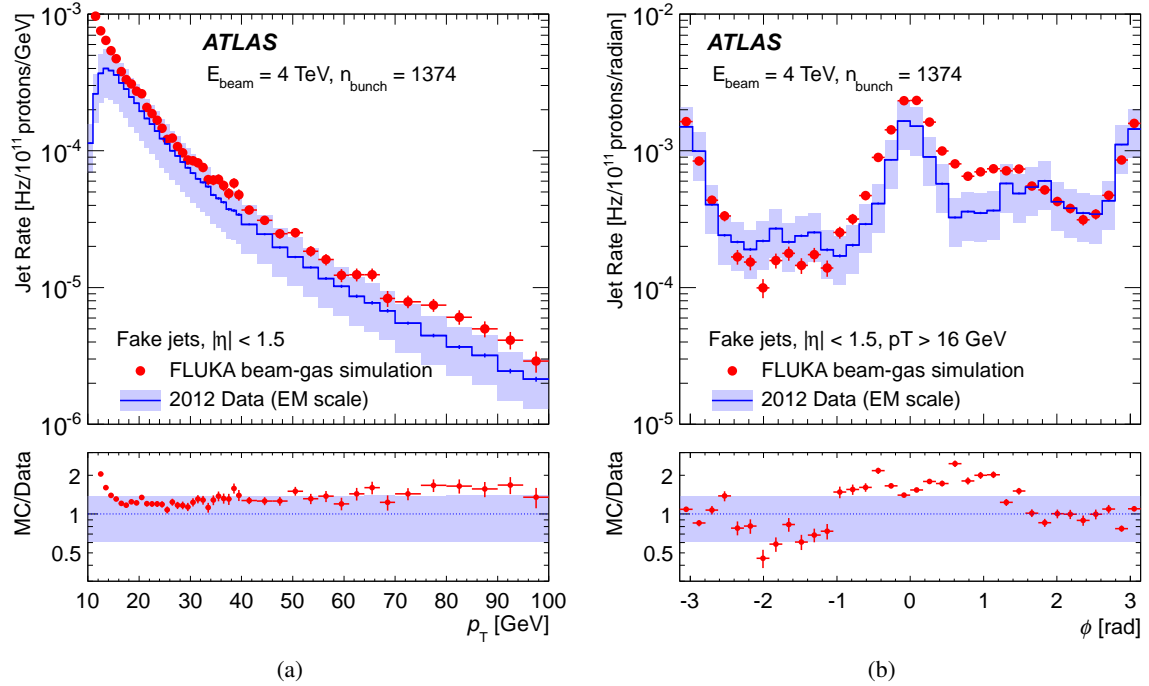


Figure 13: Distributions of (a) transverse momentum p_T and (b) azimuthal angle ϕ of fake jets with pseudorapidity $|\eta| < 1.5$ in data (blue histogram) compared with those of energy deposition clusters from FLUKA beam–gas simulations in the same η range (red circles). The p_T spectrum indicates that the ATLAS jet trigger reaches full efficiency only around 15 GeV. Therefore an additional requirement of $p_T > 16$ GeV is applied to events in the azimuthal-angle distribution. The errors shown on the simulation results are statistical only. The blue band indicates the fill-to-fill variation of the data, while the small blue error bars show the uncertainty in the mean of all fills. Data from entire fills have been used in order to minimise statistical uncertainties. The simulations, which correspond to the start-of-fill conditions have been scaled by the ratio of the total "All Fill" to "Fill Start" rates, shown in Table 3.

qualitative level. The characteristic peaks at $\pm\pi$ and 0 are mainly due to the bending in the horizontal plane that occurs in the D1 and D2 dipoles and the LHC arc [15]. The lower rate at $-\pi/2$ compared to $\pi/2$ is due to the tunnel floor reducing the muon flux, as seen from the contours in Figure 10. A tendency of the simulation to overestimate the data between $\phi = -1$ and $\phi = \pi/2$ and to underestimate around $\phi = -\pi/2$ is seen. A comparison with Figure 10 suggests that these effects might be related to the tunnel geometry: the simulations underestimate at $-y$, where the tunnel floor reduces the free drift space for pion and kaon decay, and overestimate around $+x$ where the horizontal offset provides extra space. Such differences could arise, for instance, if the z -distribution of the beam–gas events is not correct. A wrong z -distribution could change the impact of the reduced, or increased, free drift space. Another possibility is an inaccurate description of material around the beam line, which would affect the free drift space available. Forthcoming background measurements, with artificially introduced local pressure bumps, may shed some light on this. Cosmic-ray muons, which can also produce fake jets, are included in the data but not in the simulation. Studies reported in Ref. [16] indicate that the fake-jet rate at low p_T arising from cosmic-ray muons is less than 10% of the total rate due to BIB. The radiative energy losses are point-like processes and since the flux of cosmic muons is uniform in space and time, the rate of fake jets produced by them should be independent of ϕ . However, due to the significant variation of the rate as a function of ϕ , a visible contribution from cosmic-ray induced fake jets cannot be entirely excluded around $\phi = -\pi/2$,

where the rates are lowest.

Although the differences in the shapes of the distributions shown in Figure 13 are not understood, the agreement can be considered good, given the complexity of the entire simulation chain. The large systematic uncertainty due to limited knowledge of the residual gas pressure distribution is the most likely cause of the differences seen, although more detailed studies with localised and well-controlled pressure bumps will be needed to verify this.

7 Origin of backgrounds

Knowledge of the z -coordinate of the origin of each simulated event provides information beyond that which can be extracted from the data. Figure 14 shows the distribution of the origins of the simulated events that give a BCM background trigger signature or generate a fake jet in the barrel calorimeters. The black histogram, which shows the z -distribution of the generated events, reflects the residual gas distribution in the beam pipe and is equivalent to Figure 6. Most of the events with a BCM background trigger signature originate from the inner-triplet region ($z \approx 22\text{--}55$ m) with a small contribution from $z \approx 150$ m, where the tertiary collimator causes a local pressure bump. This result is consistent with the observations made in the data, that the BCM background trigger rate correlates with the residual gas pressure measured by vacuum gauges at $z = 22$ m [16]. The fake jets, on the contrary, originate predominantly from more distant beam losses with pronounced spikes at the locations of the 4.5 K magnets. According to the simulations, about 10% of fake-jet events are associated with beam–gas events in the LHC arc ($z > 270$ m), but this fraction depends strongly on the relative pressure in 4.5 K and 1.9 K sections. The lower plot in Figure 14 shows the cumulative distributions corresponding to the histograms in the upper plot. These highlight that practically all BCM background events originate from $z < 60$ m while only $\sim 1\%$ of fake-jet events are associated with beam–gas collisions in that z -range. Since the simulations disfavour any significant correlation between BCM background and fake jets in the barrel calorimeters, they suggest that BCM and fake-jet rates, seen in the data, can be used to disentangle backgrounds originating from different regions in z . As discussed before, the residual gas pressure depends on local properties of the beam pipe, such as material and temperature, and also on the radiation intensity. Therefore the pressure in different z -regions, as well as its uncertainties, can be considered to be uncorrelated. In particular, the prediction of BCM background, which originates predominantly from the inner triplet, depends on the accuracy of the pressure simulations within 1.9 K magnets. Most of the fake jets originate from the beam–gas events within 4.5 K magnets where the desorption characteristics and, therefore, the gas composition, are different. Thus it is not surprising to find, in Tables 3 and 4, better agreement in one observable than in the other.

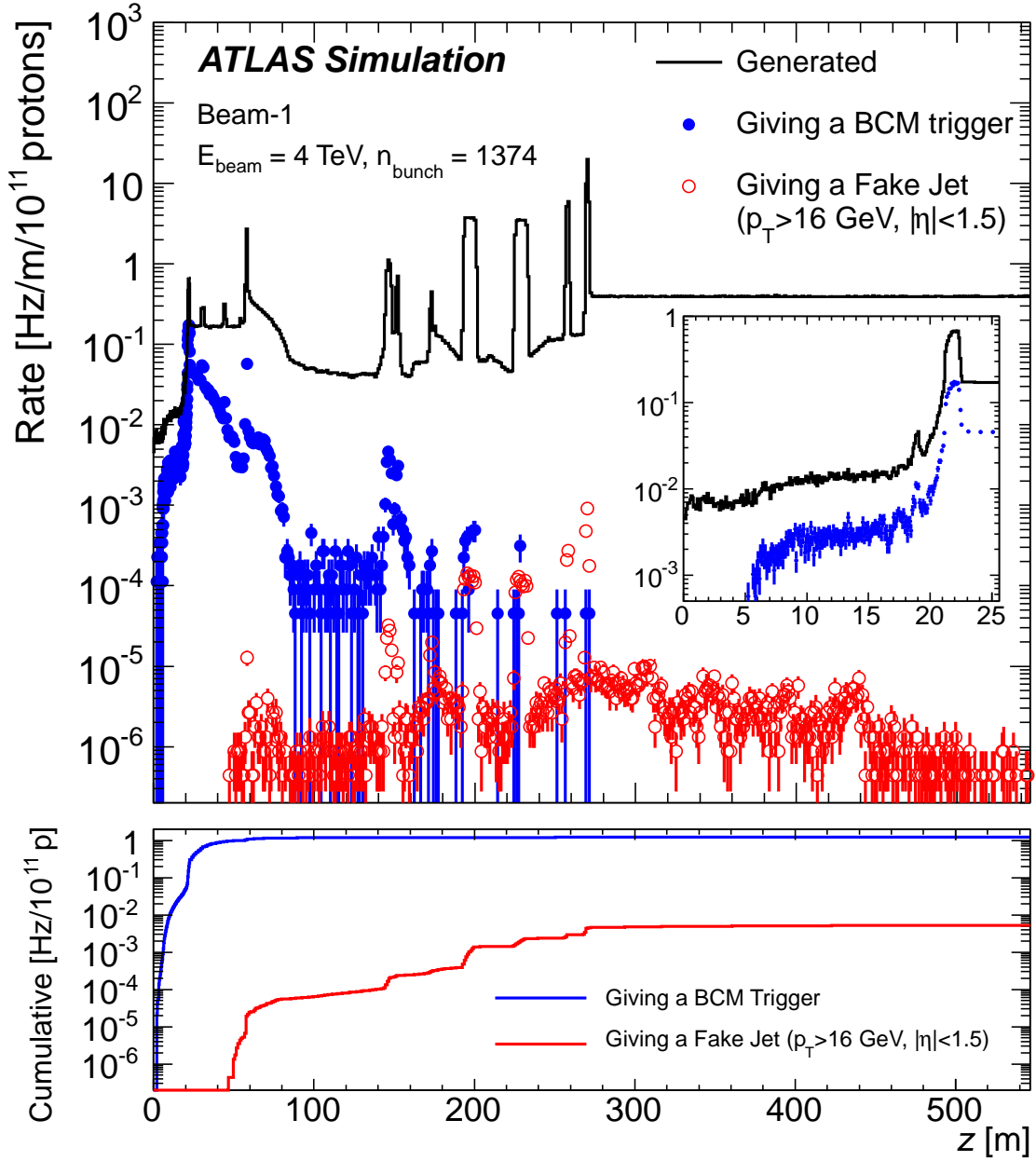


Figure 14: Distributions of the z -coordinate of the origin of simulated beam–gas events giving a BIB signature in ATLAS detectors. The solid blue circles show the z -distribution of events that give a BCM beam background signature while the open red circles show the z -distribution of beam–gas events that result in energy deposition clusters with $p_T > 16 \text{ GeV}$ and $|\eta| < 1.5$ in the calorimeters. The z -distribution of the generated events (black line) corresponds to the beam–gas rate shown in Figure 6, i.e. reflects the residual gas distribution in the beam pipe. The small inset shows the region $z < 25 \text{ m}$ in more detail. The lower plot shows the cumulative rate, as a function of z , of events resulting in BCM background events or fake jets. At large z these two histograms converge to the total simulated rates given in Tables 3 and 4 respectively.

8 Conclusion

Beam-induced background measurements in ATLAS during the 2012 LHC run with 4 TeV proton beams are compared with dedicated FLUKA Monte Carlo simulations of the background due to inelastic beam–gas interactions. Methods of extracting fake jets and BCM trigger signatures from a FLUKA simulation were developed and applied during simulations and the post-processing of the results, i.e. reconstruction of the background signatures. The simulations, performed using a two-step method, agree within a factor of two with the rate of background trigger signatures in the BCM detector and the fake-jet rates observed in the ATLAS data. This is well within the uncertainty in the residual gas pressure in the beam pipe.

Simulations reproduce rather well the shape of the time distribution of hits in the BCM as well as that of the fake jets in the pseudorapidity–time plane. The simulated spectrum of energy depositions in the calorimeters agrees with the spectrum of reconstructed transverse momenta of the observed fake jets although there is an indication of an overestimate towards higher p_T . In the azimuthal distribution of the fake jets, the characteristic peaks in the horizontal plane are reproduced by the simulations, but differences are seen in some details of the structure in azimuthal angle. These might be related either to inaccuracies in the pressure distribution or incomplete modelling of material close to the beam line.

The simulations indicate that background seen by the BCM originates mainly from the inner triplet region ($z < 55$ m) while the majority of fake jets induced by beam–gas interactions have an origin at a distance of $z \gtrsim 150$ m from the interaction point.

The level of agreement between the simulations and measurement demonstrates the good understanding of beam background that has been reached in the ATLAS experiment. It also illustrates the capability of the various simulation tools to reproduce the beam background through a complex chain involving simulation of the residual gas pressure distribution, taking into account various dynamic effects from the beam, transport of the beam–gas secondaries over long distances in the LHC magnet lattice and through the ATLAS detector, and finally the modelling of the reconstructed background signatures in ATLAS.

Acknowledgements

We thank CERN for the very successful operation of the LHC, as well as the support staff from our institutions without whom ATLAS could not be operated efficiently. The residual pressure map used in this study is courtesy of C. Yin Vallgren.

We acknowledge the support of ANPCyT, Argentina; YerPhI, Armenia; ARC, Australia; BMWFW and FWF, Austria; ANAS, Azerbaijan; SSTC, Belarus; CNPq and FAPESP, Brazil; NSERC, NRC and CFI, Canada; CERN; CONICYT, Chile; CAS, MOST and NSFC, China; COLCIENCIAS, Colombia; MSMT CR, MPO CR and VSC CR, Czech Republic; DNRF and DNSRC, Denmark; IN2P3-CNRS, CEA-DRF/IRFU, France; SRNSFG, Georgia; BMBF, HGF, and MPG, Germany; GSRT, Greece; RGC, Hong Kong SAR, China; ISF and Benozio Center, Israel; INFN, Italy; MEXT and JSPS, Japan; CNRST, Morocco; NWO, Netherlands; RCN, Norway; MNiSW and NCN, Poland; FCT, Portugal; MNE/IFA, Romania; MES of Russia and NRC KI, Russian Federation; JINR; MESTD, Serbia; MSSR, Slovakia; ARRS and MIZŠ, Slovenia; DST/NRF, South Africa; MINECO, Spain; SRC and Wallenberg Foundation, Sweden; SERI, SNSF and Cantons of Bern and Geneva, Switzerland; MOST, Taiwan; TAEK, Turkey; STFC, United Kingdom; DOE and NSF, United States of America. In addition, individual groups and members have received support from BCKDF, CANARIE, CRC and Compute Canada, Canada; COST,

ERC, ERDF, Horizon 2020, and Marie Skłodowska-Curie Actions, European Union; Investissements d’Avenir Labex and Idex, ANR, France; DFG and AvH Foundation, Germany; Herakleitos, Thales and Aristeia programmes co-financed by EU-ESF and the Greek NSRF, Greece; BSF-NSF and GIF, Israel; CERCA Programme Generalitat de Catalunya, Spain; The Royal Society and Leverhulme Trust, United Kingdom.

The crucial computing support from all WLCG partners is acknowledged gratefully, in particular from CERN, the ATLAS Tier-1 facilities at TRIUMF (Canada), NDGF (Denmark, Norway, Sweden), CC-IN2P3 (France), KIT/GridKA (Germany), INFN-CNAF (Italy), NL-T1 (Netherlands), PIC (Spain), ASGC (Taiwan), RAL (UK) and BNL (USA), the Tier-2 facilities worldwide and large non-WLCG resource providers. Major contributors of computing resources are listed in Ref. [35].

References

- [1] ATLAS Collaboration, *The ATLAS Experiment at the CERN Large Hadron Collider*, *JINST* **3** (2008) S08003.
- [2] J. M. Thompson, *Operational Experience with the CMS Pixel Detector*, *Nucl. Phys. B Proc. Suppl.* **215** (2011) 133.
- [3] ATLAS Collaboration, *Search for new phenomena with the monojet and missing transverse momentum signature using the ATLAS detector in $\sqrt{s} = 7$ TeV proton–proton collisions*, *Phys. Lett. B* **705** (2011) 294, arXiv: 1106.5327 [hep-ex].
- [4] ATLAS Collaboration, *Search for long-lived stopped R-hadrons decaying out of time with pp collisions using the ATLAS detector*, *Phys. Rev. D* **88** (2013) 112003, arXiv: 1310.6584 [hep-ex].
- [5] ATLAS Collaboration, *Search for pair-produced long-lived neutral particles decaying to jets in the ATLAS hadronic calorimeter in pp collisions at $\sqrt{s} = 8$ TeV*, *Phys. Lett. B* **743** (2015) 15, arXiv: 1501.04020 [hep-ex].
- [6] ATLAS Collaboration, *Search for dark matter and other new phenomena in events with an energetic jet and large missing transverse momentum using the ATLAS detector*, *JHEP* **01** (2018) 126, arXiv: 1711.03301 [hep-ex].
- [7] R. J. Tesarek, *Beam induced backgrounds: CDF experience*, FERMILAB-CONF-08-131-AD-E, 2008, URL: http://lss.fnal.gov/cgi-bin/find_paper.pl?conf-08-131.
- [8] V. Andreev et al., *Technical Report on the Beam Induced Backgrounds in the H1 Detector*, H1 note H1-10/02-606, 2002, URL: <http://www-h1.desy.de/publications/bgrep.pdf>.
- [9] R. Alemany-Fernández et al., *LHC Workshop on Experimental Conditions and Beam-Induced Detector Backgrounds*, CERN-2009-003, 2009, URL: <http://cdsweb.cern.ch/record/1184436>.
- [10] A. I. Drozhdin, M. Huhtinen and N. V. Mokhov, *Accelerator related background in the CMS detector at LHC*, *Nucl. Instr. and Meth. A* **381** (1996) 531.
- [11] A. I. Drozhdin, N. V. Mokhov and S. I. Striganov, *Beam Losses and Background Loads on Collider Detectors due to Beam-Gas Interactions in the LHC*, FERMILAB-CONF-09-172-APC, 2009, URL: http://lss.fnal.gov/cgi-bin/find_paper.pl?conf-09-172.
- [12] N. V. Mokhov and T. Weiler, *Machine-Induced Backgrounds: their Origin and Loads on ATLAS/CMS*, FERMILAB-CONF-08-147-APC, 2008, URL: http://lss.fnal.gov/cgi-bin/find_paper.pl?conf-08-147.
- [13] R. B. Appleby et al., *Simulation of Machine Induced Background in the LHCb Experiment: Methodology and Implementation*, *IEEE Trans. Nucl. Sci.* **59** (2012) 1681.
- [14] R. Bruce et al., *Sources of machine-induced background in the ATLAS and CMS detectors at the CERN Large Hadron Collider*, *Nucl. Instr. and Meth. A* **729** (2013) 825.
- [15] ATLAS Collaboration, *Characterisation and mitigation of beam-induced backgrounds observed in the ATLAS detector during the 2011 proton–proton run*, *JINST* **8** (2013) P07004, arXiv: 1303.0223 [hep-ex].

- [16] ATLAS Collaboration, *Beam-induced and cosmic-ray backgrounds observed in the ATLAS detector during the LHC 2012 proton–proton running period*, *JINST* **11** (2016) P05013, arXiv: [1603.09202](https://arxiv.org/abs/1603.09202) [[hep-ex](#)].
- [17] T. T. Böhlen et al., *The FLUKA Code: Developments and Challenges for High Energy and Medical Applications*, *Nucl. Data Sheets* **120** (2014) 211.
- [18] A. Ferrari, P. R. Sala, A. Fassò and J. Ranft, *FLUKA: A multi-particle transport code*, CERN-2005-010, 2005, URL: <https://cds.cern.ch/record/898301>.
- [19] O. S. Brüning et al., *LHC Design Report*, CERN-2004-003, 2004, URL: <https://cds.cern.ch/record/782076>.
- [20] R. Bruce et al., *Reaching record-low β^* at the CERN Large Hadron Collider using a novel scheme of collimator settings and optics*, *Nucl. Instr. and Meth A* **848** (2017) 19.
- [21] V. Cindro et al., *The ATLAS beam conditions monitor*, *JINST* **3** (2008) P02004.
- [22] ATLAS Collaboration, *ATLAS inner detector: Technical Design Report, 1*, CERN-LHCC-97-016, 1997, URL: <https://cds.cern.ch/record/331063>.
- [23] R. Bruce et al., *Simulations and measurements of beam loss patterns at the CERN Large Hadron Collider*, *Phys. Rev. ST Accel. Beams* **17** (2014) 081004.
- [24] ATLAS Collaboration, *Beam backgrounds in the ATLAS detector during LHC loss map tests at $\beta^* = 40$ cm and $\beta^* = 80$ cm at $E_{\text{beam}} = 6.5$ TeV*, ATL-DAPR-PUB-2017-001, 2017, URL: <https://cds.cern.ch/record/2286836>.
- [25] C. Benvenuti, P Chiggiato, F Cicora and V Ruzinov, *Decreasing surface outgassing by thin film getter coatings*, *Vacuum* **50** (1998) 57, URL: <https://cds.cern.ch/record/364588>.
- [26] G. Bregliozzi, G. Lanza, V. Baglin and J. M. Jimenez, *Vacuum stability and residual gas density estimation for the vacuum chamber upgrade of the ATLAS interaction region of the Large Hadron Collider*, *Vacuum* **86** (2012) 1682, (We would like to thank R. Kersevan for helpful discussions on the residual gas composition).
- [27] M. Cacciari, G. P. Salam and G. Soyez, *The anti- k_t jet clustering algorithm*, *JHEP* **04** (2008) 063, arXiv: [0802.1189](https://arxiv.org/abs/0802.1189) [[hep-ph](#)].
- [28] M. Cacciari, G. P. Salam and G. Soyez, *FastJet user manual*, *Eur. Phys. J. C* **72** (2012) 1896, arXiv: [1111.6097](https://arxiv.org/abs/1111.6097) [[hep-ph](#)].
- [29] ATLAS Collaboration, *Jet energy measurement and its systematic uncertainty in proton–proton collisions at $\sqrt{s} = 7$ TeV with the ATLAS detector*, *Eur. Phys. J. C* **75** (2015) 17, arXiv: [1406.0076](https://arxiv.org/abs/1406.0076) [[hep-ex](#)].
- [30] ATLAS Collaboration, *Monitoring and data quality assessment of the ATLAS liquid argon calorimeter*, *JINST* **9** (2014) P07024, arXiv: [1405.3768](https://arxiv.org/abs/1405.3768) [[hep-ex](#)].
- [31] R. Kwee-Hinzmann et al., *Machine-induced Background Simulation Studies for LHC Run 1, Run 2 and HL-LHC*, CERN-ACC-2017-0025, 2017, URL: <https://cds.cern.ch/record/2261862>.

- [32] S. Baranov et al., *Estimation of Radiation Background, Impact on Detectors, Activation and Shielding Optimization in ATLAS*, ATL-GEN-2005-001, 2005,
URL: <https://cds.cern.ch/record/814823>.
- [33] ATLAS Collaboration, *The ATLAS Simulation Infrastructure*, *Eur. Phys. J. C* **70** (2010) 823,
arXiv: [1005.4568](https://arxiv.org/abs/1005.4568) [[physics.ins-det](https://arxiv.org/archive/physics)].
- [34] S. Agostinelli et al., *GEANT4 – a Simulation toolkit*, *Nucl. Instr. and Meth. A* **506** (2003) 250.
- [35] ATLAS Collaboration, *ATLAS Computing Acknowledgements*, ATL-GEN-PUB-2016-002,
URL: <https://cds.cern.ch/record/2202407>.

The ATLAS Collaboration

M. Aaboud^{34d}, G. Aad⁹⁹, B. Abbott¹²⁴, O. Abdinov^{13,*}, B. Abeloos¹²⁸, S.H. Abidi¹⁶⁵, O.S. AbouZeid¹⁴³, N.L. Abraham¹⁵³, H. Abramowicz¹⁵⁹, H. Abreu¹⁵⁸, Y. Abulaiti⁶, B.S. Acharya^{64a,64b,p}, S. Adachi¹⁶¹, L. Adamczyk^{81a}, J. Adelman¹¹⁹, M. Adersberger¹¹², A. Adiguzel^{12c,aj}, T. Adye¹⁴¹, A.A. Affolder¹⁴³, Y. Afik¹⁵⁸, C. Agheorghiesei^{27c}, J.A. Aguilar-Saavedra^{136f,136a}, F. Ahmadov^{77,ah}, G. Aielli^{71a,71b}, S. Akatsuka⁸³, T.P.A. Åkesson⁹⁴, E. Akilli⁵², A.V. Akimov¹⁰⁸, G.L. Alberghi^{23b,23a}, J. Albert¹⁷⁴, P. Albicocco⁴⁹, M.J. Alconada Verzini⁸⁶, S. Alderweireldt¹¹⁷, M. Aleksa³⁵, I.N. Aleksandrov⁷⁷, C. Alexa^{27b}, G. Alexander¹⁵⁹, T. Alexopoulos¹⁰, M. Alhroob¹²⁴, B. Ali¹³⁸, G. Alimonti^{66a}, J. Alison³⁶, S.P. Alkire¹⁴⁵, C. Allaire¹²⁸, B.M.M. Allbrooke¹⁵³, B.W. Allen¹²⁷, P.P. Allport²¹, A. Aloisio^{67a,67b}, A. Alonso³⁹, F. Alonso⁸⁶, C. Alpigiani¹⁴⁵, A.A. Alshehri⁵⁵, M.I. Alstary⁹⁹, B. Alvarez Gonzalez³⁵, D. Álvarez Piqueras¹⁷², M.G. Alvigi^{67a,67b}, B.T. Amadio¹⁸, Y. Amaral Coutinho^{78b}, L. Ambroz¹³¹, C. Amelung²⁶, D. Amidei¹⁰³, S.P. Amor Dos Santos^{136a,136c}, S. Amoroso³⁵, C.S. Amrouche⁵², C. Anastopoulos¹⁴⁶, L.S. Ancu⁵², N. Andari²¹, T. Andeen¹¹, C.F. Anders^{59b}, J.K. Anders²⁰, K.J. Anderson³⁶, A. Andreazza^{66a,66b}, V. Andrei^{59a}, S. Angelidakis³⁷, I. Angelozzi¹¹⁸, A. Angerami³⁸, A.V. Anisenkov^{120b,120a}, A. Annovi^{69a}, C. Antel^{59a}, M.T. Anthony¹⁴⁶, M. Antonelli⁴⁹, D.J.A. Antrim¹⁶⁹, F. Anulli^{70a}, M. Aoki⁷⁹, L. Aperio Bella³⁵, G. Arabidze¹⁰⁴, Y. Arai⁷⁹, J.P. Araque^{136a}, V. Araujo Ferraz^{78b}, R. Araujo Pereira^{78b}, A.T.H. Arce⁴⁷, R.E. Ardell⁹¹, F.A. Arduh⁸⁶, J-F. Arguin¹⁰⁷, S. Argyropoulos⁷⁵, A.J. Armbruster³⁵, L.J. Armitage⁹⁰, O. Arnaez¹⁶⁵, H. Arnold¹¹⁸, M. Arratia³¹, O. Arslan²⁴, A. Artamonov^{109,*}, G. Artoni¹³¹, S. Artz⁹⁷, S. Asai¹⁶¹, N. Asbah⁴⁴, A. Ashkenazi¹⁵⁹, E.M. Asimakopoulou¹⁷⁰, L. Asquith¹⁵³, K. Assamagan²⁹, R. Astalos^{28a}, R.J. Atkin^{32a}, M. Atkinson¹⁷¹, N.B. Atlay¹⁴⁸, K. Augsten¹³⁸, G. Avolio³⁵, R. Avramidou^{58a}, B. Axen¹⁸, M.K. Ayoub^{15a}, G. Azuelos^{107,ax}, A.E. Baas^{59a}, M.J. Baca²¹, H. Bachacou¹⁴², K. Bachas^{65a,65b}, M. Backes¹³¹, P. Bagnaia^{70a,70b}, M. Bahmani⁸², H. Bahrasemani¹⁴⁹, A.J. Bailey¹⁷², J.T. Baines¹⁴¹, M. Bajic³⁹, O.K. Baker¹⁸¹, P.J. Bakker¹¹⁸, D. Bakshi Gupta⁹³, E.M. Baldin^{120b,120a}, P. Balek¹⁷⁸, F. Balli¹⁴², W.K. Balunas¹³³, E. Banas⁸², A. Bandyopadhyay²⁴, S. Banerjee^{179,1}, A.A.E. Bannoura¹⁸⁰, L. Barak¹⁵⁹, W.M. Barbe³⁷, E.L. Barberio¹⁰², D. Barberis^{53b,53a}, M. Barbero⁹⁹, T. Barillari¹¹³, M-S. Barisits³⁵, J. Barkeloo¹²⁷, T. Barklow¹⁵⁰, N. Barlow³¹, R. Barnea¹⁵⁸, S.L. Barnes^{58c}, B.M. Barnett¹⁴¹, R.M. Barnett¹⁸, Z. Barnovska-Blenessy^{58a}, A. Baroncelli^{72a}, G. Barone²⁶, A.J. Barr¹³¹, L. Barranco Navarro¹⁷², F. Barreiro⁹⁶, J. Barreiro Guimarães da Costa^{15a}, R. Bartoldus¹⁵⁰, A.E. Barton⁸⁷, P. Bartos^{28a}, A. Basalae¹³⁴, A. Bassalat¹²⁸, R.L. Bates⁵⁵, S.J. Batista¹⁶⁵, S. Batlamous^{34e}, J.R. Batley³¹, M. Battaglia¹⁴³, M. Bauce^{70a,70b}, F. Bauer¹⁴², K.T. Bauer¹⁶⁹, H.S. Bawa^{150,n}, J.B. Beacham¹²², M.D. Beattie⁸⁷, T. Beau¹³², P.H. Beauchemin¹⁶⁸, P. Bechtel²⁴, H.C. Beck⁵¹, H.P. Beck^{20,t}, K. Becker⁵⁰, M. Becker⁹⁷, C. Becot¹²¹, A. Beddall^{12d}, A.J. Beddall^{12a}, V.A. Bednyakov⁷⁷, M. Bedognetti¹¹⁸, C.P. Bee¹⁵², T.A. Beermann³⁵, M. Begalli^{78b}, M. Begel²⁹, A. Behera¹⁵², J.K. Behr⁴⁴, A.S. Bell⁹², G. Bella¹⁵⁹, L. Bellagamba^{23b}, A. Bellerive³³, M. Bellomo¹⁵⁸, K. Belotskiy¹¹⁰, N.L. Belyaev¹¹⁰, O. Benary^{159,*}, D. Benchechroun^{34a}, M. Bender¹¹², N. Benekos¹⁰, Y. Benhammou¹⁵⁹, E. Benhar Noccioli¹⁸¹, J. Benitez⁷⁵, D.P. Benjamin⁴⁷, M. Benoit⁵², J.R. Bensinger²⁶, S. Bentvelsen¹¹⁸, L. Beresford¹³¹, M. Beretta⁴⁹, D. Berge⁴⁴, E. Bergeas Kuutmann¹⁷⁰, N. Berger⁵, L.J. Bergsten²⁶, J. Beringer¹⁸, S. Berlendis⁵⁶, N.R. Bernard¹⁰⁰, G. Bernardi¹³², C. Bernius¹⁵⁰, F.U. Bernlochner²⁴, T. Berry⁹¹, P. Berta⁹⁷, C. Bertella^{15a}, G. Bertoli^{43a,43b}, I.A. Bertram⁸⁷, G.J. Besjes³⁹, O. Bessidskaia Bylund^{43a,43b}, M. Bessner⁴⁴, N. Besson¹⁴², A. Bethani⁹⁸, S. Bethke¹¹³, A. Betti²⁴, A.J. Bevan⁹⁰, J. Beyer¹¹³, R.M. Bianchi¹³⁵, O. Biebel¹¹², D. Biedermann¹⁹, R. Bielski⁹⁸, K. Bierwagen⁹⁷, N.V. Biesuz^{69a,69b}, M. Biglietti^{72a}, T.R.V. Billoud¹⁰⁷, M. Bindi⁵¹, A. Bingul^{12d}, C. Bini^{70a,70b}, S. Biondi^{23b,23a}, T. Bisanz⁵¹, J.P. Biswal¹⁵⁹, C. Bittrich⁴⁶, D.M. Bjergaard⁴⁷, J.E. Black¹⁵⁰, K.M. Black²⁵, R.E. Blair⁶, T. Blazek^{28a}, I. Bloch⁴⁴, C. Blocker²⁶, A. Blue⁵⁵, U. Blumenschein⁹⁰,

Dr. Blunier^{144a}, G.J. Bobbink¹¹⁸, V.S. Bobrovnikov^{120b,120a}, S.S. Bocchetta⁹⁴, A. Bocci⁴⁷, D. Boerner¹⁸⁰, D. Bogavac¹¹², A.G. Bogdanchikov^{120b,120a}, C. Bohm^{43a}, V. Boisvert⁹¹, P. Bokan¹⁷⁰, T. Bold^{81a}, A.S. Boldyrev¹¹¹, A.E. Bolz^{59b}, M. Bomben¹³², M. Bona⁹⁰, J.S. Bonilla¹²⁷, M. Boonekamp¹⁴², A. Borisov¹⁴⁰, G. Borissov⁸⁷, J. Bortfeldt³⁵, D. Bortolotto¹³¹, V. Bortolotto^{71a,61b,61c,71b}, D. Boscherini^{23b}, M. Bosman¹⁴, J.D. Bossio Sola³⁰, J. Boudreau¹³⁵, E.V. Bouhova-Thacker⁸⁷, D. Boumediene³⁷, C. Bourdarios¹²⁸, S.K. Boutle⁵⁵, A. Boveia¹²², J. Boyd³⁵, I.R. Boyko⁷⁷, A.J. Bozson⁹¹, J. Bracinik²¹, N. Brahimi⁹⁹, A. Brandt⁸, G. Brandt¹⁸⁰, O. Brandt^{59a}, F. Braren⁴⁴, U. Bratzler¹⁶², B. Brau¹⁰⁰, J.E. Brau¹²⁷, W.D. Breaden Madden⁵⁵, K. Brendlinger⁴⁴, A.J. Brennan¹⁰², L. Brenner⁴⁴, R. Brenner¹⁷⁰, S. Bressler¹⁷⁸, B. Brickwedde⁹⁷, D.L. Briglin²¹, D. Britton⁵⁵, D. Britzger^{59b}, I. Brock²⁴, R. Brock¹⁰⁴, G. Brooijmans³⁸, T. Brooks⁹¹, W.K. Brooks^{144b}, E. Brost¹¹⁹, J.H. Broughton²¹, R. Bruce³⁵, P.A. Bruckman de Renstrom⁸², D. Bruncko^{28b}, A. Bruni^{23b}, G. Bruni^{23b}, L.S. Bruni¹¹⁸, S. Bruno^{71a,71b}, B.H. Brunt³¹, M. Bruschi^{23b}, N. Bruscinò¹³⁵, P. Bryant³⁶, L. Bryngemark⁴⁴, T. Buanes¹⁷, Q. Buat³⁵, P. Buchholz¹⁴⁸, A.G. Buckley⁵⁵, I.A. Budagov⁷⁷, M.K. Bugge¹³⁰, F. Bühner⁵⁰, O. Bulekov¹¹⁰, D. Bullock⁸, T.J. Burch¹¹⁹, S. Burdin⁸⁸, C.D. Burgard¹¹⁸, A.M. Burger⁵, B. Burghgrave¹¹⁹, K. Burka⁸², S. Burke¹⁴¹, I. Burmeister⁴⁵, J.T.P. Burr¹³¹, D. Büscher⁵⁰, V. Büscher⁹⁷, E. Buschmann⁵¹, P. Bussey⁵⁵, J.M. Butler²⁵, C.M. Buttar⁵⁵, J.M. Butterworth⁹², P. Butti³⁵, W. Buttinger³⁵, A. Buzatu¹⁵⁵, A.R. Buzykaev^{120b,120a}, G. Cabras^{23b,23a}, S. Cabrera Urbán¹⁷², D. Caforio¹³⁸, H. Cai¹⁷¹, V.M.M. Cairo², O. Cakir^{4a}, N. Calace⁵², P. Calafiura¹⁸, A. Calandri⁹⁹, G. Calderini¹³², P. Calfayan⁶³, G. Callea^{40b,40a}, L.P. Caloba^{78b}, S. Calvente Lopez⁹⁶, D. Calvet³⁷, S. Calvet³⁷, T.P. Calvet¹⁵², M. Calvetti^{69a,69b}, R. Camacho Toro¹³², S. Camarda³⁵, P. Camarri^{71a,71b}, D. Cameron¹³⁰, R. Caminal Armadans¹⁰⁰, C. Camincher³⁵, S. Campana³⁵, M. Campanelli⁹², A. Camplani^{66a,66b}, A. Campoverde¹⁴⁸, V. Canale^{67a,67b}, M. Cano Bret^{58c}, J. Cantero¹²⁵, T. Cao¹⁵⁹, Y. Cao¹⁷¹, M.D.M. Capeans Garrido³⁵, I. Caprini^{27b}, M. Caprini^{27b}, M. Capua^{40b,40a}, R.M. Carbone³⁸, R. Cardarelli^{71a}, F.C. Cardillo⁵⁰, I. Carli¹³⁹, T. Carli³⁵, G. Carlino^{67a}, B.T. Carlson¹³⁵, L. Carminati^{66a,66b}, R.M.D. Carney^{43a,43b}, S. Caron¹¹⁷, E. Carquin^{144b}, S. Carrá^{66a,66b}, G.D. Carrillo-Montoya³⁵, D. Casadei^{32b}, M.P. Casado^{14,h}, A.F. Casha¹⁶⁵, M. Casolino¹⁴, D.W. Casper¹⁶⁹, R. Castelijin¹¹⁸, V. Castillo Gimenez¹⁷², N.F. Castro^{136a,136e}, A. Catinaccio³⁵, J.R. Catmore¹³⁰, A. Cattai³⁵, J. Caudron²⁴, V. Cavaliere²⁹, E. Cavallaro¹⁴, D. Cavalli^{66a}, M. Cavalli-Sforza¹⁴, V. Cavasinni^{69a,69b}, E. Celebi^{12b}, F. Ceradini^{72a,72b}, L. Cerda Alberich¹⁷², A.S. Cerqueira^{78a}, A. Cerri¹⁵³, L. Cerrito^{71a,71b}, F. Cerutti¹⁸, A. Cervelli^{23b,23a}, S.A. Cetin^{12b}, A. Chafaq^{34a}, D. Chakraborty¹¹⁹, S.K. Chan⁵⁷, W.S. Chan¹¹⁸, Y.L. Chan^{61a}, P. Chang¹⁷¹, J.D. Chapman³¹, D.G. Charlton²¹, C.C. Chau³³, C.A. Chavez Barajas¹⁵³, S. Che¹²², A. Chegwidan¹⁰⁴, S. Chekanov⁶, S.V. Chekulaev^{166a}, G.A. Chelkov^{77,aw}, M.A. Chelstowska³⁵, C. Chen^{58a}, C.H. Chen⁷⁶, H. Chen²⁹, J. Chen^{58a}, J. Chen³⁸, S. Chen¹³³, S.J. Chen^{15c}, X. Chen^{15b,av}, Y. Chen⁸⁰, Y-H. Chen⁴⁴, H.C. Cheng¹⁰³, H.J. Cheng^{15d}, A. Cheplakov⁷⁷, E. Cheremushkina¹⁴⁰, R. Cherkaoui El Moursli^{34e}, E. Cheu⁷, K. Cheung⁶², L. Chevalier¹⁴², V. Chiarella⁴⁹, G. Chiarelli^{69a}, G. Chiodini^{65a}, A.S. Chisholm³⁵, A. Chitan^{27b}, I. Chiu¹⁶¹, Y.H. Chiu¹⁷⁴, M.V. Chizhov⁷⁷, K. Choi⁶³, A.R. Chomont¹²⁸, S. Chouridou¹⁶⁰, Y.S. Chow¹¹⁸, V. Christodoulou⁹², M.C. Chu^{61a}, J. Chudoba¹³⁷, A.J. Chuinard¹⁰¹, J.J. Chwastowski⁸², L. Chytka¹²⁶, D. Cinca⁴⁵, V. Cindro⁸⁹, I.A. Cioară²⁴, A. Ciocio¹⁸, F. Ciroto^{67a,67b}, Z.H. Citron¹⁷⁸, M. Citterio^{66a}, A. Clark⁵², M.R. Clark³⁸, P.J. Clark⁴⁸, C. Clement^{43a,43b}, Y. Coadou⁹⁹, M. Cobal^{64a,64c}, A. Coccaro^{53b,53a}, J. Cochran⁷⁶, A.E.C. Coimbra¹⁷⁸, L. Colasurdo¹¹⁷, B. Cole³⁸, A.P. Colijn¹¹⁸, J. Collot⁵⁶, P. Conde Muñio^{136a,136b}, E. Coniavitis⁵⁰, S.H. Connell^{32b}, I.A. Connelly⁹⁸, S. Constantinescu^{27b}, F. Conventi^{67a,ay}, A.M. Cooper-Sarkar¹³¹, F. Cormier¹⁷³, K.J.R. Cormier¹⁶⁵, M. Corradi^{70a,70b}, E.E. Corrigan⁹⁴, F. Corriveau^{101,af}, A. Cortes-Gonzalez³⁵, M.J. Costa¹⁷², D. Costanzo¹⁴⁶, G. Cottin³¹, G. Cowan⁹¹, B.E. Cox⁹⁸, J. Crane⁹⁸, K. Cranmer¹²¹, S.J. Crawley⁵⁵, R.A. Creager¹³³, G. Cree³³, S. Crépe-Renaudin⁵⁶, F. Crescioli¹³², M. Cristinziani²⁴, V. Croft¹²¹, G. Crosetti^{40b,40a}, A. Cueto⁹⁶, T. Cuhadar Donszelmann¹⁴⁶, A.R. Cukierman¹⁵⁰, M. Curatolo⁴⁹, J. Cúth⁹⁷, S. Czekierda⁸², P. Czodrowski³⁵, M.J. Da Cunha Sargedas De Sousa^{58b}, C. Da Via⁹⁸,

W. Dabrowski^{81a}, T. Dado^{28a,aa}, S. Dahbi^{34e}, T. Dai¹⁰³, F. Dallaire¹⁰⁷, C. Dallapiccola¹⁰⁰, M. Dam³⁹,
 G. D'amen^{23b,23a}, J.R. Dandoy¹³³, M.F. Daneri³⁰, N.P. Dang^{179,1}, N.D. Dann⁹⁸, M. Danninger¹⁷³,
 V. Dao³⁵, G. Darbo^{53b}, S. Darmora⁸, O. Dartsis⁵, A. Dattagupta¹²⁷, T. Daubney⁴⁴, S. D'Auria⁵⁵,
 W. Davey²⁴, C. David⁴⁴, T. Davidek¹³⁹, D.R. Davis⁴⁷, E. Dawe¹⁰², I. Dawson¹⁴⁶, K. De⁸,
 R. De Asmundis^{67a}, A. De Benedetti¹²⁴, S. De Castro^{23b,23a}, S. De Cecco^{70a,70b}, N. De Groot¹¹⁷,
 P. de Jong¹¹⁸, H. De la Torre¹⁰⁴, F. De Lorenzi⁷⁶, A. De Maria^{51,v}, D. De Pedis^{70a}, A. De Salvo^{70a},
 U. De Sanctis^{71a,71b}, A. De Santo¹⁵³, K. De Vasconcelos Corga⁹⁹, J.B. De Vivie De Regie¹²⁸,
 C. Debenedetti¹⁴³, D.V. Dedovich⁷⁷, N. Dehghanian³, M. Del Gaudio^{40b,40a}, J. Del Peso⁹⁶,
 D. Delgove¹²⁸, F. Deliot¹⁴², C.M. Delitzsch⁷, M. Della Pietra^{67a,67b}, D. Della Volpe⁵², A. Dell'Acqua³⁵,
 L. Dell'Asta²⁵, M. Delmastro⁵, C. Delporte¹²⁸, P.A. Delsart⁵⁶, D.A. DeMarco¹⁶⁵, S. Demers¹⁸¹,
 M. Demichev⁷⁷, S.P. Denisov¹⁴⁰, D. Denysiuk¹¹⁸, L. D'Eramo¹³², D. Derendarz⁸², J.E. Derkaoui^{34d},
 F. Derue¹³², P. Dervan⁸⁸, K. Desch²⁴, C. Deterre⁴⁴, K. Dette¹⁶⁵, M.R. Devesa³⁰, P.O. Deviveiros³⁵,
 A. Dewhurst¹⁴¹, S. Dhaliwal²⁶, F.A. Di Bello⁵², A. Di Ciaccio^{71a,71b}, L. Di Ciaccio⁵,
 W.K. Di Clemente¹³³, C. Di Donato^{67a,67b}, A. Di Girolamo³⁵, B. Di Micco^{72a,72b}, R. Di Nardo³⁵,
 K.F. Di Petrillo⁵⁷, A. Di Simone⁵⁰, R. Di Sipio¹⁶⁵, D. Di Valentino³³, C. Diaconu⁹⁹, M. Diamond¹⁶⁵,
 F.A. Dias³⁹, T. Dias Do Vale^{136a}, M.A. Diaz^{144a}, J. Dickinson¹⁸, E.B. Diehl¹⁰³, J. Dietrich¹⁹,
 S. Díez Cornell⁴⁴, A. Dimitrievska¹⁸, J. Dingfelder²⁴, F. Dittus³⁵, F. Djama⁹⁹, T. Djobava^{157b},
 J.I. Djuvsland^{59a}, M.A.B. Do Vale^{78c}, M. Dobre^{27b}, D. Dodsworth²⁶, C. Doglioni⁹⁴, J. Dolejsi¹³⁹,
 Z. Dolezal¹³⁹, M. Donadelli^{78d}, J. Donini³⁷, A. D'onofrio⁹⁰, M. D'onofrio⁸⁸, J. Dopke¹⁴¹, A. Doria^{67a},
 M.T. Dova⁸⁶, A.T. Doyle⁵⁵, E. Drechsler⁵¹, E. Dreyer¹⁴⁹, T. Dreyer⁵¹, M. Dris¹⁰, Y. Du^{58b},
 J. Duarte-Campderros¹⁵⁹, F. Dubinin¹⁰⁸, A. Dubreuil⁵², E. Duchovni¹⁷⁸, G. Duckeck¹¹²,
 A. Ducourthial¹³², O.A. Ducu^{107,z}, D. Duda¹¹³, A. Dudarev³⁵, A.C. Dudder⁹⁷, E.M. Duffield¹⁸,
 L. Dufflot¹²⁸, M. Dührssen³⁵, C. Dülsen¹⁸⁰, M. Dumancic¹⁷⁸, A.E. Dumitriu^{27b,f}, A.K. Duncan⁵⁵,
 M. Dunford^{59a}, A. Duperrin⁹⁹, H. Duran Yildiz^{4a}, M. Düren⁵⁴, A. Durglishvili^{157b}, D. Duschinger⁴⁶,
 B. Dutta⁴⁴, D. Duvnjak¹, M. Dyndal⁴⁴, B.S. Dziedzic⁸², C. Eckardt⁴⁴, K.M. Ecker¹¹³, R.C. Edgar¹⁰³,
 T. Eifert³⁵, G. Eigen¹⁷, K. Einsweiler¹⁸, T. Ekelof¹⁷⁰, M. El Kacimi^{34c}, R. El Kousseifi⁹⁹, V. Ellajosyula⁹⁹,
 M. Ellert¹⁷⁰, F. Ellinghaus¹⁸⁰, A.A. Elliot⁹⁰, N. Ellis³⁵, J. Elmsheuser²⁹, M. Elsing³⁵, D. Emeliyanov¹⁴¹,
 Y. Enari¹⁶¹, J.S. Ennis¹⁷⁶, M.B. Epland⁴⁷, J. Erdmann⁴⁵, A. Ereditato²⁰, S. Errede¹⁷¹, M. Escalier¹²⁸,
 C. Escobar¹⁷², B. Esposito⁴⁹, O. Estrada Pastor¹⁷², A.I. Etienne¹⁴², E. Etzion¹⁵⁹, H. Evans⁶³,
 A. Ezhilov¹³⁴, M. Ezzi^{34e}, F. Fabbri⁵⁵, L. Fabbri^{23b,23a}, V. Fabiani¹¹⁷, G. Facini⁹²,
 R.M. Faisca Rodrigues Pereira^{136a}, R.M. Fakhruddinov¹⁴⁰, S. Falciano^{70a}, P.J. Falke⁵, S. Falke⁵,
 J. Faltova¹³⁹, Y. Fang^{15a}, M. Fanti^{66a,66b}, A. Farbin⁸, A. Farilla^{72a}, E.M. Farina^{68a,68b}, T. Farooque¹⁰⁴,
 S. Farrell¹⁸, S.M. Farrington¹⁷⁶, P. Farthouat³⁵, F. Fassi^{34e}, P. Fassnacht³⁵, D. Fassouliotis⁹,
 M. Fauci Giannelli⁴⁸, A. Favareto^{53b,53a}, W.J. Fawcett⁵², L. Fayard¹²⁸, O.L. Fedin^{134,r}, W. Fedorko¹⁷³,
 M. Feickert⁴¹, S. Feigl¹³⁰, L. Feligioni⁹⁹, C. Feng^{58b}, E.J. Feng³⁵, M. Feng⁴⁷, M.J. Fenton⁵⁵,
 A.B. Fenyuk¹⁴⁰, L. Feremenga⁸, J. Ferrando⁴⁴, A. Ferrari¹⁷⁰, P. Ferrari¹¹⁸, R. Ferrari^{68a},
 D.E. Ferreira de Lima^{59b}, A. Ferrer¹⁷², D. Ferrere⁵², C. Ferretti¹⁰³, F. Fiedler⁹⁷, A. Filipčič⁸⁹,
 F. Filthaut¹¹⁷, M. Fincke-Keeler¹⁷⁴, K.D. Finelli²⁵, M.C.N. Fiolhais^{136a,136c,b}, L. Fiorini¹⁷², C. Fischer¹⁴,
 W.C. Fisher¹⁰⁴, N. Flaschel⁴⁴, I. Fleck¹⁴⁸, P. Fleischmann¹⁰³, R.R.M. Fletcher¹³³, T. Flick¹⁸⁰,
 B.M. Flierl¹¹², L.M. Flores¹³³, L.R. Flores Castillo^{61a}, N. Fomin¹⁷, G.T. Forcolin⁹⁸, A. Formica¹⁴²,
 F.A. Förster¹⁴, A.C. Forti⁹⁸, A.G. Foster²¹, D. Fournier¹²⁸, H. Fox⁸⁷, S. Fracchia¹⁴⁶, P. Francavilla^{69a,69b},
 M. Franchini^{23b,23a}, S. Franchino^{59a}, D. Francis³⁵, L. Franconi¹³⁰, M. Franklin⁵⁷, M. Frate¹⁶⁹,
 M. Fraternali^{68a,68b}, D. Freeborn⁹², S.M. Fressard-Batraneanu³⁵, B. Freund¹⁰⁷, W.S. Freund^{78b},
 D. Froidevaux³⁵, J.A. Frost¹³¹, C. Fukunaga¹⁶², T. Fusayasu¹¹⁴, J. Fuster¹⁷², O. Gabizon¹⁵⁸,
 A. Gabrielli^{23b,23a}, A. Gabrielli¹⁸, G.P. Gach^{81a}, S. Gadatsch⁵², P. Gadow¹¹³, G. Gagliardi^{53b,53a},
 L.G. Gagnon¹⁰⁷, C. Galea^{27b}, B. Galhardo^{136a,136c}, E.J. Gallas¹³¹, B.J. Gallop¹⁴¹, P. Gallus¹³⁸,
 G. Galster³⁹, R. Gamboa Goni⁹⁰, K.K. Gan¹²², S. Ganguly¹⁷⁸, Y. Gao⁸⁸, Y.S. Gao^{150,n}, C. García¹⁷²,

J.E. García Navarro¹⁷², J.A. García Pascual^{15a}, M. Garcia-Sciveres¹⁸, R.W. Gardner³⁶, N. Garelli¹⁵⁰, V. Garonne¹³⁰, K. Gasnikova⁴⁴, A. Gaudiello^{53b,53a}, G. Gaudio^{68a}, I.L. Gavrilenko¹⁰⁸, A. Gavrilyuk¹⁰⁹, C. Gay¹⁷³, G. Gaycken²⁴, E.N. Gazis¹⁰, C.N.P. Gee¹⁴¹, J. Geisen⁵¹, M. Geisen⁹⁷, M.P. Geisler^{59a}, K. Gellerstedt^{43a,43b}, C. Gemme^{53b}, M.H. Genest⁵⁶, C. Geng¹⁰³, S. Gentile^{70a,70b}, C. Gentsos¹⁶⁰, S. George⁹¹, D. Gerbaudo¹⁴, G. Gessner⁴⁵, S. Ghasemi¹⁴⁸, M. Ghneimat²⁴, B. Giacobbe^{23b}, S. Giagu^{70a,70b}, N. Giangiacomi^{23b,23a}, P. Giannetti^{69a}, S.M. Gibson⁹¹, M. Gignac¹⁴³, D. Gillberg³³, G. Gilles¹⁸⁰, D.M. Gingrich^{3,ax}, M.P. Giordani^{64a,64c}, F.M. Giorgi^{23b}, P.F. Giraud¹⁴², P. Giromini⁵⁷, G. Giugliarelli^{64a,64c}, D. Giugni^{66a}, F. Giuli¹³¹, M. Giulini^{59b}, S. Gkaitatzis¹⁶⁰, I. Gkialas^{9,k}, E.L. Gkoukousis¹⁴, P. Gkountoumis¹⁰, L.K. Gladilin¹¹¹, C. Glasman⁹⁶, J. Glatzer¹⁴, P.C.F. Glaysher⁴⁴, A. Glazov⁴⁴, M. Goblirsch-Kolb²⁶, J. Godlewski⁸², S. Goldfarb¹⁰², T. Golling⁵², D. Golubkov¹⁴⁰, A. Gomes^{136a,136b,136d}, R. Goncalves Gama^{78a}, R. Gonçalo^{136a}, G. Gonella⁵⁰, L. Gonella²¹, A. Gongadze⁷⁷, F. Gonnella²¹, J.L. Gonski⁵⁷, S. González de la Hoz¹⁷², S. Gonzalez-Sevilla⁵², L. Goossens³⁵, P.A. Gorbounov¹⁰⁹, H.A. Gordon²⁹, B. Gorini³⁵, E. Gorini^{65a,65b}, A. Gorišek⁸⁹, A.T. Goshaw⁴⁷, C. Gössling⁴⁵, M.I. Gostkin⁷⁷, C.A. Gottardo²⁴, C.R. Goudet¹²⁸, D. Goujdami^{34c}, A.G. Goussiou¹⁴⁵, N. Govender^{32b,d}, C. Goy⁵, E. Gozani¹⁵⁸, I. Grabowska-Bold^{81a}, P.O.J. Gradin¹⁷⁰, E.C. Graham⁸⁸, J. Gramling¹⁶⁹, E. Gramstad¹³⁰, S. Grancagnolo¹⁹, V. Gratchev¹³⁴, P.M. Gravila^{27f}, C. Gray⁵⁵, H.M. Gray¹⁸, Z.D. Greenwood^{93,al}, C. Grefe²⁴, K. Gregersen⁹², I.M. Gregor⁴⁴, P. Grenier¹⁵⁰, K. Grevtsov⁴⁴, J. Griffiths⁸, A.A. Grillo¹⁴³, K. Grimm^{150,c}, S. Grinstein^{14,ab}, Ph. Gris³⁷, J.-F. Grivaz¹²⁸, S. Groh⁹⁷, E. Gross¹⁷⁸, J. Grosse-Knetter⁵¹, G.C. Grossi⁹³, Z.J. Grout⁹², C. Grud¹⁰³, A. Grummer¹¹⁶, L. Guan¹⁰³, W. Guan¹⁷⁹, J. Guenther³⁵, A. Guerguichon¹²⁸, F. Guescini^{166a}, D. Guest¹⁶⁹, R. Gugel⁵⁰, B. Gui¹²², T. Guillemín⁵, S. Guindon³⁵, U. Gul⁵⁵, C. Gumpert³⁵, J. Guo^{58c}, W. Guo¹⁰³, Y. Guo^{58a,u}, Z. Guo⁹⁹, R. Gupta⁴¹, S. Gurbuz^{12c}, G. Gustavino¹²⁴, B.J. Gutelman¹⁵⁸, P. Gutierrez¹²⁴, C. Gutschow⁹², C. Guyot¹⁴², M.P. Guzik^{81a}, C. Gwenlan¹³¹, C.B. Gwilliam⁸⁸, A. Haas¹²¹, C. Haber¹⁸, H.K. Hadavand⁸, N. Haddad^{34e}, A. Hader^{58a}, S. Hageböck²⁴, M. Hagihara¹⁶⁷, H. Hakobyan^{182,*}, M. Haleem¹⁷⁵, J. Haley¹²⁵, G. Halladjian¹⁰⁴, G.D. Hallewell⁹⁹, K. Hamacher¹⁸⁰, P. Hamal¹²⁶, K. Hamano¹⁷⁴, A. Hamilton^{32a}, G.N. Hamity¹⁴⁶, K. Han^{58a,ak}, L. Han^{58a}, S. Han^{15d}, K. Hanagaki^{79,x}, M. Hance¹⁴³, D.M. Handl¹¹², B. Haney¹³³, R. Hankache¹³², P. Hanke^{59a}, E. Hansen⁹⁴, J.B. Hansen³⁹, J.D. Hansen³⁹, M.C. Hansen²⁴, P.H. Hansen³⁹, K. Hara¹⁶⁷, A.S. Hard¹⁷⁹, T. Harenberg¹⁸⁰, S. Harkusha¹⁰⁵, P.F. Harrison¹⁷⁶, N.M. Hartmann¹¹², Y. Hasegawa¹⁴⁷, A. Hasib⁴⁸, S. Hassani¹⁴², S. Haug²⁰, R. Hauser¹⁰⁴, L. Hauswald⁴⁶, L.B. Havener³⁸, M. Havranek¹³⁸, C.M. Hawkes²¹, R.J. Hawkings³⁵, D. Hayden¹⁰⁴, C. Hayes¹⁵², C.P. Hays¹³¹, J.M. Hays⁹⁰, H.S. Hayward⁸⁸, S.J. Haywood¹⁴¹, M.P. Heath⁴⁸, V. Hedberg⁹⁴, L. Heelan⁸, S. Heer²⁴, K.K. Heidegger⁵⁰, J. Heilman³³, S. Heim⁴⁴, T. Heim¹⁸, B. Heinemann^{44,as}, J.J. Heinrich¹¹², L. Heinrich¹²¹, C. Heinz⁵⁴, J. Hejbal¹³⁷, L. Helary³⁵, A. Held¹⁷³, S. Hellesund¹³⁰, S. Hellman^{43a,43b}, C. Helsens³⁵, R.C.W. Henderson⁸⁷, Y. Heng¹⁷⁹, S. Henkelmann¹⁷³, A.M. Henriques Correia³⁵, G.H. Herbert¹⁹, H. Herde²⁶, V. Herget¹⁷⁵, Y. Hernández Jiménez^{32c}, H. Herr⁹⁷, G. Herten⁵⁰, R. Hertenberger¹¹², L. Hervas³⁵, T.C. Herwig¹³³, G.G. Hesketh⁹², N.P. Hessey^{166a}, J.W. Hetherly⁴¹, S. Higashino⁷⁹, E. Higón-Rodriguez¹⁷², K. Hildebrand³⁶, E. Hill¹⁷⁴, J.C. Hill³¹, K.K. Hill²⁹, K.H. Hiller⁴⁴, S.J. Hillier²¹, M. Hils⁴⁶, I. Hinchliffe¹⁸, M. Hirose¹²⁹, D. Hirschbuehl¹⁸⁰, B. Hiti⁸⁹, O. Hladik¹³⁷, D.R. Hlaluku^{32c}, X. Hoad⁴⁸, J. Hobbs¹⁵², N. Hod^{166a}, M.C. Hodgkinson¹⁴⁶, A. Hoecker³⁵, M.R. Hoferkamp¹¹⁶, F. Hoenig¹¹², D. Hohn²⁴, D. Hohov¹²⁸, T.R. Holmes³⁶, M. Holzbock¹¹², M. Homann⁴⁵, S. Honda¹⁶⁷, T. Honda⁷⁹, T.M. Hong¹³⁵, A. Hönle¹¹³, B.H. Hooberman¹⁷¹, W.H. Hopkins¹²⁷, Y. Horii¹¹⁵, P. Horn⁴⁶, A.J. Horton¹⁴⁹, L.A. Horyn³⁶, J-Y. Hostachy⁵⁶, A. Hostiuc¹⁴⁵, S. Hou¹⁵⁵, A. Hoummada^{34a}, J. Howarth⁹⁸, J. Hoya⁸⁶, M. Hrabovsky¹²⁶, J. Hrdinka³⁵, I. Hristova¹⁹, J. Hrivnac¹²⁸, A. Hrynevich¹⁰⁶, T. Hryn'ova⁵, P.J. Hsu⁶², S.-C. Hsu¹⁴⁵, Q. Hu²⁹, S. Hu^{58c}, Y. Huang^{15a}, Z. Hubacek¹³⁸, F. Hubaut⁹⁹, M. Huebner²⁴, F. Huegging²⁴, T.B. Huffman¹³¹, E.W. Hughes³⁸, M. Huhtinen³⁵, R.F.H. Hunter³³, P. Huo¹⁵², A.M. Hupe³³, N. Huseynov^{77,ah}, J. Huston¹⁰⁴, J. Huth⁵⁷, R. Hyneman¹⁰³, G. Iacobucci⁵², G. Iakovidis²⁹,

I. Ibragimov¹⁴⁸, L. Iconomidou-Fayard¹²⁸, Z. Idrissi^{34e}, P. Iengo³⁵, R. Ignazzi³⁹, O. Igonkina^{118,ad},
 R. Iguchi¹⁶¹, T. Iizawa¹⁷⁷, Y. Ikegami⁷⁹, M. Ikeno⁷⁹, D. Iliadis¹⁶⁰, N. Ilic¹⁵⁰, F. Iltzsche⁴⁶,
 G. Introzzi^{68a,68b}, M. Iodice^{72a}, K. Iordanidou³⁸, V. Ippolito^{70a,70b}, M.F. Isacson¹⁷⁰, N. Ishijima¹²⁹,
 M. Ishino¹⁶¹, M. Ishitsuka¹⁶³, C. Issever¹³¹, S. Istin^{12c,aq}, F. Ito¹⁶⁷, J.M. Iturbe Ponce^{61a}, R. Iuppa^{73a,73b},
 A. Ivina¹⁷⁸, H. Iwasaki⁷⁹, J.M. Izen⁴², V. Izzo^{67a}, S. Jabbar³, P. Jacka¹³⁷, P. Jackson¹, R.M. Jacobs²⁴,
 V. Jain², G. Jäkel¹⁸⁰, K.B. Jakobi⁹⁷, K. Jakobs⁵⁰, S. Jakobsen⁷⁴, T. Jakoubek¹³⁷, D.O. Jamin¹²⁵,
 D.K. Jana⁹³, R. Jansky⁵², J. Janssen²⁴, M. Janus⁵¹, P.A. Janus^{81a}, G. Jarlskog⁹⁴, N. Javadov^{77,ah},
 T. Javůrek⁵⁰, M. Javurkova⁵⁰, F. Jeanneau¹⁴², L. Jeanty¹⁸, J. Jejelava^{157a,ai}, A. Jelinskas¹⁷⁶, P. Jenni^{50,e},
 J. Jeong⁴⁴, C. Jeske¹⁷⁶, S. Jézéquel⁵, H. Ji¹⁷⁹, J. Jia¹⁵², H. Jiang⁷⁶, Y. Jiang^{58a}, Z. Jiang^{150,s}, S. Jiggins⁵⁰,
 F.A. Jimenez Morales³⁷, J. Jimenez Pena¹⁷², S. Jin^{15c}, A. Jinaru^{27b}, O. Jinnouchi¹⁶³, H. Jivan^{32c},
 P. Johansson¹⁴⁶, K.A. Johns⁷, C.A. Johnson⁶³, W.J. Johnson¹⁴⁵, K. Jon-And^{43a,43b}, R.W.L. Jones⁸⁷,
 S.D. Jones¹⁵³, S. Jones⁷, T.J. Jones⁸⁸, J. Jongmanns^{59a}, P.M. Jorge^{136a,136b}, J. Jovicevic^{166a}, X. Ju¹⁷⁹,
 J.J. Junggeburth¹¹³, A. Juste Rozas^{14,ab}, A. Kaczmarska⁸², M. Kado¹²⁸, H. Kagan¹²², M. Kagan¹⁵⁰,
 T. Kaji¹⁷⁷, E. Kajomovitz¹⁵⁸, C.W. Kalderon⁹⁴, A. Kaluza⁹⁷, S. Kama⁴¹, A. Kamenshchikov¹⁴⁰,
 L. Kanjir⁸⁹, Y. Kano¹⁶¹, V.A. Kantserov¹¹⁰, J. Kanzaki⁷⁹, B. Kaplan¹²¹, L.S. Kaplan¹⁷⁹, D. Kar^{32c},
 M.J. Kareem^{166b}, E. Karentzos¹⁰, S.N. Karpov⁷⁷, Z.M. Karpova⁷⁷, V. Kartvelishvili⁸⁷,
 A.N. Karyukhin¹⁴⁰, K. Kasahara¹⁶⁷, L. Kashif¹⁷⁹, R.D. Kass¹²², A. Kastanas¹⁵¹, Y. Kataoka¹⁶¹,
 C. Kato¹⁶¹, J. Katzy⁴⁴, K. Kawade⁸⁰, K. Kawagoe⁸⁵, T. Kawamoto¹⁶¹, G. Kawamura⁵¹, E.F. Kay⁸⁸,
 V.F. Kazanin^{120b,120a}, R. Keeler¹⁷⁴, R. Kehoe⁴¹, J.S. Keller³³, E. Kellermann⁹⁴, J.J. Kempster²¹,
 J. Kendrick²¹, O. Kepka¹³⁷, S. Kersten¹⁸⁰, B.P. Kerševan⁸⁹, R.A. Keyes¹⁰¹, M. Khader¹⁷¹,
 F. Khalil-Zada¹³, A. Khanov¹²⁵, A.G. Kharlamov^{120b,120a}, T. Kharlamova^{120b,120a}, A. Khodinov¹⁶⁴,
 T.J. Khoo⁵², E. Khramov⁷⁷, J. Khubua^{157b}, S. Kido⁸⁰, M. Kiehn⁵², C.R. Kilby⁹¹, S.H. Kim¹⁶⁷,
 Y.K. Kim³⁶, N. Kimura^{64a,64c}, O.M. Kind¹⁹, B.T. King⁸⁸, D. Kirchmeier⁴⁶, J. Kirk¹⁴¹, A.E. Kiryunin¹¹³,
 T. Kishimoto¹⁶¹, D. Kisielewska^{81a}, V. Kitali⁴⁴, O. Kivernyk⁵, E. Kladiva^{28b,*},
 T. Klapdor-Kleingrothaus⁵⁰, M.H. Klein¹⁰³, M. Klein⁸⁸, U. Klein⁸⁸, K. Kleinknecht⁹⁷, P. Klimek¹¹⁹,
 A. Klimentov²⁹, R. Klingenberg^{45,*}, T. Klingl²⁴, T. Klioutchnikova³⁵, F.F. Klitzner¹¹², P. Kluit¹¹⁸,
 S. Kluth¹¹³, E. Kneringer⁷⁴, E.B.F.G. Knoops⁹⁹, A. Knue⁵⁰, A. Kobayashi¹⁶¹, D. Kobayashi⁸⁵,
 T. Kobayashi¹⁶¹, M. Kobel⁴⁶, M. Kocian¹⁵⁰, P. Kodys¹³⁹, T. Koffas³³, E. Koffeman¹¹⁸, N.M. Köhler¹¹³,
 T. Koi¹⁵⁰, M. Kolb^{59b}, I. Koletsou⁵, T. Kondo⁷⁹, N. Kondrashova^{58c}, K. Köneke⁵⁰, A.C. König¹¹⁷,
 T. Kono⁷⁹, R. Konoplich^{121,an}, N. Konstantinidis⁹², B. Konya⁹⁴, R. Kopeliansky⁶³, S. Koperny^{81a},
 K. Korcyl⁸², K. Kordas¹⁶⁰, A. Korn⁹², I. Korolkov¹⁴, E.V. Korolkova¹⁴⁶, O. Kortner¹¹³, S. Kortner¹¹³,
 T. Kosek¹³⁹, V.V. Kostyukhin²⁴, A. Kotwal⁴⁷, A. Koulouris¹⁰, A. Kourkoumeli-Charalampidi^{68a,68b},
 C. Kourkoumelis⁹, E. Kourlitis¹⁴⁶, V. Kouskoura²⁹, A.B. Kowalewska⁸², R. Kowalewski¹⁷⁴,
 T.Z. Kowalski^{81a}, C. Kozakai¹⁶¹, W. Kozanecki¹⁴², A.S. Kozhin¹⁴⁰, V.A. Kramarenko¹¹¹,
 G. Kramberger⁸⁹, D. Krasnopevtsev¹¹⁰, M.W. Krasny¹³², A. Krasznahorkay³⁵, D. Krauss¹¹³,
 J.A. Kremer^{81a}, J. Kretzschmar⁸⁸, P. Krieger¹⁶⁵, K. Krizka¹⁸, K. Kroeninger⁴⁵, H. Kroha¹¹³, J. Kroll¹³⁷,
 J. Kroll¹³³, J. Krstic¹⁶, U. Kruchonak⁷⁷, H. Krüger²⁴, N. Krumnack⁷⁶, M.C. Kruse⁴⁷, T. Kubota¹⁰²,
 S. Kuday^{4b}, J.T. Kuechler¹⁸⁰, S. Kuehn³⁵, A. Kugel^{59a}, F. Kuger¹⁷⁵, T. Kuhl⁴⁴, V. Kukhtin⁷⁷, R. Kukla⁹⁹,
 Y. Kulchitsky¹⁰⁵, S. Kuleshov^{144b}, Y.P. Kulinich¹⁷¹, M. Kuna⁵⁶, T. Kunigo⁸³, A. Kupco¹³⁷, T. Kupfer⁴⁵,
 O. Kuprash¹⁵⁹, H. Kurashige⁸⁰, L.L. Kurchaninov^{166a}, Y.A. Kurochkin¹⁰⁵, M.G. Kurth^{15d},
 E.S. Kuwertz¹⁷⁴, M. Kuze¹⁶³, J. Kvita¹²⁶, T. Kwan¹⁷⁴, R. Kwee-Hinzmann⁹¹, A. La Rosa¹¹³,
 J.L. La Rosa Navarro^{78d}, L. La Rotonda^{40b,40a}, F. La Ruffa^{40b,40a}, C. Lacasta¹⁷², F. Lacava^{70a,70b},
 J. Lacey⁴⁴, D.P.J. Lack⁹⁸, H. Lacker¹⁹, D. Lacour¹³², E. Ladygin⁷⁷, R. Lafaye⁵, B. Laforge¹³²,
 T. Lagouri^{32c}, S. Lai⁵¹, S. Lammers⁶³, W. Lampl⁷, E. Lançon²⁹, U. Landgraf⁵⁰, M.P.J. Landon⁹⁰,
 M.C. Lanfermann⁵², V.S. Lang⁴⁴, J.C. Lange¹⁴, R.J. Langenberg³⁵, A.J. Lankford¹⁶⁹, F. Lanni²⁹,
 K. Lantzsck²⁴, A. Lanza^{68a}, A. Lapertosa^{53b,53a}, S. Laplace¹³², J.F. Laporte¹⁴², T. Lari^{66a},
 F. Lasagni Manghi^{23b,23a}, M. Lassnig³⁵, T.S. Lau^{61a}, A. Laudrain¹²⁸, A.T. Law¹⁴³, P. Laycock⁸⁸,

M. Lazzaroni^{66a,66b}, B. Le¹⁰², O. Le Dortz¹³², E. Le Guirriec⁹⁹, E.P. Le Quilleuc¹⁴², M. LeBlanc⁷,
T. LeCompte⁶, F. Ledroit-Guillon⁵⁶, C.A. Lee²⁹, G.R. Lee^{144a}, L. Lee⁵⁷, S.C. Lee¹⁵⁵, B. Lefebvre¹⁰¹,
M. Lefebvre¹⁷⁴, F. Legger¹¹², C. Leggett¹⁸, G. Lehmann Miotto³⁵, W.A. Leight⁴⁴, A. Leisos^{160,y},
M.A.L. Leite^{78d}, R. Leitner¹³⁹, D. Lellouch¹⁷⁸, B. Lemmer⁵¹, K.J.C. Leney⁹², T. Lenz²⁴, B. Lenzi³⁵,
R. Leone⁷, S. Leone^{69a}, C. Leonidopoulos⁴⁸, G. Lerner¹⁵³, C. Leroy¹⁰⁷, R. Les¹⁶⁵, A.A.J. Lesage¹⁴²,
C.G. Lester³¹, M. Levchenko¹³⁴, J. Levêque⁵, D. Levin¹⁰³, L.J. Levinson¹⁷⁸, D. Lewis⁹⁰, B. Li¹⁰³,
C-Q. Li^{58a,am}, H. Li^{58b}, L. Li^{58c}, Q. Li^{15d}, Q.Y. Li^{58a}, S. Li^{58d,58c}, X. Li^{58c}, Y. Li¹⁴⁸, Z. Liang^{15a},
B. Liberti^{71a}, A. Liblong¹⁶⁵, K. Lie^{61c}, S. Liem¹¹⁸, A. Limosani¹⁵⁴, C.Y. Lin³¹, K. Lin¹⁰⁴, S.C. Lin¹⁵⁶,
T.H. Lin⁹⁷, R.A. Linck⁶³, B.E. Lindquist¹⁵², A.L. Lioni⁵², E. Lipeles¹³³, A. Lipniacka¹⁷, M. Lisovyi^{59b},
T.M. Liss^{171,au}, A. Lister¹⁷³, A.M. Litke¹⁴³, J.D. Little⁸, B. Liu⁷⁶, B.L. Liu⁶, H.B. Liu²⁹, H. Liu¹⁰³,
J.B. Liu^{58a}, J.K.K. Liu¹³¹, K. Liu¹³², M. Liu^{58a}, P. Liu¹⁸, Y.L. Liu^{58a}, Y.W. Liu^{58a}, M. Livan^{68a,68b},
A. Lleres⁵⁶, J. Llorente Merino^{15a}, S.L. Lloyd⁹⁰, C.Y. Lo^{61b}, F. Lo Sterzo⁴¹, E.M. Lobodzinska⁴⁴,
P. Loch⁷, F.K. Loebinger⁹⁸, K.M. Loew²⁶, T. Lohse¹⁹, K. Lohwasser¹⁴⁶, M. Lokajicek¹³⁷, B.A. Long²⁵,
J.D. Long¹⁷¹, R.E. Long⁸⁷, L. Longo^{65a,65b}, K.A. Looper¹²², J.A. Lopez^{144b}, I. Lopez Paz¹⁴,
A. Lopez Solis¹³², J. Lorenz¹¹², N. Lorenzo Martinez⁵, M. Losada²², P.J. Lösel¹¹², A. Lösle⁵⁰, X. Lou⁴⁴,
X. Lou^{15a}, A. Lounis¹²⁸, J. Love⁶, P.A. Love⁸⁷, J.J. Lozano Bahilo¹⁷², H. Lu^{61a}, N. Lu¹⁰³, Y.J. Lu⁶²,
H.J. Lubatti¹⁴⁵, C. Luci^{70a,70b}, A. Lucotte⁵⁶, C. Luedtke⁵⁰, F. Luehring⁶³, I. Luise¹³², W. Lukas⁷⁴,
L. Luminari^{70a}, B. Lund-Jensen¹⁵¹, M.S. Lutz¹⁰⁰, P.M. Luzi¹³², D. Lynn²⁹, R. Lysak¹³⁷, E. Lytken⁹⁴,
F. Lyu^{15a}, V. Lyubushkin⁷⁷, H. Ma²⁹, L.L. Ma^{58b}, Y. Ma^{58b}, G. Maccarrone⁴⁹, A. Macchiolo¹¹³,
C.M. Macdonald¹⁴⁶, J. Machado Miguens^{133,136b}, D. Madaffari¹⁷², R. Madar³⁷, W.F. Mader⁴⁶,
A. Madsen⁴⁴, N. Madysa⁴⁶, J. Maeda⁸⁰, S. Maeland¹⁷, T. Maeno²⁹, A.S. Maevskiy¹¹¹, V. Magerl⁵⁰,
C. Maidantchik^{78b}, T. Maier¹¹², A. Maio^{136a,136b,136d}, O. Majersky^{28a}, S. Majewski¹²⁷, Y. Makida⁷⁹,
N. Makovec¹²⁸, B. Malaescu¹³², Pa. Malecki⁸², V.P. Maleev¹³⁴, F. Malek⁵⁶, U. Mallik⁷⁵, D. Malon⁶,
C. Malone³¹, S. Maltezos¹⁰, S. Malyukov³⁵, J. Mamuzic¹⁷², G. Mancini⁴⁹, I. Mandić⁸⁹, J. Maneira^{136a},
L. Manhaes de Andrade Filho^{78a}, J. Manjarres Ramos⁴⁶, K.H. Mankinen⁹⁴, A. Mann¹¹², A. Manousos⁷⁴,
B. Mansoulie¹⁴², J.D. Mansour^{15a}, M. Mantoani⁵¹, S. Manzoni^{66a,66b}, G. Marceca³⁰, L. March⁵²,
L. Marchese¹³¹, G. Marchiori¹³², M. Marcisovsky¹³⁷, C.A. Marin Tobon³⁵, M. Marjanovic³⁷,
D.E. Marley¹⁰³, F. Marroquim^{78b}, Z. Marshall¹⁸, M.U.F. Martensson¹⁷⁰, S. Marti-Garcia¹⁷²,
C.B. Martin¹²², T.A. Martin¹⁷⁶, V.J. Martin⁴⁸, B. Martin dit Latour¹⁷, M. Martinez^{14,ab},
V.I. Martinez Outschoorn¹⁰⁰, S. Martin-Haugh¹⁴¹, V.S. Martoiu^{27b}, A.C. Martyniuk⁹², A. Marzin³⁵,
L. Masetti⁹⁷, T. Mashimo¹⁶¹, R. Mashinistov¹⁰⁸, J. Masik⁹⁸, A.L. Maslennikov^{120b,120a}, L.H. Mason¹⁰²,
L. Massa^{71a,71b}, P. Mastrandrea⁵, A. Mastroberardino^{40b,40a}, T. Masubuchi¹⁶¹, P. Mättig¹⁸⁰, J. Maurer^{27b},
B. Maček⁸⁹, S.J. Maxfield⁸⁸, D.A. Maximov^{120b,120a}, R. Mazini¹⁵⁵, I. Maznas¹⁶⁰, S.M. Mazza¹⁴³,
N.C. Mc Fadden¹¹⁶, G. Mc Goldrick¹⁶⁵, S.P. Mc Kee¹⁰³, A. McCarn¹⁰³, T.G. McCarthy¹¹³,
L.I. McClymont⁹², E.F. McDonald¹⁰², J.A. McFayden³⁵, G. Mchedlidze⁵¹, M.A. McKay⁴¹,
K.D. McLean¹⁷⁴, S.J. McMahon¹⁴¹, P.C. McNamara¹⁰², C.J. McNicol¹⁷⁶, R.A. McPherson^{174,af},
J.E. Mdhlu^{32c}, Z.A. Meadows¹⁰⁰, S. Meehan¹⁴⁵, T.M. Megy⁵⁰, S. Mehlhase¹¹², A. Mehta⁸⁸,
T. Meideck⁵⁶, B. Meirose⁴², D. Melini^{172,i}, B.R. Mellado Garcia^{32c}, J.D. Mellenthin⁵¹, M. Melo^{28a},
F. Meloni²⁰, A. Melzer²⁴, S.B. Menary⁹⁸, L. Meng⁸⁸, X.T. Meng¹⁰³, A. Mengarelli^{23b,23a}, S. Menke¹¹³,
E. Meoni^{40b,40a}, S. Mergelmeyer¹⁹, C. Merlassino²⁰, P. Mermod⁵², L. Merola^{67a,67b}, C. Meroni^{66a},
F.S. Merritt³⁶, A. Messina^{70a,70b}, J. Metcalfe⁶, A.S. Mete¹⁶⁹, C. Meyer¹³³, J. Meyer¹⁵⁸, J-P. Meyer¹⁴²,
H. Meyer Zu Theenhausen^{59a}, F. Miano¹⁵³, R.P. Middleton¹⁴¹, L. Mijović⁴⁸, G. Mikenberg¹⁷⁸,
M. Mikestikova¹³⁷, M. Mikuž⁸⁹, M. Milesi¹⁰², A. Milic¹⁶⁵, D.A. Millar⁹⁰, D.W. Miller³⁶, A. Milov¹⁷⁸,
D.A. Milstead^{43a,43b}, A.A. Minaenko¹⁴⁰, I.A. Minashvili^{157b}, A.I. Mincer¹²¹, B. Mindur^{81a},
M. Mineev⁷⁷, Y. Minegishi¹⁶¹, Y. Ming¹⁷⁹, L.M. Mir¹⁴, A. Mirto^{65a,65b}, K.P. Mistry¹³³, T. Mitani¹⁷⁷,
J. Mitrevski¹¹², V.A. Mitsou¹⁷², A. Miucci²⁰, P.S. Miyagawa¹⁴⁶, A. Mizukami⁷⁹, J.U. Mjörnmark⁹⁴,
T. Mkrtchyan¹⁸², M. Mlynarikova¹³⁹, T. Moa^{43a,43b}, K. Mochizuki¹⁰⁷, P. Mogg⁵⁰, S. Mohapatra³⁸,

S. Molander^{43a,43b}, R. Moles-Valls²⁴, M.C. Mondragon¹⁰⁴, K. Mönig⁴⁴, J. Monk³⁹, E. Monnier⁹⁹,
 A. Montalbano¹⁴⁹, J. Montejo Berlingen³⁵, F. Monticelli⁸⁶, S. Monzani^{66a}, R.W. Moore³, N. Morange¹²⁸,
 D. Moreno²², M. Moreno Llácer³⁵, P. Morettini^{53b}, M. Morgenstern¹¹⁸, S. Morgenstern³⁵, D. Mori¹⁴⁹,
 T. Mori¹⁶¹, M. Morii⁵⁷, M. Morinaga¹⁷⁷, V. Morisbak¹³⁰, A.K. Morley³⁵, G. Mornacchi³⁵, J.D. Morris⁹⁰,
 L. Morvaj¹⁵², P. Moschovakos¹⁰, M. Mosidze^{157b}, H.J. Moss¹⁴⁶, J. Moss^{150,o}, K. Motohashi¹⁶³,
 R. Mount¹⁵⁰, E. Mountricha²⁹, E.J.W. Moyse¹⁰⁰, S. Muanza⁹⁹, F. Mueller¹¹³, J. Mueller¹³⁵,
 R.S.P. Mueller¹¹², D. Muenstermann⁸⁷, P. Mullen⁵⁵, G.A. Mullier²⁰, F.J. Munoz Sanchez⁹⁸, P. Murin^{28b},
 W.J. Murray^{176,141}, A. Murrone^{66a,66b}, M. Muškinja⁸⁹, C. Mwewa^{32a}, A.G. Myagkov^{140,ao}, J. Myers¹²⁷,
 M. Myska¹³⁸, B.P. Nachman¹⁸, O. Nackenhorst⁴⁵, K. Nagai¹³¹, R. Nagai^{79,ar}, K. Nagano⁷⁹,
 Y. Nagasaka⁶⁰, K. Nagata¹⁶⁷, M. Nagel⁵⁰, E. Nagy⁹⁹, A.M. Nairz³⁵, Y. Nakahama¹¹⁵, K. Nakamura⁷⁹,
 T. Nakamura¹⁶¹, I. Nakano¹²³, F. Napolitano^{59a}, R.F. Naranjo Garcia⁴⁴, R. Narayan¹¹,
 D.I. Narrias Villar^{59a}, I. Naryshkin¹³⁴, T. Naumann⁴⁴, G. Navarro²², R. Nayyar⁷, H.A. Neal^{103,*},
 P.Y. Nechaeva¹⁰⁸, T.J. Neep¹⁴², A. Negri^{68a,68b}, M. Negrini^{23b}, S. Nektarijevic¹¹⁷, C. Nellist⁵¹,
 M.E. Nelson¹³¹, S. Nemecek¹³⁷, P. Nemethy¹²¹, M. Nessi^{35,g}, M.S. Neubauer¹⁷¹, M. Neumann¹⁸⁰,
 P.R. Newman²¹, T.Y. Ng^{61c}, Y.S. Ng¹⁹, H.D.N. Nguyen⁹⁹, T. Nguyen Manh¹⁰⁷, E. Nibigira³⁷,
 R.B. Nickerson¹³¹, R. Nicolaidou¹⁴², J. Nielsen¹⁴³, N. Nikipforou¹¹, V. Nikolaenko^{140,ao},
 I. Nikolic-Audit¹³², K. Nikolopoulos²¹, P. Nilsson²⁹, Y. Ninomiya⁷⁹, A. Nisati^{70a}, N. Nishu^{58c},
 R. Nisius¹¹³, I. Nitsche⁴⁵, T. Nitta¹⁷⁷, T. Nobe¹⁶¹, Y. Noguchi⁸³, M. Nomachi¹²⁹, I. Nomidis³³,
 M.A. Nomura²⁹, T. Nooney⁹⁰, M. Nordberg³⁵, N. Norjoharuddeen¹³¹, T. Novak⁸⁹, O. Novgorodova⁴⁶,
 R. Novotny¹³⁸, M. Nozaki⁷⁹, L. Nozka¹²⁶, K. Ntekas¹⁶⁹, E. Nurse⁹², F. Nuti¹⁰², F.G. Oakham^{33,ax},
 H. Oberlack¹¹³, T. Obermann²⁴, J. Ocariz¹³², A. Ochi⁸⁰, I. Ochoa³⁸, J.P. Ochoa-Ricoux^{144a},
 K. O'Connor²⁶, S. Oda⁸⁵, S. Odaka⁷⁹, A. Oh⁹⁸, S.H. Oh⁴⁷, C.C. Ohm¹⁵¹, H. Oide^{53b,53a}, H. Okawa¹⁶⁷,
 Y. Okazaki⁸³, Y. Okumura¹⁶¹, T. Okuyama⁷⁹, A. Olariu^{27b}, L.F. Oleiro Seabra^{136a},
 S.A. Olivares Pino^{144a}, D. Oliveira Damazio²⁹, J.L. Oliver¹, M.J.R. Olsson³⁶, A. Olszewski⁸²,
 J. Olszowska⁸², D.C. O'Neil¹⁴⁹, A. Onofre^{136a,136e}, K. Onogi¹¹⁵, P.U.E. Onyisi¹¹, H. Oppen¹³⁰,
 M.J. Oreglia³⁶, Y. Oren¹⁵⁹, D. Orestano^{72a,72b}, E.C. Orgill⁹⁸, N. Orlando^{61b}, A.A. O'Rourke⁴⁴,
 R.S. Orr¹⁶⁵, B. Osculati^{53b,53a,*}, V. O'Shea⁵⁵, R. Ospanov^{58a}, G. Otero y Garzon³⁰, H. Otono⁸⁵,
 M. Ouchrif^{34d}, F. Ould-Saada¹³⁰, A. Ouraou¹⁴², Q. Ouyang^{15a}, M. Owen⁵⁵, R.E. Owen²¹, V.E. Ozcan^{12c},
 N. Ozturk⁸, J. Pacalt¹²⁶, H.A. Pacey³¹, K. Pachal¹⁴⁹, A. Pacheco Pages¹⁴, L. Pacheco Rodriguez¹⁴²,
 C. Padilla Aranda¹⁴, S. Pagan Griso¹⁸, M. Paganini¹⁸¹, G. Palacino⁶³, S. Palazzo^{40b,40a}, S. Palestini³⁵,
 M. Palka^{81b}, D. Pallin³⁷, I. Panagoulis¹⁰, C.E. Pandini³⁵, J.G. Panduro Vazquez⁹¹, P. Pani³⁵,
 L. Paolozzi⁵², T.D. Papadopoulou¹⁰, K. Papageorgiou^{9,k}, A. Paramonov⁶, D. Paredes Hernandez^{61b},
 B. Parida^{58c}, A.J. Parker⁸⁷, K.A. Parker⁴⁴, M.A. Parker³¹, F. Parodi^{53b,53a}, J.A. Parsons³⁸, U. Parzefall⁵⁰,
 V.R. Pascuzzi¹⁶⁵, J.M.P. Pasner¹⁴³, E. Pasqualucci^{70a}, S. Passaggio^{53b}, F. Pastore⁹¹, P. Pasuwan^{43a,43b},
 S. Pataraiá⁹⁷, J.R. Pater⁹⁸, A. Pathak^{179,1}, T. Pauly³⁵, B. Pearson¹¹³, M. Pedersen¹³⁰, S. Pedraza Lopez¹⁷²,
 R. Pedro^{136a,136b}, S.V. Peleganchuk^{120b,120a}, O. Penc¹³⁷, C. Peng^{15d}, H. Peng^{58a}, B.S. Peralva^{78a},
 M.M. Perego¹⁴², A.P. Pereira Peixoto^{136a}, D.V. Perepelitsa²⁹, F. Peri¹⁹, L. Perini^{66a,66b}, H. Pernegger³⁵,
 S. Perrella^{67a,67b}, V.D. Peshekhonov^{77,*}, K. Peters⁴⁴, R.F.Y. Peters⁹⁸, B.A. Petersen³⁵, T.C. Petersen³⁹,
 E. Petit⁵⁶, A. Petridis¹, C. Petridou¹⁶⁰, P. Petroff¹²⁸, E. Petrolo^{70a}, M. Petrov¹³¹, F. Petrucci^{72a,72b},
 N.E. Pettersson¹⁰⁰, A. Peyaud¹⁴², R. Pezoa^{144b}, T. Pham¹⁰², F.H. Phillips¹⁰⁴, P.W. Phillips¹⁴¹,
 G. Piacquadio¹⁵², E. Pianori¹⁸, A. Picazio¹⁰⁰, M.A. Pickering¹³¹, R. Piegaiá³⁰, J.E. Pilcher³⁶,
 A.D. Pilkington⁹⁸, M. Pinamonti^{71a,71b}, J.L. Pinfold³, M. Pitt¹⁷⁸, M.-A. Pleier²⁹, V. Pleskot¹³⁹,
 E. Plotnikova⁷⁷, D. Pluth⁷⁶, P. Podberezko^{120b,120a}, R. Poettgen⁹⁴, R. Poggi^{68a,68b}, L. Poggioli¹²⁸,
 I. Pogrebnyak¹⁰⁴, D. Pohl²⁴, I. Pokharel⁵¹, G. Polesello^{68a}, A. Poley⁴⁴, A. Policicchio^{40b,40a}, R. Polifka³⁵,
 A. Polini^{23b}, C.S. Pollard⁴⁴, V. Polychronakos²⁹, D. Ponomarenko¹¹⁰, L. Pontecorvo³⁵,
 G.A. Popeneciu^{27d}, D.M. Portillo Quintero¹³², S. Pospisil¹³⁸, K. Potamianos⁴⁴, I.N. Potrap⁷⁷,
 C.J. Potter³¹, H. Potti¹¹, T. Poulsen⁹⁴, J. Poveda³⁵, T.D. Powell¹⁴⁶, M.E. Pozo Astigarraga³⁵,

P. Pralavorio⁹⁹, S. Prell⁷⁶, D. Price⁹⁸, M. Primavera^{65a}, S. Prince¹⁰¹, N. Proklova¹¹⁰, K. Prokofiev^{61c},
 F. Prokoshin^{144b}, S. Protopopescu²⁹, J. Proudfoot⁶, M. Przybycien^{81a}, A. Puri¹⁷¹, P. Puzo¹²⁸, J. Qian¹⁰³,
 Y. Qin⁹⁸, A. Quadt⁵¹, M. Queitsch-Maitland⁴⁴, A. Qureshi¹, P. Rados¹⁰², F. Ragusa^{66a,66b}, G. Rahal⁹⁵,
 J.A. Raine⁹⁸, S. Rajagopalan²⁹, T. Rashid¹²⁸, S. Raspopov⁵, M.G. Ratti^{66a,66b}, D.M. Rauch⁴⁴,
 F. Rauscher¹¹², S. Rave⁹⁷, B. Ravina¹⁴⁶, I. Ravinovich¹⁷⁸, J.H. Rawling⁹⁸, M. Raymond³⁵, A.L. Read¹³⁰,
 N.P. Readioff⁵⁶, M. Reale^{65a,65b}, D.M. Rebuzzi^{68a,68b}, A. Redelbach¹⁷⁵, G. Redlinger²⁹, R. Reece¹⁴³,
 R.G. Reed^{32c}, K. Reeves⁴², L. Rehnisch¹⁹, J. Reichert¹³³, A. Reiss⁹⁷, C. Rembser³⁵, H. Ren^{15d},
 M. Rescigno^{70a}, S. Resconi^{66a}, E.D. Resseguie¹³³, S. Rettie¹⁷³, E. Reynolds²¹, O.L. Rezanova^{120b,120a},
 P. Reznicek¹³⁹, R. Richter¹¹³, S. Richter⁹², E. Richter-Was^{81b}, O. Ricken²⁴, M. Ridel¹³², P. Rieck¹¹³,
 C.J. Riegel¹⁸⁰, O. Rifki⁴⁴, M. Rijssenbeek¹⁵², A. Rimoldi^{68a,68b}, M. Rimoldi²⁰, L. Rinaldi^{23b},
 G. Ripellino¹⁵¹, B. Ristić⁸⁷, E. Ritsch³⁵, I. Riu¹⁴, J.C. Rivera Vergara^{144a}, F. Rizatdinova¹²⁵, E. Rizvi⁹⁰,
 C. Rizzi¹⁴, R.T. Roberts⁹⁸, S.H. Robertson^{101,af}, A. Robichaud-Veronneau¹⁰¹, D. Robinson³¹,
 J.E.M. Robinson⁴⁴, A. Robson⁵⁵, E. Rocco⁹⁷, C. Roda^{69a,69b}, Y. Rodina⁹⁹, S. Rodriguez Bosca¹⁷²,
 A. Rodriguez Perez¹⁴, D. Rodriguez Rodriguez¹⁷², A.M. Rodríguez Vera^{166b}, S. Roe³⁵, C.S. Rogan⁵⁷,
 O. Røhne¹³⁰, R. Röhrig¹¹³, C.P.A. Roland⁶³, J. Roloff⁵⁷, A. Romaniouk¹¹⁰, M. Romano^{23b,23a},
 N. Rompotis⁸⁸, M. Ronzani¹²¹, L. Roos¹³², S. Rosati^{70a}, K. Rosbach⁵⁰, P. Rose¹⁴³, N-A. Rosien⁵¹,
 E. Rossi^{67a,67b}, L.P. Rossi^{53b}, L. Rossini^{66a,66b}, J.H.N. Rosten³¹, R. Rosten¹⁴⁵, M. Rotaru^{27b},
 J. Rothberg¹⁴⁵, D. Rousseau¹²⁸, D. Roy^{32c}, A. Rozanov⁹⁹, Y. Rozen¹⁵⁸, X. Ruan^{32c}, F. Rubbo¹⁵⁰,
 F. Rühr⁵⁰, A. Ruiz-Martinez³³, Z. Rurikova⁵⁰, N.A. Rusakovich⁷⁷, H.L. Russell¹⁰¹, J.P. Rutherford⁷,
 N. Ruthmann³⁵, E.M. Rüttinger^{44,m}, Y.F. Ryabov¹³⁴, M. Rybar¹⁷¹, G. Rybkin¹²⁸, S. Ryu⁶, A. Ryzhov¹⁴⁰,
 G.F. Rzehorz⁵¹, P. Sabatini⁵¹, G. Sabato¹¹⁸, S. Sacerdoti¹²⁸, H.F-W. Sadrozinski¹⁴³, R. Sadykov⁷⁷,
 F. Safai Tehrani^{70a}, P. Saha¹¹⁹, M. Sahinsoy^{59a}, A. Sahu¹⁸⁰, M. Saimpert⁴⁴, M. Saito¹⁶¹, T. Saito¹⁶¹,
 H. Sakamoto¹⁶¹, A. Sakharov^{121,an}, D. Salamani⁵², G. Salamanna^{72a,72b}, J.E. Salazar Loyola^{144b},
 D. Salek¹¹⁸, P.H. Sales De Bruin¹⁷⁰, D. Salihagic¹¹³, A. Salnikov¹⁵⁰, J. Salt¹⁷², D. Salvatore^{40b,40a},
 F. Salvatore¹⁵³, A. Salvucci^{61a,61b,61c}, A. Salzburger³⁵, D. Sammel⁵⁰, D. Sampsonidis¹⁶⁰,
 D. Sampsonidou¹⁶⁰, J. Sánchez¹⁷², A. Sanchez Pineda^{64a,64c}, H. Sandaker¹³⁰, C.O. Sander⁴⁴,
 M. Sandhoff¹⁸⁰, C. Sandoval²², D.P.C. Sankey¹⁴¹, M. Sannino^{53b,53a}, Y. Sano¹¹⁵, A. Sansoni⁴⁹,
 C. Santoni³⁷, H. Santos^{136a}, I. Santoyo Castillo¹⁵³, A. Sapronov⁷⁷, J.G. Saraiva^{136a,136d}, O. Sasaki⁷⁹,
 K. Sato¹⁶⁷, E. Sauvan⁵, P. Savard^{165,ax}, N. Savic¹¹³, R. Sawada¹⁶¹, C. Sawyer¹⁴¹, L. Sawyer^{93,al},
 C. Sbarra^{23b}, A. Sbrizzi^{23b,23a}, T. Scanlon⁹², D.A. Scannicchio¹⁶⁹, J. Schaarschmidt¹⁴⁵, P. Schacht¹¹³,
 B.M. Schachtner¹¹², D. Schaefer³⁶, L. Schaefer¹³³, J. Schaeffer⁹⁷, S. Schaepe³⁵, U. Schäfer⁹⁷,
 A.C. Schaffer¹²⁸, D. Schaile¹¹², R.D. Schamberger¹⁵², N. Scharmberg⁹⁸, V.A. Schegelsky¹³⁴,
 D. Scheirich¹³⁹, F. Schenck¹⁹, M. Schernau¹⁶⁹, C. Schiavi^{53b,53a}, S. Schier¹⁴³, L.K. Schildgen²⁴,
 Z.M. Schillaci²⁶, E.J. Schioppa³⁵, M. Schioppa^{40b,40a}, K.E. Schleicher⁵⁰, S. Schlenker³⁵,
 K.R. Schmidt-Sommerfeld¹¹³, K. Schmieden³⁵, C. Schmitt⁹⁷, S. Schmitt⁴⁴, S. Schmitz⁹⁷, U. Schnoor⁵⁰,
 L. Schoeffel¹⁴², A. Schoening^{59b}, E. Schopf²⁴, M. Schott⁹⁷, J.F.P. Schouwenberg¹¹⁷, J. Schovancova³⁵,
 S. Schramm⁵², N. Schuh⁹⁷, A. Schulte⁹⁷, H-C. Schultz-Coulon^{59a}, M. Schumacher⁵⁰, B.A. Schumm¹⁴³,
 Ph. Schune¹⁴², A. Schwartzman¹⁵⁰, T.A. Schwarz¹⁰³, H. Schweiger⁹⁸, Ph. Schwemling¹⁴²,
 R. Schwienhorst¹⁰⁴, A. Sciandra²⁴, G. Sciolla²⁶, M. Scornajenghi^{40b,40a}, F. Scuri^{69a}, F. Scutti¹⁰²,
 L.M. Scyboz¹¹³, J. Searcy¹⁰³, C.D. Sebastiani^{70a,70b}, P. Seema²⁴, S.C. Seidel¹¹⁶, A. Seiden¹⁴³, T. Seiss³⁶,
 J.M. Seixas^{78b}, G. Sekhniaidze^{67a}, K. Sekhon¹⁰³, S.J. Sekula⁴¹, N. Semprini-Cesari^{23b,23a}, S. Sen⁴⁷,
 S. Senkin³⁷, C. Serfon¹³⁰, L. Serin¹²⁸, L. Serkin^{64a,64b}, M. Sessa^{72a,72b}, H. Severini¹²⁴, F. Sforza¹⁶⁸,
 A. Sfyrla⁵², E. Shabalina⁵¹, J.D. Shahinian¹⁴³, N.W. Shaikh^{43a,43b}, L.Y. Shan^{15a}, R. Shang¹⁷¹,
 J.T. Shank²⁵, M. Shapiro¹⁸, A.S. Sharma¹, A. Sharma¹³¹, P.B. Shatalov¹⁰⁹, K. Shaw^{64a,64b}, S.M. Shaw⁹⁸,
 A. Shcherbakova¹³⁴, C.Y. Shehu¹⁵³, Y. Shen¹²⁴, N. Sherafati³³, A.D. Sherman²⁵, P. Sherwood⁹²,
 L. Shi^{155,at}, S. Shimizu⁸⁰, C.O. Shimmin¹⁸¹, M. Shimojima¹¹⁴, I.P.J. Shipsey¹³¹, S. Shirabe⁸⁵,
 M. Shiyakova⁷⁷, J. Shlomi¹⁷⁸, A. Shmeleva¹⁰⁸, D. Shoaleh Saadi¹⁰⁷, M.J. Shochet³⁶, S. Shojaii¹⁰²,

D.R. Shope¹²⁴, S. Shrestha¹²², E. Shulga¹¹⁰, P. Sicho¹³⁷, A.M. Sickles¹⁷¹, P.E. Sidebo¹⁵¹,
 E. Sideras Haddad^{32c}, O. Sidiropoulou¹⁷⁵, A. Sidoti^{23b,23a}, F. Siegert⁴⁶, Dj. Sijacki¹⁶, J. Silva^{136a},
 M. Silva Jr.¹⁷⁹, S.B. Silverstein^{43a}, L. Simic⁷⁷, S. Simion¹²⁸, E. Simioni⁹⁷, M. Simon⁹⁷, P. Sinervo¹⁶⁵,
 N.B. Sinev¹²⁷, M. Sioli^{23b,23a}, G. Siragusa¹⁷⁵, I. Siral¹⁰³, S.Yu. Sivoklokov¹¹¹, J. Sjölin^{43a,43b},
 M.B. Skinner⁸⁷, P. Skubic¹²⁴, M. Slater²¹, T. Slavicek¹³⁸, M. Slawinska⁸², K. Sliwa¹⁶⁸, R. Slovak¹³⁹,
 V. Smakhtin¹⁷⁸, B.H. Smart⁵, J. Smiesko^{28a}, N. Smirnov¹¹⁰, S.Yu. Smirnov¹¹⁰, Y. Smirnov¹¹⁰,
 L.N. Smirnova¹¹¹, O. Smirnova⁹⁴, J.W. Smith⁵¹, M.N.K. Smith³⁸, R.W. Smith³⁸, M. Smizanska⁸⁷,
 K. Smolek¹³⁸, A.A. Snesarev¹⁰⁸, I.M. Snyder¹²⁷, S. Snyder²⁹, R. Sobie^{174,af}, A.M. Soffa¹⁶⁹, A. Soffer¹⁵⁹,
 A. Sjøgaard⁴⁸, D.A. Soh¹⁵⁵, G. Sokhrannyi⁸⁹, C.A. Solans Sanchez³⁵, M. Solar¹³⁸, E.Yu. Soldatov¹¹⁰,
 U. Soldevila¹⁷², A.A. Solodkov¹⁴⁰, A. Soloshenko⁷⁷, O.V. Solovyanov¹⁴⁰, V. Solovyev¹³⁴, P. Sommer¹⁴⁶,
 H. Son¹⁶⁸, W. Song¹⁴¹, A. Sopczak¹³⁸, F. Sopkova^{28b}, D. Sosa^{59b}, C.L. Sotiropoulou^{69a,69b},
 S. Sottocornola^{68a,68b}, R. Soualah^{64a,64c,j}, A.M. Soukharev^{120b,120a}, D. South⁴⁴, B.C. Sowden⁹¹,
 S. Spagnolo^{65a,65b}, M. Spalla¹¹³, M. Spangenberg¹⁷⁶, F. Spanò⁹¹, D. Sperlich¹⁹, F. Spettel¹¹³,
 T.M. Spieker^{59a}, R. Spighi^{23b}, G. Spigo³⁵, L.A. Spiller¹⁰², M. Spousta¹³⁹, A. Stabile^{66a,66b}, R. Stamen^{59a},
 S. Stamm¹⁹, E. Stanecka⁸², R.W. Stanek⁶, C. Stanescu^{72a}, M.M. Stanitzki⁴⁴, B. Stapf¹¹⁸, S. Stapnes¹³⁰,
 E.A. Starchenko¹⁴⁰, G.H. Stark³⁶, J. Stark⁵⁶, S.H. Stark³⁹, P. Staroba¹³⁷, P. Starovoitov^{59a}, S. Stärz³⁵,
 R. Staszewski⁸², M. Stegler⁴⁴, P. Steinberg²⁹, B. Stelzer¹⁴⁹, H.J. Stelzer³⁵, O. Stelzer-Chilton^{166a},
 H. Stenzel⁵⁴, T.J. Stevenson⁹⁰, G.A. Stewart⁵⁵, M.C. Stockton¹²⁷, G. Stoicea^{27b}, P. Stolte⁵¹,
 S. Stonjek¹¹³, A. Straessner⁴⁶, J. Strandberg¹⁵¹, S. Strandberg^{43a,43b}, M. Strauss¹²⁴, P. Strizenec^{28b},
 R. Ströhmer¹⁷⁵, D.M. Strom¹²⁷, R. Stroynowski⁴¹, A. Strubig⁴⁸, S.A. Stucci²⁹, B. Stugu¹⁷, J. Stupak¹²⁴,
 N.A. Styles⁴⁴, D. Su¹⁵⁰, J. Su¹³⁵, S. Suchek^{59a}, Y. Sugaya¹²⁹, M. Suk¹³⁸, V.V. Sulin¹⁰⁸, D.M.S. Sultan⁵²,
 S. Sultansoy^{4c}, T. Sumida⁸³, S. Sun¹⁰³, X. Sun³, K. Suruliz¹⁵³, C.J.E. Suster¹⁵⁴, M.R. Sutton¹⁵³,
 S. Suzuki⁷⁹, M. Svatos¹³⁷, M. Swiatlowski³⁶, S.P. Swift², A. Sydorenko⁹⁷, I. Sykora^{28a}, T. Sykora¹³⁹,
 D. Ta⁹⁷, K. Tackmann^{44,ac}, J. Taenzer¹⁵⁹, A. Taffard¹⁶⁹, R. Tafirout^{166a}, E. Tahirovic⁹⁰, N. Taiblum¹⁵⁹,
 H. Takai²⁹, R. Takashima⁸⁴, E.H. Takasugi¹¹³, K. Takeda⁸⁰, T. Takeshita¹⁴⁷, Y. Takubo⁷⁹, M. Talby⁹⁹,
 A.A. Talyshv^{120b,120a}, J. Tanaka¹⁶¹, M. Tanaka¹⁶³, R. Tanaka¹²⁸, R. Tanioka⁸⁰, B.B. Tannenwald¹²²,
 S. Tapia Araya^{144b}, S. Tapprogge⁹⁷, A. Tarek Abouelfadl Mohamed¹³², S. Tarem¹⁵⁸, G. Tarna^{27b,f},
 G.F. Tartarelli^{66a}, P. Tas¹³⁹, M. Tasevsky¹³⁷, T. Tashiro⁸³, E. Tassi^{40b,40a}, A. Tavares Delgado^{136a,136b},
 Y. Tayalati^{34e}, A.C. Taylor¹¹⁶, A.J. Taylor⁴⁸, G.N. Taylor¹⁰², P.T.E. Taylor¹⁰², W. Taylor^{166b}, A.S. Tee⁸⁷,
 P. Teixeira-Dias⁹¹, D. Temple¹⁴⁹, H. Ten Kate³⁵, P.K. Teng¹⁵⁵, J.J. Teoh¹²⁹, F. Tepel¹⁸⁰, S. Terada⁷⁹,
 K. Terashi¹⁶¹, J. Terron⁹⁶, S. Terzo¹⁴, M. Testa⁴⁹, R.J. Teuscher^{165,af}, S.J. Thais¹⁸¹,
 T. Thevenaux-Pelzer⁴⁴, F. Thiele³⁹, J.P. Thomas²¹, A.S. Thompson⁵⁵, P.D. Thompson²¹,
 L.A. Thomsen¹⁸¹, E. Thomson¹³³, Y. Tian³⁸, R.E. Ticse Torres⁵¹, V.O. Tikhomirov^{108,ap},
 Yu.A. Tikhonov^{120b,120a}, S. Timoshenko¹¹⁰, P. Tipton¹⁸¹, S. Tisserant⁹⁹, K. Todome¹⁶³,
 S. Todorova-Nova⁵, S. Todt⁴⁶, J. Tojo⁸⁵, S. Tokár^{28a}, K. Tokushuku⁷⁹, E. Tolley¹²², M. Tomoto¹¹⁵,
 L. Tompkins^{150,s}, K. Toms¹¹⁶, B. Tong⁵⁷, P. Tornambe⁵⁰, E. Torrence¹²⁷, H. Torres⁴⁶, E. Torrón Pastor¹⁴⁵,
 C. Toscirri¹³¹, J. Toth^{99,ae}, F. Touchard⁹⁹, D.R. Tovey¹⁴⁶, C.J. Treado¹²¹, T. Trefzger¹⁷⁵, F. Tresoldi¹⁵³,
 A. Tricoli²⁹, I.M. Trigger^{166a}, S. Trincaz-Duvoid¹³², M.F. Tripiana¹⁴, W. Trischuk¹⁶⁵, B. Trocmé⁵⁶,
 A. Trofymov¹²⁸, C. Troncon^{66a}, M. Trovatelli¹⁷⁴, F. Trovato¹⁵³, L. Truong^{32b}, M. Trzebinski⁸²,
 A. Trzupek⁸², F. Tsai⁴⁴, J.C-L. Tseng¹³¹, P.V. Tsiarshka¹⁰⁵, N. Tsirintanis⁹, V. Tsiskaridze¹⁵²,
 E.G. Tskhadadze^{157a}, I.I. Tsukerman¹⁰⁹, V. Tsulaia¹⁸, S. Tsuno⁷⁹, D. Tsybychev¹⁵², Y. Tu^{61b},
 A. Tudorache^{27b}, V. Tudorache^{27b}, T.T. Tulbure^{27a}, A.N. Tuna⁵⁷, S. Turchikhin⁷⁷, D. Turgeman¹⁷⁸,
 I. Turk Cakir^{4b,w}, R. Turra^{66a}, P.M. Tuts³⁸, E. Tzovara⁹⁷, G. Ucchielli^{23b,23a}, I. Ueda⁷⁹, M. Ughetto^{43a,43b},
 F. Ukegawa¹⁶⁷, G. Unal³⁵, A. Undrus²⁹, G. Unel¹⁶⁹, F.C. Ungaro¹⁰², Y. Unno⁷⁹, K. Uno¹⁶¹, J. Urban^{28b},
 P. Urquijo¹⁰², P. Urrejola⁹⁷, G. Usai⁸, J. Usui⁷⁹, L. Vacavant⁹⁹, V. Vacek¹³⁸, B. Vachon¹⁰¹,
 K.O.H. Vadla¹³⁰, A. Vaidya⁹², C. Valderanis¹¹², E. Valdes Santurio^{43a,43b}, M. Valente⁵²,
 S. Valentineti^{23b,23a}, A. Valero¹⁷², L. Valéry⁴⁴, R.A. Vallance²¹, A. Vallier⁵, J.A. Valls Ferrer¹⁷²,

T.R. Van Daalen¹⁴, W. Van Den Wollenberg¹¹⁸, H. Van der Graaf¹¹⁸, P. Van Gemmeren⁶, J. Van Nieuwkoop¹⁴⁹, I. Van Vulpen¹¹⁸, M.C. van Woerden¹¹⁸, M. Vanadia^{71a,71b}, W. Vandelli³⁵, A. Vaniachine¹⁶⁴, P. Vankov¹¹⁸, R. Vari^{70a}, E.W. Varnes⁷, C. Varni^{53b,53a}, T. Varol⁴¹, D. Varouchas¹²⁸, A. Vartapetian⁸, K.E. Varvell¹⁵⁴, G.A. Vasquez^{144b}, J.G. Vasquez¹⁸¹, F. Vazeille³⁷, D. Vazquez Furelos¹⁴, T. Vazquez Schroeder¹⁰¹, J. Veatch⁵¹, V. Vecchio^{72a,72b}, L.M. Veloce¹⁶⁵, F. Veloso^{136a,136c}, S. Veneziano^{70a}, A. Ventura^{65a,65b}, M. Venturi¹⁷⁴, N. Venturi³⁵, V. Vercesi^{68a}, M. Verducci^{72a,72b}, W. Verkerke¹¹⁸, A.T. Vermeulen¹¹⁸, J.C. Vermeulen¹¹⁸, M.C. Vetterli^{149,ax}, N. Viaux Maira^{144b}, O. Viazlo⁹⁴, I. Vichou^{171,*}, T. Vickey¹⁴⁶, O.E. Vickey Boeriu¹⁴⁶, G.H.A. Viehhauser¹³¹, S. Viel¹⁸, L. Vigani¹³¹, M. Villa^{23b,23a}, M. Villaplana Perez^{66a,66b}, E. Vilucchi⁴⁹, M.G. Vincter³³, V.B. Vinogradov⁷⁷, A. Vishwakarma⁴⁴, C. Vittori^{23b,23a}, I. Vivarelli¹⁵³, S. Vlachos¹⁰, M. Vogel¹⁸⁰, P. Vokac¹³⁸, G. Volpi¹⁴, S.E. von Buddenbrock^{32c}, E. Von Toerne²⁴, V. Vorobel¹³⁹, K. Vorobev¹¹⁰, M. Vos¹⁷², J.H. Vosseveld⁸⁸, N. Vranjes¹⁶, M. Vranjes Milosavljevic¹⁶, V. Vrba¹³⁸, M. Vreeswijk¹¹⁸, T. Šfiligoj⁸⁹, R. Vuillermet³⁵, I. Vukotic³⁶, T. Ženiš^{28a}, L. Živković¹⁶, P. Wagner²⁴, W. Wagner¹⁸⁰, J. Wagner-Kuhr¹¹², H. Wahlberg⁸⁶, S. Wahrmund⁴⁶, K. Wakamiya⁸⁰, J. Walder⁸⁷, R. Walker¹¹², W. Walkowiak¹⁴⁸, V. Wallangen^{43a,43b}, A.M. Wang⁵⁷, C. Wang^{58b,f}, F. Wang¹⁷⁹, H. Wang¹⁸, H. Wang³, J. Wang¹⁵⁴, J. Wang^{59b}, P. Wang⁴¹, Q. Wang¹²⁴, R.-J. Wang¹³², R. Wang^{58a}, R. Wang⁶, S.M. Wang¹⁵⁵, W. Wang^{155,q}, W.X. Wang^{58a,ag}, Y. Wang^{58a,am}, Z. Wang^{58c}, C. Wanotayaroj⁴⁴, A. Warburton¹⁰¹, C.P. Ward³¹, D.R. Wardrope⁹², A. Washbrook⁴⁸, P.M. Watkins²¹, A.T. Watson²¹, M.F. Watson²¹, G. Watts¹⁴⁵, S. Watts⁹⁸, B.M. Waugh⁹², A.F. Webb¹¹, S. Webb⁹⁷, C. Weber¹⁸¹, M.S. Weber²⁰, S.A. Weber³³, S.M. Weber^{59a}, J.S. Webster⁶, A.R. Weidberg¹³¹, B. Weinert⁶³, J. Weingarten⁵¹, M. Weirich⁹⁷, C. Weiser⁵⁰, P.S. Wells³⁵, T. Wenaus²⁹, T. Wengler³⁵, S. Wenig³⁵, N. Wermes²⁴, M.D. Werner⁷⁶, P. Werner³⁵, M. Wessels^{59a}, T.D. Weston²⁰, K. Whalen¹²⁷, N.L. Whallon¹⁴⁵, A.M. Wharton⁸⁷, A.S. White¹⁰³, A. White⁸, M.J. White¹, R. White^{144b}, D. Whiteson¹⁶⁹, B.W. Whitmore⁸⁷, F.J. Wickens¹⁴¹, W. Wiedenmann¹⁷⁹, M. Wielers¹⁴¹, C. Wiglesworth³⁹, L.A.M. Wiik-Fuchs⁵⁰, A. Wildauer¹¹³, F. Wilk⁹⁸, H.G. Wilkens³⁵, H.H. Williams¹³³, S. Williams³¹, C. Willis¹⁰⁴, S. Willocq¹⁰⁰, J.A. Wilson²¹, I. Wingerter-Seez⁵, E. Winkels¹⁵³, F. Winklmeier¹²⁷, O.J. Winston¹⁵³, B.T. Winter²⁴, M. Wittgen¹⁵⁰, M. Wobisch⁹³, A. Wolf⁹⁷, T.M.H. Wolf¹¹⁸, R. Wolff⁹⁹, M.W. Wolter⁸², H. Wolters^{136a,136c}, V.W.S. Wong¹⁷³, N.L. Woods¹⁴³, S.D. Worm²¹, B.K. Wosiek⁸², K.W. Woźniak⁸², K. Wraight⁵⁵, M. Wu³⁶, S.L. Wu¹⁷⁹, X. Wu⁵², Y. Wu^{58a}, T.R. Wyatt⁹⁸, B.M. Wynne⁴⁸, S. Xella³⁹, Z. Xi¹⁰³, L. Xia¹⁷⁶, D. Xu^{15a}, H. Xu^{58a,f}, L. Xu²⁹, T. Xu¹⁴², W. Xu¹⁰³, B. Yabsley¹⁵⁴, S. Yacoub^{32a}, K. Yajima¹²⁹, D.P. Yallup⁹², D. Yamaguchi¹⁶³, Y. Yamaguchi¹⁶³, A. Yamamoto⁷⁹, T. Yamanaka¹⁶¹, F. Yamane⁸⁰, M. Yamatani¹⁶¹, T. Yamazaki¹⁶¹, Y. Yamazaki⁸⁰, Z. Yan²⁵, H.J. Yang^{58c,58d}, H.T. Yang¹⁸, S. Yang⁷⁵, Y. Yang¹⁶¹, Y. Yang¹⁵⁵, Z. Yang¹⁷, W.-M. Yao¹⁸, Y.C. Yap⁴⁴, Y. Yasu⁷⁹, E. Yatsenko⁵, J. Ye⁴¹, S. Ye²⁹, I. Yeletsikh⁷⁷, E. Yigitbasi²⁵, E. Yildirim⁹⁷, K. Yorita¹⁷⁷, K. Yoshihara¹³³, C.J.S. Young³⁵, C. Young¹⁵⁰, J. Yu⁸, J. Yu⁷⁶, X. Yue^{59a}, S.P.Y. Yuen²⁴, I. Yusuff^{31,a}, B. Zabinski⁸², G. Zacharis¹⁰, E. Zaffaroni⁵², R. Zaidan¹⁴, A.M. Zaitsev^{140,ao}, N. Zakharchuk⁴⁴, J. Zalieckas¹⁷, S. Zambito⁵⁷, D. Zanzi³⁵, D.R. Zaripovas⁵⁵, C. Zeitnitz¹⁸⁰, G. Zemaityte¹³¹, J.C. Zeng¹⁷¹, Q. Zeng¹⁵⁰, O. Zenin¹⁴⁰, D. Zerwas¹²⁸, M. Zgubić¹³¹, D.F. Zhang^{58b}, D. Zhang¹⁰³, F. Zhang¹⁷⁹, G. Zhang^{58a,ag}, H. Zhang^{15c}, J. Zhang⁶, L. Zhang⁵⁰, L. Zhang^{58a}, M. Zhang¹⁷¹, P. Zhang^{15c}, R. Zhang^{58a,f}, R. Zhang²⁴, X. Zhang^{58b}, Y. Zhang^{15d}, Z. Zhang¹²⁸, X. Zhao⁴¹, Y. Zhao^{58b,128,ak}, Z. Zhao^{58a}, A. Zhemchugov⁷⁷, B. Zhou¹⁰³, C. Zhou¹⁷⁹, L. Zhou⁴¹, M.S. Zhou^{15d}, M. Zhou¹⁵², N. Zhou^{58c}, Y. Zhou⁷, C.G. Zhu^{58b}, H.L. Zhu^{58a}, H. Zhu^{15a}, J. Zhu¹⁰³, Y. Zhu^{58a}, X. Zhuang^{15a}, K. Zhukov¹⁰⁸, V. Zhulanov^{120b,120a}, A. Zibell¹⁷⁵, D. Zieminska⁶³, N.I. Zimine⁷⁷, S. Zimmermann⁵⁰, Z. Zinonos¹¹³, M. Zinser⁹⁷, M. Ziolkowski¹⁴⁸, G. Zobernig¹⁷⁹, A. Zoccoli^{23b,23a}, K. Zoch⁵¹, T.G. Zorbas¹⁴⁶, R. Zou³⁶, M. Zur Nedden¹⁹, L. Zwalinski³⁵.

¹Department of Physics, University of Adelaide, Adelaide; Australia.

- ²Physics Department, SUNY Albany, Albany NY; United States of America.
- ³Department of Physics, University of Alberta, Edmonton AB; Canada.
- ⁴(^a)Department of Physics, Ankara University, Ankara; (^b)Istanbul Aydin University, Istanbul; (^c)Division of Physics, TOBB University of Economics and Technology, Ankara; Turkey.
- ⁵LAPP, Université Grenoble Alpes, Université Savoie Mont Blanc, CNRS/IN2P3, Annecy; France.
- ⁶High Energy Physics Division, Argonne National Laboratory, Argonne IL; United States of America.
- ⁷Department of Physics, University of Arizona, Tucson AZ; United States of America.
- ⁸Department of Physics, University of Texas at Arlington, Arlington TX; United States of America.
- ⁹Physics Department, National and Kapodistrian University of Athens, Athens; Greece.
- ¹⁰Physics Department, National Technical University of Athens, Zografou; Greece.
- ¹¹Department of Physics, University of Texas at Austin, Austin TX; United States of America.
- ¹²(^a)Bahcesehir University, Faculty of Engineering and Natural Sciences, Istanbul; (^b)Istanbul Bilgi University, Faculty of Engineering and Natural Sciences, Istanbul; (^c)Department of Physics, Bogazici University, Istanbul; (^d)Department of Physics Engineering, Gaziantep University, Gaziantep; Turkey.
- ¹³Institute of Physics, Azerbaijan Academy of Sciences, Baku; Azerbaijan.
- ¹⁴Institut de Física d'Altes Energies (IFAE), Barcelona Institute of Science and Technology, Barcelona; Spain.
- ¹⁵(^a)Institute of High Energy Physics, Chinese Academy of Sciences, Beijing; (^b)Physics Department, Tsinghua University, Beijing; (^c)Department of Physics, Nanjing University, Nanjing; (^d)University of Chinese Academy of Science (UCAS), Beijing; China.
- ¹⁶Institute of Physics, University of Belgrade, Belgrade; Serbia.
- ¹⁷Department for Physics and Technology, University of Bergen, Bergen; Norway.
- ¹⁸Physics Division, Lawrence Berkeley National Laboratory and University of California, Berkeley CA; United States of America.
- ¹⁹Institut für Physik, Humboldt Universität zu Berlin, Berlin; Germany.
- ²⁰Albert Einstein Center for Fundamental Physics and Laboratory for High Energy Physics, University of Bern, Bern; Switzerland.
- ²¹School of Physics and Astronomy, University of Birmingham, Birmingham; United Kingdom.
- ²²Centro de Investigaciones, Universidad Antonio Nariño, Bogota; Colombia.
- ²³(^a)Dipartimento di Fisica e Astronomia, Università di Bologna, Bologna; (^b)INFN Sezione di Bologna; Italy.
- ²⁴Physikalisches Institut, Universität Bonn, Bonn; Germany.
- ²⁵Department of Physics, Boston University, Boston MA; United States of America.
- ²⁶Department of Physics, Brandeis University, Waltham MA; United States of America.
- ²⁷(^a)Transilvania University of Brasov, Brasov; (^b)Horia Hulubei National Institute of Physics and Nuclear Engineering, Bucharest; (^c)Department of Physics, Alexandru Ioan Cuza University of Iasi, Iasi; (^d)National Institute for Research and Development of Isotopic and Molecular Technologies, Physics Department, Cluj-Napoca; (^e)University Politehnica Bucharest, Bucharest; (^f)West University in Timisoara, Timisoara; Romania.
- ²⁸(^a)Faculty of Mathematics, Physics and Informatics, Comenius University, Bratislava; (^b)Department of Subnuclear Physics, Institute of Experimental Physics of the Slovak Academy of Sciences, Kosice; Slovak Republic.
- ²⁹Physics Department, Brookhaven National Laboratory, Upton NY; United States of America.
- ³⁰Departamento de Física, Universidad de Buenos Aires, Buenos Aires; Argentina.
- ³¹Cavendish Laboratory, University of Cambridge, Cambridge; United Kingdom.
- ³²(^a)Department of Physics, University of Cape Town, Cape Town; (^b)Department of Mechanical Engineering Science, University of Johannesburg, Johannesburg; (^c)School of Physics, University of the

Witwatersrand, Johannesburg; South Africa.

³³Department of Physics, Carleton University, Ottawa ON; Canada.

^{34(a)}Faculté des Sciences Ain Chock, Réseau Universitaire de Physique des Hautes Energies - Université Hassan II, Casablanca;^(b)Centre National de l'Energie des Sciences Techniques Nucleaires (CNESTEN), Rabat;^(c)Faculté des Sciences Semlalia, Université Cadi Ayyad, LPHEA-Marrakech;^(d)Faculté des Sciences, Université Mohamed Premier and LTPM, Oujda;^(e)Faculté des sciences, Université Mohammed V, Rabat; Morocco.

³⁵CERN, Geneva; Switzerland.

³⁶Enrico Fermi Institute, University of Chicago, Chicago IL; United States of America.

³⁷LPC, Université Clermont Auvergne, CNRS/IN2P3, Clermont-Ferrand; France.

³⁸Nevis Laboratory, Columbia University, Irvington NY; United States of America.

³⁹Niels Bohr Institute, University of Copenhagen, Copenhagen; Denmark.

^{40(a)}Dipartimento di Fisica, Università della Calabria, Rende;^(b)INFN Gruppo Collegato di Cosenza, Laboratori Nazionali di Frascati; Italy.

⁴¹Physics Department, Southern Methodist University, Dallas TX; United States of America.

⁴²Physics Department, University of Texas at Dallas, Richardson TX; United States of America.

^{43(a)}Department of Physics, Stockholm University;^(b)Oskar Klein Centre, Stockholm; Sweden.

⁴⁴Deutsches Elektronen-Synchrotron DESY, Hamburg and Zeuthen; Germany.

⁴⁵Lehrstuhl für Experimentelle Physik IV, Technische Universität Dortmund, Dortmund; Germany.

⁴⁶Institut für Kern- und Teilchenphysik, Technische Universität Dresden, Dresden; Germany.

⁴⁷Department of Physics, Duke University, Durham NC; United States of America.

⁴⁸SUPA - School of Physics and Astronomy, University of Edinburgh, Edinburgh; United Kingdom.

⁴⁹INFN e Laboratori Nazionali di Frascati, Frascati; Italy.

⁵⁰Physikalisches Institut, Albert-Ludwigs-Universität Freiburg, Freiburg; Germany.

⁵¹II. Physikalisches Institut, Georg-August-Universität Göttingen, Göttingen; Germany.

⁵²Département de Physique Nucléaire et Corpusculaire, Université de Genève, Genève; Switzerland.

^{53(a)}Dipartimento di Fisica, Università di Genova, Genova;^(b)INFN Sezione di Genova; Italy.

⁵⁴II. Physikalisches Institut, Justus-Liebig-Universität Giessen, Giessen; Germany.

⁵⁵SUPA - School of Physics and Astronomy, University of Glasgow, Glasgow; United Kingdom.

⁵⁶LPSC, Université Grenoble Alpes, CNRS/IN2P3, Grenoble INP, Grenoble; France.

⁵⁷Laboratory for Particle Physics and Cosmology, Harvard University, Cambridge MA; United States of America.

^{58(a)}Department of Modern Physics and State Key Laboratory of Particle Detection and Electronics, University of Science and Technology of China, Hefei;^(b)Institute of Frontier and Interdisciplinary Science and Key Laboratory of Particle Physics and Particle Irradiation (MOE), Shandong University, Qingdao;^(c)School of Physics and Astronomy, Shanghai Jiao Tong University, KLPPAC-MoE, SKLPPC, Shanghai;^(d)Tsung-Dao Lee Institute, Shanghai; China.

^{59(a)}Kirchhoff-Institut für Physik, Ruprecht-Karls-Universität Heidelberg, Heidelberg;^(b)Physikalisches Institut, Ruprecht-Karls-Universität Heidelberg, Heidelberg; Germany.

⁶⁰Faculty of Applied Information Science, Hiroshima Institute of Technology, Hiroshima; Japan.

^{61(a)}Department of Physics, Chinese University of Hong Kong, Shatin, N.T., Hong Kong;^(b)Department of Physics, University of Hong Kong, Hong Kong;^(c)Department of Physics and Institute for Advanced Study, Hong Kong University of Science and Technology, Clear Water Bay, Kowloon, Hong Kong; China.

⁶²Department of Physics, National Tsing Hua University, Hsinchu; Taiwan.

⁶³Department of Physics, Indiana University, Bloomington IN; United States of America.

^{64(a)}INFN Gruppo Collegato di Udine, Sezione di Trieste, Udine;^(b)ICTP, Trieste;^(c)Dipartimento di

- Chimica, Fisica e Ambiente, Università di Udine, Udine; Italy.
- 65^(a)INFN Sezione di Lecce;^(b)Dipartimento di Matematica e Fisica, Università del Salento, Lecce; Italy.
- 66^(a)INFN Sezione di Milano;^(b)Dipartimento di Fisica, Università di Milano, Milano; Italy.
- 67^(a)INFN Sezione di Napoli;^(b)Dipartimento di Fisica, Università di Napoli, Napoli; Italy.
- 68^(a)INFN Sezione di Pavia;^(b)Dipartimento di Fisica, Università di Pavia, Pavia; Italy.
- 69^(a)INFN Sezione di Pisa;^(b)Dipartimento di Fisica E. Fermi, Università di Pisa, Pisa; Italy.
- 70^(a)INFN Sezione di Roma;^(b)Dipartimento di Fisica, Sapienza Università di Roma, Roma; Italy.
- 71^(a)INFN Sezione di Roma Tor Vergata;^(b)Dipartimento di Fisica, Università di Roma Tor Vergata, Roma; Italy.
- 72^(a)INFN Sezione di Roma Tre;^(b)Dipartimento di Matematica e Fisica, Università Roma Tre, Roma; Italy.
- 73^(a)INFN-TIFPA;^(b)Università degli Studi di Trento, Trento; Italy.
- 74Institut für Astro- und Teilchenphysik, Leopold-Franzens-Universität, Innsbruck; Austria.
- 75University of Iowa, Iowa City IA; United States of America.
- 76Department of Physics and Astronomy, Iowa State University, Ames IA; United States of America.
- 77Joint Institute for Nuclear Research, Dubna; Russia.
- 78^(a)Departamento de Engenharia Elétrica, Universidade Federal de Juiz de Fora (UFJF), Juiz de Fora;^(b)Universidade Federal do Rio De Janeiro COPPE/EE/IF, Rio de Janeiro;^(c)Universidade Federal de São João del Rei (UFSJ), São João del Rei;^(d)Instituto de Física, Universidade de São Paulo, São Paulo; Brazil.
- 79KEK, High Energy Accelerator Research Organization, Tsukuba; Japan.
- 80Graduate School of Science, Kobe University, Kobe; Japan.
- 81^(a)AGH University of Science and Technology, Faculty of Physics and Applied Computer Science, Krakow;^(b)Marian Smoluchowski Institute of Physics, Jagiellonian University, Krakow; Poland.
- 82Institute of Nuclear Physics Polish Academy of Sciences, Krakow; Poland.
- 83Faculty of Science, Kyoto University, Kyoto; Japan.
- 84Kyoto University of Education, Kyoto; Japan.
- 85Research Center for Advanced Particle Physics and Department of Physics, Kyushu University, Fukuoka ; Japan.
- 86Instituto de Física La Plata, Universidad Nacional de La Plata and CONICET, La Plata; Argentina.
- 87Physics Department, Lancaster University, Lancaster; United Kingdom.
- 88Oliver Lodge Laboratory, University of Liverpool, Liverpool; United Kingdom.
- 89Department of Experimental Particle Physics, Jožef Stefan Institute and Department of Physics, University of Ljubljana, Ljubljana; Slovenia.
- 90School of Physics and Astronomy, Queen Mary University of London, London; United Kingdom.
- 91Department of Physics, Royal Holloway University of London, Egham; United Kingdom.
- 92Department of Physics and Astronomy, University College London, London; United Kingdom.
- 93Louisiana Tech University, Ruston LA; United States of America.
- 94Fysiska institutionen, Lunds universitet, Lund; Sweden.
- 95Centre de Calcul de l'Institut National de Physique Nucléaire et de Physique des Particules (IN2P3), Villeurbanne; France.
- 96Departamento de Física Teórica C-15 and CIAFF, Universidad Autónoma de Madrid, Madrid; Spain.
- 97Institut für Physik, Universität Mainz, Mainz; Germany.
- 98School of Physics and Astronomy, University of Manchester, Manchester; United Kingdom.
- 99CPPM, Aix-Marseille Université, CNRS/IN2P3, Marseille; France.
- 100Department of Physics, University of Massachusetts, Amherst MA; United States of America.
- 101Department of Physics, McGill University, Montreal QC; Canada.

- ¹⁰²School of Physics, University of Melbourne, Victoria; Australia.
- ¹⁰³Department of Physics, University of Michigan, Ann Arbor MI; United States of America.
- ¹⁰⁴Department of Physics and Astronomy, Michigan State University, East Lansing MI; United States of America.
- ¹⁰⁵B.I. Stepanov Institute of Physics, National Academy of Sciences of Belarus, Minsk; Belarus.
- ¹⁰⁶Research Institute for Nuclear Problems of Byelorussian State University, Minsk; Belarus.
- ¹⁰⁷Group of Particle Physics, University of Montreal, Montreal QC; Canada.
- ¹⁰⁸P.N. Lebedev Physical Institute of the Russian Academy of Sciences, Moscow; Russia.
- ¹⁰⁹Institute for Theoretical and Experimental Physics (ITEP), Moscow; Russia.
- ¹¹⁰National Research Nuclear University MEPhI, Moscow; Russia.
- ¹¹¹D.V. Skobeltsyn Institute of Nuclear Physics, M.V. Lomonosov Moscow State University, Moscow; Russia.
- ¹¹²Fakultät für Physik, Ludwig-Maximilians-Universität München, München; Germany.
- ¹¹³Max-Planck-Institut für Physik (Werner-Heisenberg-Institut), München; Germany.
- ¹¹⁴Nagasaki Institute of Applied Science, Nagasaki; Japan.
- ¹¹⁵Graduate School of Science and Kobayashi-Maskawa Institute, Nagoya University, Nagoya; Japan.
- ¹¹⁶Department of Physics and Astronomy, University of New Mexico, Albuquerque NM; United States of America.
- ¹¹⁷Institute for Mathematics, Astrophysics and Particle Physics, Radboud University Nijmegen/Nikhef, Nijmegen; Netherlands.
- ¹¹⁸Nikhef National Institute for Subatomic Physics and University of Amsterdam, Amsterdam; Netherlands.
- ¹¹⁹Department of Physics, Northern Illinois University, DeKalb IL; United States of America.
- ¹²⁰(^a)Budker Institute of Nuclear Physics, SB RAS, Novosibirsk; (^b)Novosibirsk State University Novosibirsk; Russia.
- ¹²¹Department of Physics, New York University, New York NY; United States of America.
- ¹²²Ohio State University, Columbus OH; United States of America.
- ¹²³Faculty of Science, Okayama University, Okayama; Japan.
- ¹²⁴Homer L. Dodge Department of Physics and Astronomy, University of Oklahoma, Norman OK; United States of America.
- ¹²⁵Department of Physics, Oklahoma State University, Stillwater OK; United States of America.
- ¹²⁶Palacký University, RCPTM, Joint Laboratory of Optics, Olomouc; Czech Republic.
- ¹²⁷Center for High Energy Physics, University of Oregon, Eugene OR; United States of America.
- ¹²⁸LAL, Université Paris-Sud, CNRS/IN2P3, Université Paris-Saclay, Orsay; France.
- ¹²⁹Graduate School of Science, Osaka University, Osaka; Japan.
- ¹³⁰Department of Physics, University of Oslo, Oslo; Norway.
- ¹³¹Department of Physics, Oxford University, Oxford; United Kingdom.
- ¹³²LPNHE, Sorbonne Université, Paris Diderot Sorbonne Paris Cité, CNRS/IN2P3, Paris; France.
- ¹³³Department of Physics, University of Pennsylvania, Philadelphia PA; United States of America.
- ¹³⁴Konstantinov Nuclear Physics Institute of National Research Centre "Kurchatov Institute", PNPI, St. Petersburg; Russia.
- ¹³⁵Department of Physics and Astronomy, University of Pittsburgh, Pittsburgh PA; United States of America.
- ¹³⁶(^a)Laboratório de Instrumentação e Física Experimental de Partículas - LIP; (^b)Departamento de Física, Faculdade de Ciências, Universidade de Lisboa, Lisboa; (^c)Departamento de Física, Universidade de Coimbra, Coimbra; (^d)Centro de Física Nuclear da Universidade de Lisboa, Lisboa; (^e)Departamento de Física, Universidade do Minho, Braga; (^f)Departamento de Física Teórica y del Cosmos, Universidad

- de Granada, Granada (Spain);^(g)Dep Física and CEFITEC of Faculdade de Ciências e Tecnologia, Universidade Nova de Lisboa, Caparica; Portugal.
- ¹³⁷Institute of Physics, Academy of Sciences of the Czech Republic, Prague; Czech Republic.
- ¹³⁸Czech Technical University in Prague, Prague; Czech Republic.
- ¹³⁹Charles University, Faculty of Mathematics and Physics, Prague; Czech Republic.
- ¹⁴⁰State Research Center Institute for High Energy Physics, NRC KI, Protvino; Russia.
- ¹⁴¹Particle Physics Department, Rutherford Appleton Laboratory, Didcot; United Kingdom.
- ¹⁴²IRFU, CEA, Université Paris-Saclay, Gif-sur-Yvette; France.
- ¹⁴³Santa Cruz Institute for Particle Physics, University of California Santa Cruz, Santa Cruz CA; United States of America.
- ¹⁴⁴^(a)Departamento de Física, Pontificia Universidad Católica de Chile, Santiago;^(b)Departamento de Física, Universidad Técnica Federico Santa María, Valparaíso; Chile.
- ¹⁴⁵Department of Physics, University of Washington, Seattle WA; United States of America.
- ¹⁴⁶Department of Physics and Astronomy, University of Sheffield, Sheffield; United Kingdom.
- ¹⁴⁷Department of Physics, Shinshu University, Nagano; Japan.
- ¹⁴⁸Department Physik, Universität Siegen, Siegen; Germany.
- ¹⁴⁹Department of Physics, Simon Fraser University, Burnaby BC; Canada.
- ¹⁵⁰SLAC National Accelerator Laboratory, Stanford CA; United States of America.
- ¹⁵¹Physics Department, Royal Institute of Technology, Stockholm; Sweden.
- ¹⁵²Departments of Physics and Astronomy, Stony Brook University, Stony Brook NY; United States of America.
- ¹⁵³Department of Physics and Astronomy, University of Sussex, Brighton; United Kingdom.
- ¹⁵⁴School of Physics, University of Sydney, Sydney; Australia.
- ¹⁵⁵Institute of Physics, Academia Sinica, Taipei; Taiwan.
- ¹⁵⁶Academia Sinica Grid Computing, Institute of Physics, Academia Sinica, Taipei; Taiwan.
- ¹⁵⁷^(a)E. Andronikashvili Institute of Physics, Iv. Javakhishvili Tbilisi State University, Tbilisi;^(b)High Energy Physics Institute, Tbilisi State University, Tbilisi; Georgia.
- ¹⁵⁸Department of Physics, Technion, Israel Institute of Technology, Haifa; Israel.
- ¹⁵⁹Raymond and Beverly Sackler School of Physics and Astronomy, Tel Aviv University, Tel Aviv; Israel.
- ¹⁶⁰Department of Physics, Aristotle University of Thessaloniki, Thessaloniki; Greece.
- ¹⁶¹International Center for Elementary Particle Physics and Department of Physics, University of Tokyo, Tokyo; Japan.
- ¹⁶²Graduate School of Science and Technology, Tokyo Metropolitan University, Tokyo; Japan.
- ¹⁶³Department of Physics, Tokyo Institute of Technology, Tokyo; Japan.
- ¹⁶⁴Tomsk State University, Tomsk; Russia.
- ¹⁶⁵Department of Physics, University of Toronto, Toronto ON; Canada.
- ¹⁶⁶^(a)TRIUMF, Vancouver BC;^(b)Department of Physics and Astronomy, York University, Toronto ON; Canada.
- ¹⁶⁷Division of Physics and Tomonaga Center for the History of the Universe, Faculty of Pure and Applied Sciences, University of Tsukuba, Tsukuba; Japan.
- ¹⁶⁸Department of Physics and Astronomy, Tufts University, Medford MA; United States of America.
- ¹⁶⁹Department of Physics and Astronomy, University of California Irvine, Irvine CA; United States of America.
- ¹⁷⁰Department of Physics and Astronomy, University of Uppsala, Uppsala; Sweden.
- ¹⁷¹Department of Physics, University of Illinois, Urbana IL; United States of America.
- ¹⁷²Instituto de Física Corpuscular (IFIC), Centro Mixto Universidad de Valencia - CSIC, Valencia; Spain.
- ¹⁷³Department of Physics, University of British Columbia, Vancouver BC; Canada.

- ¹⁷⁴Department of Physics and Astronomy, University of Victoria, Victoria BC; Canada.
- ¹⁷⁵Fakultät für Physik und Astronomie, Julius-Maximilians-Universität Würzburg, Würzburg; Germany.
- ¹⁷⁶Department of Physics, University of Warwick, Coventry; United Kingdom.
- ¹⁷⁷Waseda University, Tokyo; Japan.
- ¹⁷⁸Department of Particle Physics, Weizmann Institute of Science, Rehovot; Israel.
- ¹⁷⁹Department of Physics, University of Wisconsin, Madison WI; United States of America.
- ¹⁸⁰Fakultät für Mathematik und Naturwissenschaften, Fachgruppe Physik, Bergische Universität Wuppertal, Wuppertal; Germany.
- ¹⁸¹Department of Physics, Yale University, New Haven CT; United States of America.
- ¹⁸²Yerevan Physics Institute, Yerevan; Armenia.
- ^a Also at Department of Physics, University of Malaya, Kuala Lumpur; Malaysia.
- ^b Also at Borough of Manhattan Community College, City University of New York, NY; United States of America.
- ^c Also at California State University, East Bay; United States of America.
- ^d Also at Centre for High Performance Computing, CSIR Campus, Rosebank, Cape Town; South Africa.
- ^e Also at CERN, Geneva; Switzerland.
- ^f Also at CPPM, Aix-Marseille Université, CNRS/IN2P3, Marseille; France.
- ^g Also at Département de Physique Nucléaire et Corpusculaire, Université de Genève, Genève; Switzerland.
- ^h Also at Departament de Física de la Universitat Autònoma de Barcelona, Barcelona; Spain.
- ⁱ Also at Departamento de Física Teórica y del Cosmos, Universidad de Granada, Granada (Spain); Spain.
- ^j Also at Department of Applied Physics and Astronomy, University of Sharjah, Sharjah; United Arab Emirates.
- ^k Also at Department of Financial and Management Engineering, University of the Aegean, Chios; Greece.
- ^l Also at Department of Physics and Astronomy, University of Louisville, Louisville, KY; United States of America.
- ^m Also at Department of Physics and Astronomy, University of Sheffield, Sheffield; United Kingdom.
- ⁿ Also at Department of Physics, California State University, Fresno CA; United States of America.
- ^o Also at Department of Physics, California State University, Sacramento CA; United States of America.
- ^p Also at Department of Physics, King's College London, London; United Kingdom.
- ^q Also at Department of Physics, Nanjing University, Nanjing; China.
- ^r Also at Department of Physics, St. Petersburg State Polytechnical University, St. Petersburg; Russia.
- ^s Also at Department of Physics, Stanford University; United States of America.
- ^t Also at Department of Physics, University of Fribourg, Fribourg; Switzerland.
- ^u Also at Department of Physics, University of Michigan, Ann Arbor MI; United States of America.
- ^v Also at Dipartimento di Fisica E. Fermi, Università di Pisa, Pisa; Italy.
- ^w Also at Giresun University, Faculty of Engineering, Giresun; Turkey.
- ^x Also at Graduate School of Science, Osaka University, Osaka; Japan.
- ^y Also at Hellenic Open University, Patras; Greece.
- ^z Also at Horia Hulubei National Institute of Physics and Nuclear Engineering, Bucharest; Romania.
- ^{aa} Also at II. Physikalisches Institut, Georg-August-Universität Göttingen, Göttingen; Germany.
- ^{ab} Also at Institutio Catalana de Recerca i Estudis Avancats, ICREA, Barcelona; Spain.
- ^{ac} Also at Institut für Experimentalphysik, Universität Hamburg, Hamburg; Germany.
- ^{ad} Also at Institute for Mathematics, Astrophysics and Particle Physics, Radboud University Nijmegen/Nikhef, Nijmegen; Netherlands.

- ae* Also at Institute for Particle and Nuclear Physics, Wigner Research Centre for Physics, Budapest; Hungary.
- af* Also at Institute of Particle Physics (IPP); Canada.
- ag* Also at Institute of Physics, Academia Sinica, Taipei; Taiwan.
- ah* Also at Institute of Physics, Azerbaijan Academy of Sciences, Baku; Azerbaijan.
- ai* Also at Institute of Theoretical Physics, Iliia State University, Tbilisi; Georgia.
- aj* Also at Istanbul University, Dept. of Physics, Istanbul; Turkey.
- ak* Also at LAL, Université Paris-Sud, CNRS/IN2P3, Université Paris-Saclay, Orsay; France.
- al* Also at Louisiana Tech University, Ruston LA; United States of America.
- am* Also at LPNHE, Sorbonne Université, Paris Diderot Sorbonne Paris Cité, CNRS/IN2P3, Paris; France.
- an* Also at Manhattan College, New York NY; United States of America.
- ao* Also at Moscow Institute of Physics and Technology State University, Dolgoprudny; Russia.
- ap* Also at National Research Nuclear University MEPhI, Moscow; Russia.
- aq* Also at Near East University, Nicosia, North Cyprus, Mersin; Turkey.
- ar* Also at O Chadai Academic Production, Ochanomizu University, Tokyo; Japan.
- as* Also at Physikalisches Institut, Albert-Ludwigs-Universität Freiburg, Freiburg; Germany.
- at* Also at School of Physics, Sun Yat-sen University, Guangzhou; China.
- au* Also at The City College of New York, New York NY; United States of America.
- av* Also at The Collaborative Innovation Center of Quantum Matter (CICQM), Beijing; China.
- aw* Also at Tomsk State University, Tomsk, and Moscow Institute of Physics and Technology State University, Dolgoprudny; Russia.
- ax* Also at TRIUMF, Vancouver BC; Canada.
- ay* Also at Università di Napoli Parthenope, Napoli; Italy.
- * Deceased